TWO-WAY COUPLING OF MULTIPHASE TRANSPORT AND VISCOELASTIC LARGE DEFORMATION OF UNSATURATED SWELLING POROUS MATERIALS

A Dissertation

Presented to the Faculty of the Graduate School

of Cornell University

In Partial Fulfillment of the Requirements for the Degree of

Doctor of Philosophy

by

Haolin Zhu

January 2012

TWO-WAY COUPLING OF MULTIPHASE TRANSPORT AND VISCOELASTIC LARGE DEFORMATION OF UNSATURATED SWELLING POROUS MATERIALS

Haolin Zhu, Ph. D.

Cornell University 2012

Multiphase transport in unsaturated swelling porous materials involves fluid mass transport, heat transfer as well as swelling of the porous solid matrix. Neglecting the deformation of the solid matrix can lead to erroneous results when modeling transport phenomena in porous materials. In particular, many porous materials exhibit viscoelastic effect upon wetting/drying, which can expedite or slow the transport process. This work presents modeling and simulation of two-way coupling of multiphase transport and viscoelastic large deformation of unsaturated swelling porous systems based on fundamental physics. The work includes the development of a thermomechanical theory for multiphase transport in unsaturated swelling porous media based on the Hybrid Mixture Theory (saturated systems can also be modeled as a special case of this general theory). The theory includes three phases: solid matrix, fluid and air and uses the Coleman-Noll procedure to obtain restrictions on the form of the constitutive equations. Derived relationships include, for example, a modified Darcy's law, which takes into account both Fickian and non-Fickian transport, and a viscoelastic constitutive relationship that relates the stress and strain tensors for the solid phase. A model is then developed based on this theory for isothermal conditions

which involves a simple form of a differential-integral equation that governs the fluid transport and is fully coupled with the solid large deformation. Numerical implementation of this model is then presented that involves a finite element analysis of water absorption of plane sheet pasta and numerical results of sorption curves show good agreement with experimental results obtained from the literature. Importance of including viscoelastic relaxation is investigated for soaking processes of pasta. Drying of potato is also considered in this work as an important example of two-way coupling of multiphase transport and viscoelastic large deformation of the solid matrix of porous materials because during drying processes, the transition of outer surface of the material from rubbery to glassy state at low moisture content can slow or stop shrinkage of the materials, and thus viscoelasticity plays an important role.

BIOGRAPHICAL SKETCH

Haolin Zhu was born in the Northwestern part of China in 1984. She went to elementary, middle and high school there. Then she moved to Shanghai in 2002 for undergraduate studies. She received her Bachelor's degree in the School of Naval Architecture, Ocean and Civil Engineering from Shanghai Jiao Tong University in 2006. She majored in Engineering Mechanics and became interested in solid mechanics and finite element analysis during her undergraduate studies. In August of 2006, she joined the department of Theoretical and Applied Mechanics at Cornell University, Ithaca, to pursue a PhD degree. She has developed interest in continuum mechanics, non-linear viscoelastic constitutive modeling, nonlinear finite element analysis and other numerical analysis during her stay at Cornell University. In addition to research presented in this dissertation, she has also taught many courses at Cornell University as either an instructor or a teaching assistant, conducted trainings for graduate teaching assistants throughout Cornell University as a Graduate Teaching Specialist and campus Master Teaching Assistant, and participated in research projects on integration of computer simulations into the mechanical engineering curriculum in engineering higher education.

To my parents, Suying An and Changjie Zhu

ACKNOWLEDGMENTS

My heart is full of gratitude throughout my stay at Cornell University as I always consider myself a lucky person who has met so many great individuals here. They have always been of help to me in one way or another, either academically, professionally or not. In particular, this dissertation would not have been possible without the guidance and the help of those who have contributed and extended their valuable assistance in the preparation and completion of this study.

First and foremost, my utmost gratitude to my dissertation supervisor and chair of my special committee, Professor Subrata Mukherjee, for his consistent support and guidance throughout my stay at Cornell. I consider myself extremely lucky to be a student and supervisee of Professor Subrata Mukherjee, one of the greatest persons I have ever met. It would be impossible for me to successfully complete this work without his help, encouragement, and patience. The numerous discussions with him are vital to the completion of this work. I also deeply appreciate his kindness, support and help for me to develop professionally and as a person. Words really fail to express my gratitude for him. I couldn't imagine having a better advisor.

It is also an honor for me to work with Professor Ashim K. Datta, who has continuously offered support for my work. I thank him for those valuable discussions and his insightful comments and encouragement, and for being part of my Special Committee. I would also like to acknowledge Professor Alan T. Zehnder for his role in my Special Committee, and for his support and help with some experiments related to this work. I also thank him for his encouragement and assistance. I sincerely thank Professor Kenneth E. Torrance and Professor Wilkins Aquino for the discussions

about numerical implementations of this work. In particular, I wish to acknowledge Professor Wilkins Aquino's course on “Nonlinear Finite Element Analysis” and Professor Kenneth E. Torrance's course on “Computational Fluid Dynamics and Heat Transfer” that introduced me to advanced topics in numerical analysis. I acknowledge Professor Pawan S. Takhar at Texas Tech University for the discussions related to the theory development of this work. I also owe thanks to Professor Wolfgang H. Sachse and Professor Yingxing Gao with whom I have worked as a teaching assistant and from whom I have gained a lot of valuable teaching experience. My thanks are also due to my supervisors at Cornell, Linda J. Tompkins, Dr. Kathryn C. Dimiduk, Dr. Rajesh Bhaskaran and Ms. Derina S. Samuel, who have provided assistance and support for me to develop professionally as an educator.

A special thanks to my colleagues in both Professor Subrata Mukherjee’s and Professor Ashim K. Datta’s research groups, Dr. Karthick Chandraseker, Dr. Ranajay Ghosh, Chao Fang, Dr. Vineet Rakesh, and Dr. Ashish Dhall, my colleagues in Theoretical and Applied Mechanics, and my officemates, for their invaluable discussions, assistance and technical support. The discussions on porous materials, transport processes and numerical implementations with them are very helpful for this work. I owe many thanks to a lot of my friends, both at Cornell and in different places all around the world, for their friendship, great company, encouragement and support that helped me in the most difficult times. I also owe many thanks to those who have helped me in the process of finding a job. Their help really means a lot to me. I am in great fear of missing out even just one name and thus refrain to list the names here.

Finally, I would like to thank the most important people in my life, my parents and my husband. I owe many thanks to my parents, Suying An and Changjie Zhu for their

unconditional love and endless support. They have always been supporting me in so many ways and encouraging me in those difficult times. Their spiritual support has made it possible for me to overcome any difficulties during the completion of this work. I owe many thanks to my husband, Min Tang. I so appreciate my loving, supportive, encouraging and patient husband for his faithful support during the final stage of this dissertation. His company, care, love, support and his dedication to the family has made it possible for me to focus on this work. I would also like to thank all my other family members who have shared love, showed care and supported me in many ways.

TABLE OF CONTENTS

LIST OF FIGURES

LIST OF TABLES

LIST OF SYMBOLS

Latin symbols

a_M	Time-moisture shift factor
a_w	Water activity
$\boldsymbol{A}^n$	Forth order material coefficient tensor
A^{α_j}	Helmholtz free energy of the *j*th component in α phase
A^{α}	Helmholtz free energy of the α phase
b^{α_j}	External entropy source for the *j*th component in α phase
b^{α}	External entropy source for the α phase
B	Material coefficient related to the bulk relaxation function
$\boldsymbol{B}$	Material coefficient
B_c	Material constant
$\boldsymbol{B}^{\alpha}$	Forth order viscous dissipation tensor
c_w	Concentration of liquid water
c_g	Concentration of gas
c_p	Specific heat capacity
c_v	Concentration of water vapor
C^{α_j}	Mass fraction of the *j*th component in α phase
C_g	Molar density
$\boldsymbol{C}^s$	Right Cauchy-Green strain tensor of the solid phase
$\overline{\boldsymbol{C}}^s$	Right Cauchy-Green strain tensor associated with $\overline{\boldsymbol{F}}^s$
$\boldsymbol{d}^{\alpha}$	Rate of deformation tensor of the α phase
d_{α}	Material constant related to the initial bulk modulus of α phase
D	Diffusion coefficient
D_g	Effective gas diffusivity
$D_{w,cap}$	Capillary diffusivity
e^{α_j}	Energy density of the *j*th component in α phase
e^{α}	Energy density of the α phase
$\hat{e}^{\beta}_{\alpha_j}$	Rate of mass transfer from phase β to the *j*th component in α phase
$\hat{e}^{\beta}_{\alpha}$	Rate of mass transfer from β phase to the α phase

$\boldsymbol{E}^s$	Lagrangian strain tensor of the solid phase
$\overline{E}(s)$	Laplace transform of the Young's modulus
$\boldsymbol{F}^s$	Deformation gradient of the solid phase
$\overline{\boldsymbol{F}}^s$	The multiplicative decomposition of the deformation gradient
$\boldsymbol{g}^{\alpha_j}$	Gravitational force on the *j*th component in α phase
$\boldsymbol{g}^{\alpha}$	Gravitational force on the α phase
$g(t)$	Normalized relaxation function
$\boldsymbol{G}(t)$	Relaxation function in shear
h	Heat transfer coefficient
h_m	Mass transfer coefficient
h^{α_j}	External supply of energy to the *j*th component in α phase
h^{α}	External supply of energy to α phase
$\boldsymbol{H}^{\alpha}$	Third order material coefficient tensor
$\hat{\boldsymbol{i}}^{\alpha_j}$	Rate of momentum gain to the *j*th component in α phase due to interaction with other species in the same phase
$\boldsymbol{I}$	Identity tensor
$\dot{I}$	Volumetric evaporation rate
I_k	Principal invariants of the right Cauchy Green tensor $\boldsymbol{C}^s$
$\bar{I}_k$	Principal invariants of $\overline{\boldsymbol{C}}^s$
J^s	Determinant of the deformation gradient
k^l	Permeability of the liquid phase
k^i	Intrinsic permeability
k^r	Relative permeability
k_{evap}	Non-equilibrium evaporation constant
k_w	Permeability of liquid water
K	Relaxation modulus
K_{α}	Thermal conductivity
K_i	Coefficients of the Prony series
$\overline{K}(s)$	Laplace transform of the bulk modulus
K^{α}	Initial bulk modulus of α phase
$\boldsymbol{K}^{\alpha}$	Second rank coefficient from linearization
L	Laplace transform operator
L_0	Total length of the domain
M	Moisture content on a dry basis
M_a	Molecular weight of air
M_v	Molecular weight of vapor
M_0	Reference moisture content on a dry basis

M^{α}	Material coefficient
$\overline{M}$	Initial moisture content
$\boldsymbol{n}$	The unit normal vector
$\boldsymbol{n}_w$	Flux of liquid water
n_k	Number of terms in the Prony series
P	Total pressure
p^{α}	Physical pressure in the α phase
p^c	Capillary pressure
$p_{v,eq}$	Equilibrium vapor pressure
$\boldsymbol{q}^{\alpha_j}$	Heat flux vector for the *j*th component in α phase
$\boldsymbol{q}^{\alpha}$	Heat flux vector for α phase
$\hat{Q}^{\alpha_j}$	Rate of energy gain to the *j*th component in α phase due to interaction with other species in the same phase
$\hat{Q}^{\beta}_{\alpha_j}$	Rate of energy transfer from phase β to the *j*th component in α phase
$\hat{Q}^{\beta}_{\alpha}$	Rate of energy transfer from phase β to α phase
$\boldsymbol{Q}_i$	Internal variables
r_i	Radius of the pores in the *i*th class
$\hat{r}^{\alpha_j}$	Rate of mass gain to the *j*th component in α phase due to interaction with other species in the same phase
R	The gas constant
$\boldsymbol{R}^a$	Resistivity tensor
$\boldsymbol{R}^l$	Resistivity tensor
s	The complex parameter in Laplace transform
S^a	Degree of air saturation
S^g	Degree of gas saturation
S^l	Degree of water saturation
$\boldsymbol{S}$	Material coefficient related to the shear relaxation function
$\boldsymbol{S}'$	The effective 2nd Piola-Kirchhoff stress
$\boldsymbol{S}^s$	Second Piola-Kirchhoff stress tensor
t	Time
$\boldsymbol{t}$	The total stress
$\boldsymbol{t}^{\alpha_j}$	Stress tensor of the *j*th component in α phase
$\boldsymbol{t}^{\alpha}$	Stress tensor of the α phase
$\boldsymbol{t}^{se}$	Terzaghi stress for the solid phase
$\boldsymbol{t}^{sh}$	Hydration stress for the solid phase
$\boldsymbol{t}'$	The effective Cauchy stress
T	Temperature
$\hat{\boldsymbol{T}}^{\beta}_{\alpha_j}$	Rate of momentum transfer to the *j*th component in α phase from β phase

$\hat{\boldsymbol{T}}_{\alpha}^{\beta}$	Rate of momentum transfer to α phase from β phase
$\boldsymbol{u}^{s}$	Displacement of the solid phase
U	Volumetric part of the energy function
$\boldsymbol{v}^{\alpha_j}$	Velocity of the *j*th component in α phase
$\boldsymbol{v}^{\alpha}$	Velocity of the α phase
v_l	Molar volume of the liquid
V^{l}	Volume of the liquid phase
V^{P}	Volume of the pores
W	Energy function
$\overline{W}$	Deviatoric part of the energy function
$\boldsymbol{x}$	Position vector in the deformed configuration
x_v	Mole fraction of vapor
$\boldsymbol{X}$	Position vector in the undeformed configuration
Z	Position coordinate in the undeformed cylindrical coordinate system

Greek symbols

δ	Dirac's delta function
β	Constant for the initial condition
$\Delta\beta_i$	Volume fraction of pores having radius r_i
ε^{α}	Volume fraction of the α phase
κ	Initial bulk modulus
η^{α_j}	Entropy of the *j*th component in α phase
η^{α}	Entropy of the α phase
$\hat{\eta}^{\alpha_j}$	Entropy gain by the *j*th component in α phase due to interaction with other species in the same phase
λ^{α}	Lagrange multiplier for the continuity equation of α phase
Λ^{α_j}	Entropy production per unit mass density for the *j*th component in α phase
Λ^{α}	Entropy production per unit mass density for α phase
μ	Viscosity of the liquid phase
μ^{α_j}	Chemical potential of the *j*th component in α phase
μ^{α}	Chemical potential of α phase
μ_{α}	Initial shear modulus of α phase
$\overline{\nu}$	Laplace transform of the Poisson's ratio

ξ	Coordinate of the parent element
ξ_M	"Shifted time"
π^l	Swelling pressure due to interaction of the solid phase and the bulk fluid
ρ^{α_j}	Density of the *j*th component in the α phase
ρ^{α}	Density of the α phase
σ	The Cauchy stress
τ	Tortuosity
τ_i	The relaxation times in the Prony series
ϕ	The porosity
$\boldsymbol{\phi}^{\alpha_j}$	Entropy flux vector for the *j*th component in α phase
$\boldsymbol{\phi}^{\alpha}$	Entropy flux vector for α phase
Φ	Position coordinate in undeformed cylindrical coordinate system
$\hat{\Phi}^{\beta}_{\alpha_j}$	Entropy transfer to the *j*th component in α phase from β phase
$\hat{\Phi}^{\beta}_{\alpha}$	Entropy transfer to α phase from β phase
ω	Weighting function
ω_a	Mass fraction of air with respect to total gas porosity
ω_v	Mass fraction of water vapor with respect to total gas porosity

Superscripts, subscripts, and other notations

a	Air phase
A	Particle composed of solid phase and the vicinal fluid
wA	Vicinal water in the particle
sA	Solid phase in the particle
f	Fluid composed of vicinal water and the bulk phase fluid
g	Gas phase
j	*j*th component of species
l	Liquid phase
s	Solid phase
w	Liquid water
v	Water vapor
vs	The viscoelastic part
$(\cdot)_0$	Initial value of $(\cdot)$
α	α phase

$\hat{(\cdot)}_{\alpha}^{\beta}$	Exchange from β phase to α phase
$(\cdot)^{\alpha,s}$	Difference of two quantities $((\cdot)^{\alpha} - (\cdot)^{s})$
$\frac{D^{\alpha_j}}{Dt}$	Material time derivative of a variable with respect to velocity of *j*th component in the α phase

CHAPTER 1

INTRODUCTION

Porous materials appear in a wide variety of applications – biomedical engineering, construction, agriculture, industrial drying of wood, ceramics and foodstuffs, drug delivery, food processing, to name a few. The focus of the thesis is on multiphase transport in unsaturated swelling porous materials which exhibit viscoelastic deformation and can experience large deformations upon wetting/drying.

1.1 Porous Materials and Multiple Phases

A porous material under consideration in this thesis consists of a porous solid with fluid or gas filled pores. The solid skeleton and the fluid or gas that exists in the pores are considered as phases in the system. The solid skeleton and the fluid(s) that exist in the pores usually have different motions. There are also interactions between the constituents. These as well as the fact that the geometry of a porous material is usually very complicated, make the modeling of mass, heat and momentum transport in swelling porous materials rather difficult. A porous system is a heterogeneous system. To treat the porous system as a system in which the properties are continuous functions of the space coordinates, a substitute model is generally used at the macroscopic scale, where the interacting constituents are assumed to fill the entire control volume. Using homogenization/averaging procedures, the distribution of

constituents in control space is obtained and then the substitute continua can be treated with the methods of continuum mechanics. This can be done by introducing the concept of representative elementary volume (REV) as is suggested by many authors (Hassanizadeh and Gray 1979a, b, 1980, 1990; Bear 1972; Bachmat and Bear 1986; Bear and Bachmat 1986; Kaviany 1991) [49-52,15,11,16,59]. Figure 1.1 illustrates a REV of a porous material consisting of three phases: solid, liquid, and gas.

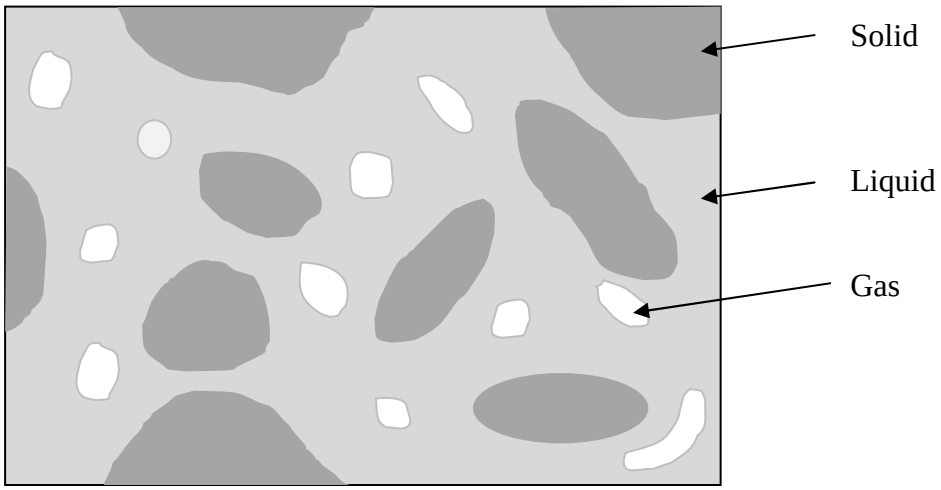

Figure 1.1: Representative elementary volume (REV) of a porous medium with three phases: solid, liquid, and gas.

1.2 Swelling Porous Materials that Exhibit Viscoelastic Relaxation

Swelling porous materials are those that swell or shrink upon liquid absorption or desorption. Examples of such materials include clays, foodstuffs, hydrogels, biomaterials and cell membranes. Studying of transport through swelling porous materials is more complicated than that for a rigid porous body. As the porous material swells, elastically or non-elastically, porosities (defined as the ratio of volume of pores and the total volume) vary and the transport of mass, momentum and heat through the material are modified. In another situation, the deformation of the porous material itself caused by moisture transport becomes important, for example, the design and fracture/failure of structures containing swelling colloids as foundations for buildings, bridges, highways, and runways. Mass, momentum, and heat transport through swelling porous materials are closely coupled with the deformation of the porous matrices and it is imperative that the mathematical models that describe the flow through or the deformations of swelling porous materials contain appropriate governing equations as well as constitutive relations that account for the swelling nature of these systems.

Swelling porous materials, such as biological tissues, food materials and polymer foams, exhibit viscoelastic behavior. The fluid transport mechanism is dependent on the relaxation of the porous materials. For example, when the transport is non-Fickian,

which is indicative of coupling of diffusional and relaxational mechanisms, Fick's law is not appropriate even if the diffusion coefficient is considered a function of fluid concentration. In this case, including viscoelastic relaxation in modelling of fluid and heat transport in swelling porous materials is important.

1.3 Fundamental Physics-based Modeling of Transport in Swelling Porous Materials

Two categories of approaches have been used in the literature to non-empirically model mass, momentum and energy transport in swelling porous materials based on fundamental physics.

In the first approach, porous materials are treated as a mixture of solid and fluid(s) and all constituents are equally important for the behavior of the mixture. Continuum approaches such as averaging; mixture theory and hybrid mixture theory are used to model such a system, which usually involve a rigorous general thermodynamic derivation to obtain the constitutive relations that accurately describe systems under consideration. In the following sections, an overview of this approach is given. Examples of modeling of transport in swelling porous materials based on this approach are Singh et al. (2003a), Weinstein et al. (2008a) and Bennethum (2007) [107,127,18].

Another approach involves development of multiphase porous media models by combining conservation laws with the fundamental transport mechanisms (for detailed discussions, please refer to the mechanistic models discussed in Datta (2007) [36]). Examples following such an approach to model transport in swelling porous materials can be found in Rakesh (2010) [95] and Dhall (2011) [39].

This dissertation focuses on the first approach and an example of modeling using the second is also presented.

1.4 Hierarchical Scales of Porous Materials

Porous materials exhibit a hierarchy of scales. This is illustrated in Figure 1.2. At the micro-scale, the porous system is composed of a solid matrix and the vicinal fluid. These two exists as separated phases. At the meso-scale, the solid matrix and the vicinal fluid is represented as a homogeneous mixture (particles) and this homogeneous mixture exist with bulk fluid(s) as separated phases. At the macro-scale, the particles (a homogeneous mixture of the solid matrix and the vicinal fluid) and the bulk fluid(s) exist as homogeneous mixtures – all the phases as well as the constituents in each phase are considered as overlaying continua defined all over space. In order to understand the phenomena that we observe at the macro-scale, for example, swelling of the porous matrix, the interactions between phases need to be understood from smaller scales: micro or meso-scales.

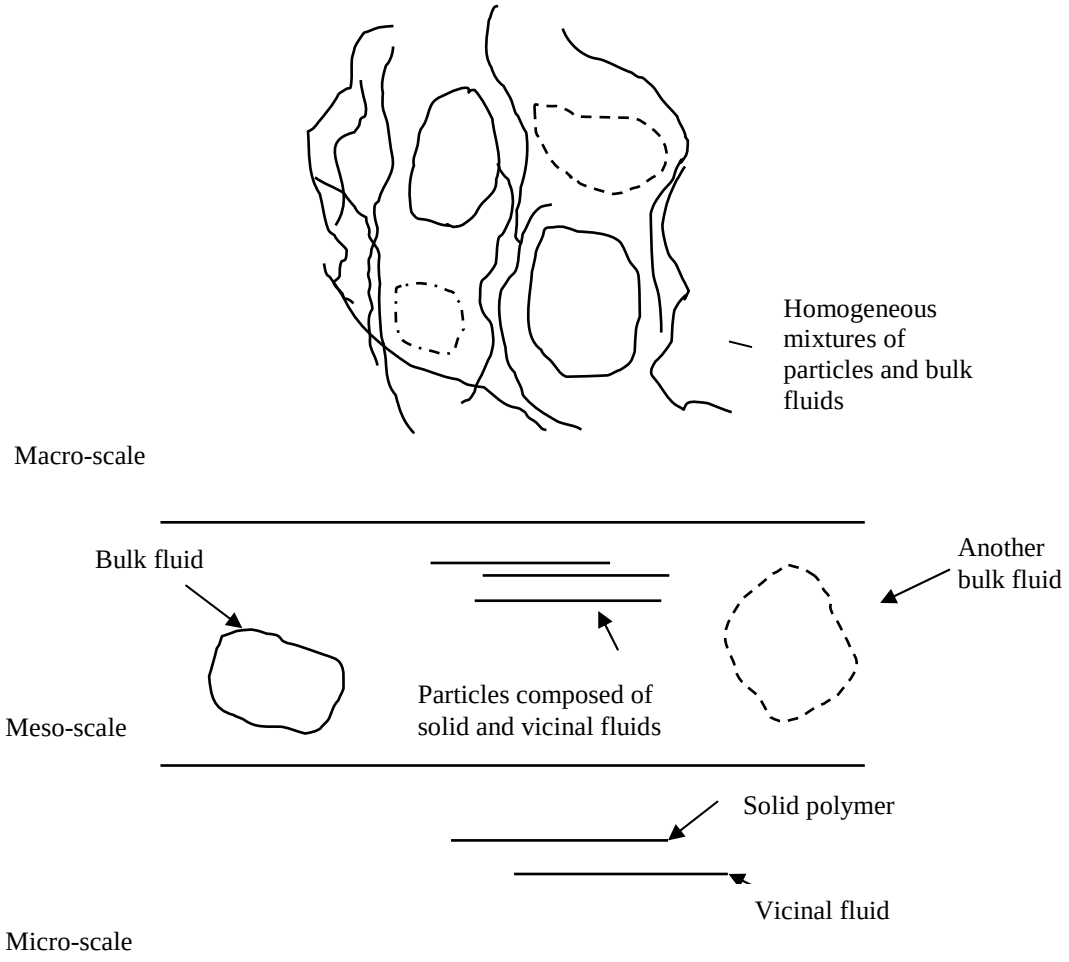

Figure 1.2: Hierarchical scales of porous materials.

1.5 Hybrid Mixture Theory

Approaches used to develop macroscopic theories can be broadly classified into three categories -- averaging or macroscopization theories, theory of mixtures, and hybrid theories of the first two. In macroscopization theories, conservation laws as well as empirical constitutive relations are introduced at the micro-scale, and then averaging is

done to obtain relationships at the meso-scale and then at the macro-scale. Using this approach, assumptions are made about the microscopic behavior of phases and interfaces. However, since the entropy inequality is not used by the macroscorpization theories, relationships among macroscopic thermodynamic variables cannot be obtained (Hassanizadeh and Gray 1990)[52]. In the theory of mixtures, conservation laws are stated at the macro-scale with additional terms in analogy with the conservation laws of single phase systems and then the constitutive relationships are directly postulated or the entropy inequality (from second law of thermodynamics) is exploited to obtain constitutive relations at the macro-scale. Even though the assumptions used in this method are usually minimum, it may overlook the essential features of multiphase systems as little information of the micro-scale is used (Hassanizadeh and Gray 1990)[52]. The third category contains various theories which are hybrids of the first two. As the name suggests, Hybrid Mixture Theory (HMT) introduced by Hassanizadeh and Gray (1979a, b)[49-50], is one of the approaches from the third category, which has been extensively used to study swelling porous systems and explore the interactions between phases at the macro-scale from smaller scales. In this approach, conservation laws are written at the micro-scale before introducing the constitutive relations, and then an averaging procedure is performed to obtain conservation equations at higher scales. The entropy inequality is then applied at the macro-scale to derive constitutive relations such as Fick's law of gas diffusion and Darcy's law of water flow. The advantages of HMT over all the other approaches are explained in detail by Achanta (1995)[2].

In this work, to investigate the coupled viscoelastic large deformation of porous materials which occurs simultaneously with mass, momentum and heat transport in porous materials, we choose to use Hybrid Mixture Theory and establish a thermomechanical theory to describe the two-way coupling of transport and viscoelastic large deformation of swelling porous systems.

1.6 Organization of the Dissertation

The dissertation is organized into six chapters. Overviews of the different chapters are given below.

Chapter 1: Introduction This chapter provides an introduction to swelling porous materials, the approach, and an overview of the dissertation.

Chapter 2: Thermomechanical Theory for Flow and Deformation in Unsaturated Swelling Porous Media In this chapter, a thermomechanical theory for flow and deformation in unsaturated swelling porous systems is developed. The development is based on the Hybrid Mixture Theory. A three-phase swelling porous system that is of viscoelastic nature upon wetting is considered. All the conservation laws for each phase are given at the micro-scale and upscaled to the macro-scale. This work focuses on the nature of the porous system and postulates independent variables that fully describe the system under consideration. Then the second law of thermodynamics is

exploited to investigate the restrictions of constitutive relationships that relate the dependent variables and the independent variables. Results include, for example, a modified Darcy's law that can account for both Fickian and non-Fickian diffusion.

Chapter 3: A Model for Flow and Deformation in Unsaturated Swelling Porous Systems under Isothermal Conditions In this chapter, a two-way coupled model that can fully capture simultaneous fluid transport and viscoelastic large deformation of unsaturated swelling porous systems is developed based on the thermomechanical theory established in chapter 2 under isothermal conditions. The model consists of a differential-integral equation that governs the flow of fluid through the swelling porous material, as a result of combining the mass conservation equation and the modified Darcy's law; the linear momentum balance that governs the motion of the solid matrix, as well as constitutive equations that describe the nonlinear viscoelastic relaxation of the material. The effect of viscoelastic relaxation as well as the deforming domain on the fluid transport is included in this model and the effect of fluid transport on the deformation is included as the driving force.

Chapter 4: Numerical Implementation: A Finite Element Analysis of Coupling between Water Absorption and Swelling of Foodstuffs during Soaking In this chapter, the model developed in chapter 3 is numerically implemented to study soaking of pasta. A finite element based code is developed to solve the coupled nonlinear system of PDEs. The model is found to successfully predict the moisture profiles of soaking of pasta as numerical results agree well with experimental results

obtained from literature. Effect of viscoelastic relaxation on fluid transport is also investigated.

Chapter 5: Drying of Foodstuffs In this chapter, another approach to study the two-way coupling of mass, momentum, energy transport in porous materials and viscoelastic large deformation of the porous matrix is presented. Three phases are considered in the system: solid, water and gas. Gas phase consists of air and water vapor. Modes of transport of water are bulk flow, capillary flow and phase change while modes of transport for water vapor are bulk flow, binary diffusion and phase change. Viscoelastic large deformation of the solid matrix is considered and ALE formulations are used.

Chapter 6: Conclusions and Future Work This chapter provides conclusions of the dissertation and suggests possible future direction of research.

CHAPTER 2

THERMOMECHANICAL THEORY FOR FLOW AND DEFORMATION IN UNSATURATED SWELLING POROUS MEDIA

2.1 Introduction and Objectives

We consider a swelling porous material, which consists of three phases: the solid phase *s*, the liquid phase *l*, and the air phase, *a*. Such a swelling porous material is considered unsaturated, i.e., the pores are only partially filled with fluids. In many practical applications, swelling porous materials can be unsaturated, for example, drying of wood and food materials (Datta 2007; Perre and Turner 1999) [36,88], and transport in soils (Carminati et al. 2008; Purandara et al. 2008) [28,92]. As is mentioned before, the swelling behavior of a porous medium results from interactions at different spatial scales, and therefore, researchers have developed multiscale thermomechanical models to study heat and mass transport in multiphase swelling porous materials (Achanta 1995; Bennethum and Cushman 1996b; Murad et al 1995; Murad and Cushman 1996, 1997, 2000; Bennethum et al 2000; Schrefler 2000; Singh et al. 2003a, b; Weinstein et al. 2008a) [2,20,78-81,23,103,107-108,127]. Among other approaches, Hybrid Mixture Theory (HMT) is advantageous as the approach to develop a macroscopic theory for multiphase swelling porous materials.

2.1.1 Viscoelastic deformation of the solid

As is mentioned before, several swelling porous materials, such as biological tissues, food materials and polymer foams, exhibit viscoelastic behavior. This viscoelastic behavior can result either from interaction between the elastic solid skeleton and the viscous fluid(s) present in the pores, or from viscoelasticity of the solid skeleton itself. For example, in the multiscale fluid transport model developed by Achanta and Cushman (1994)[3], Achanta et al. (1994)[3] and Achanta (1995)[2], the solid phase is assumed to be elastic at the micro-scale, and the interaction between the elastic solid and the viscous fluid results in only short memory at the macro-scale. This short memory may not be adequate to fully capture the viscoelastic effects in all situations. Therefore, in Singh's work (Singh et al. 2003a, b; Singh 2002)[107,108,106], the viscoelastic effects are captured by including higher order material time derivatives of the macroscopic Green strain tensor of the solid phase, $\overset{(n)s}{\boldsymbol{E}}$, in order to obtain a generalized Kelvin-Voigt model.

Many of the detailed transport studies on swelling porous media have been on saturated systems, where the deformation of the solid is given by change in fluid volume fraction only, and the solid deformation equation is not required. Few researchers discuss the deformation of the solid phase or the coupling between the liquid transport and the solid deformation. Singh et al. (2003a, b)[107, 108] considered an unsaturated system; however, the second fluid phase is assumed to be immobile.

The immobility of one fluid phase makes the system essentially saturated; and under these conditions, the ratio of volume fraction of the immobile phase to the volume fraction of the solid skeleton remains constant. Many simplifications can be made based on this constant ratio. If we assume that the second bulk phase is able to move freely, this constant ratio relationship does not hold anymore. In such a case, the fluid transport equation needs to be solved simultaneously with the solid phase equations.

Murad and Cushman (1996)[79] considered deformation for an elastic solid and assumed linearity, which only allows for small strain. Schrefler (2002)[103] proposed a constitutive model for the solid deformation, however, elastoplasticity has been assumed. Bennethum (2007)[18] discussed deformation and derived a generalized Terzaghi stress principle for swelling porous materials considering a saturated swelling porous system. However, a detailed study on the deformation of the non-linear viscoelastic solid in unsaturated swelling systems is not available in the literature.

2.1.2 Three-scale swelling systems

While developing HMT for a swelling system, interactions at two or three spatial scales are usually considered; depending on the requirements and complexity of the modeling system. While applying the Hybrid Mixture Theory (HMT) to a particular system, many studies consider phenomena at three spatial scales: micro-, meso- and

macro-scale. At the micro-scale, the vicinal fluid and the solid matrix exist as separate phases. At the meso-scale, the solid matrix and the vicinal fluid are considered together a homogenous mixture representing a particle; and the liquid(s) and/or gaseous bulk fluid(s) are separated from this particle. At the macro-scale, the particle and the bulk fluid(s) form overlaying continua. Although a three-scale theory seems to be a more general approach of developing a model for swelling systems, complexities arise in the treatment of vicinal and bulk phases of a fluid; and while coupling the transport equation with the deformation of the solid in an unsaturated case.

In the three-scale model developed by Singh et al. (2002, 2003a, b) [106-108], the vicinal phase and the bulk phase conservation equations of a mobile fluid were added to obtain a combined transport equation for the fluid. This addition of equations is necessary as only overall transport properties of the fluid can be obtained through experiments. Separate information about the vicinal phase and the bulk phase is not available. The major assumptions made to obtain a single transport equation for the mobile fluid are that the micro and macropores drain at the same rate, i.e., the permeabilities of the micro and the macro-pores are equal, and the volume fraction of the vicinal phase of the fluid is always proportional to the volume fraction of the bulk fluid. However, both the assumptions are difficult to justify. For example, in plants the permeability of cell wall (micropores) is of the order of $10^{-21}\,\mathrm{m}^2$, while the permeability of extracellular space (macropores) is $10^{-17}\,\mathrm{m}^2$. Similarly, in the wood drying literature, it is well established that until the moisture content reaches the Fiber Saturation Point (FSP), all the moisture is in a vicinal state. Another problem with the

three-scale model is that the separation of the volume fractions of the solid phase and the vicinal fluid cannot be achieved as the volume fraction of the particle (composed of the solid phase and the vicinal water) is chosen as an independent variable. The upscaling technique is slightly modified in Cushman et al. (2004) [34] and, in the conservation equations, whenever the volume fraction and the density of the vicinal fluid appear as a product, the volume fraction of vicinal water is separated. However, in all other cases, it remains difficult to separate them without making further assumptions, which are not always justifiable (Refer to Appendix B for details).

To summarize, although the three scale theory is more general, it also has more parameters, and thus, its implementation requires much more information about the system than what is available from experiments. Current applications of the three scale theory make assumptions to simply the system, some of which are not justified under all conditions. (See Appendix B)

2.1.3 Objectives

The objective here is to develop a two-scale thermomechanical theory for an unsaturated swellable porous system, which includes a solid porous skeleton, a liquid and an air phase. The solid skeleton is considered as viscoelastic of generalized Kelvin-Voigt type, while both the liquid and air phases are considered as viscous.

Large deformation of the solid is considered and discussed in detail in this dissertation.

In this chapter, modified constitutive equations, Darcy's law for the liquid and Cauchy stress-strain relationship for the solid are derived.

2.2 Theory Development: Constitutive Relations

The methodology followed to arrive at the constitutive relations is outlined in Figure 2.1. Mass, momentum, energy and entropy conservation equations are written for all the phases at the micro-scale and then, upscaled to the macro-scale. Then, we select a set of macroscopic independent variables which are assumed to fully capture the behavior of the system. Helmholtz free energy of each of the phases is assumed to be dependent on a subset of the independent variables. Using these dependencies, the total entropy for the system is then obtained by adding the entropies of all the constituents. Restrictions on the constitutive relationships are then obtained by exploiting the entropy inequality in the sense of Coleman and Noll (1963) [31].

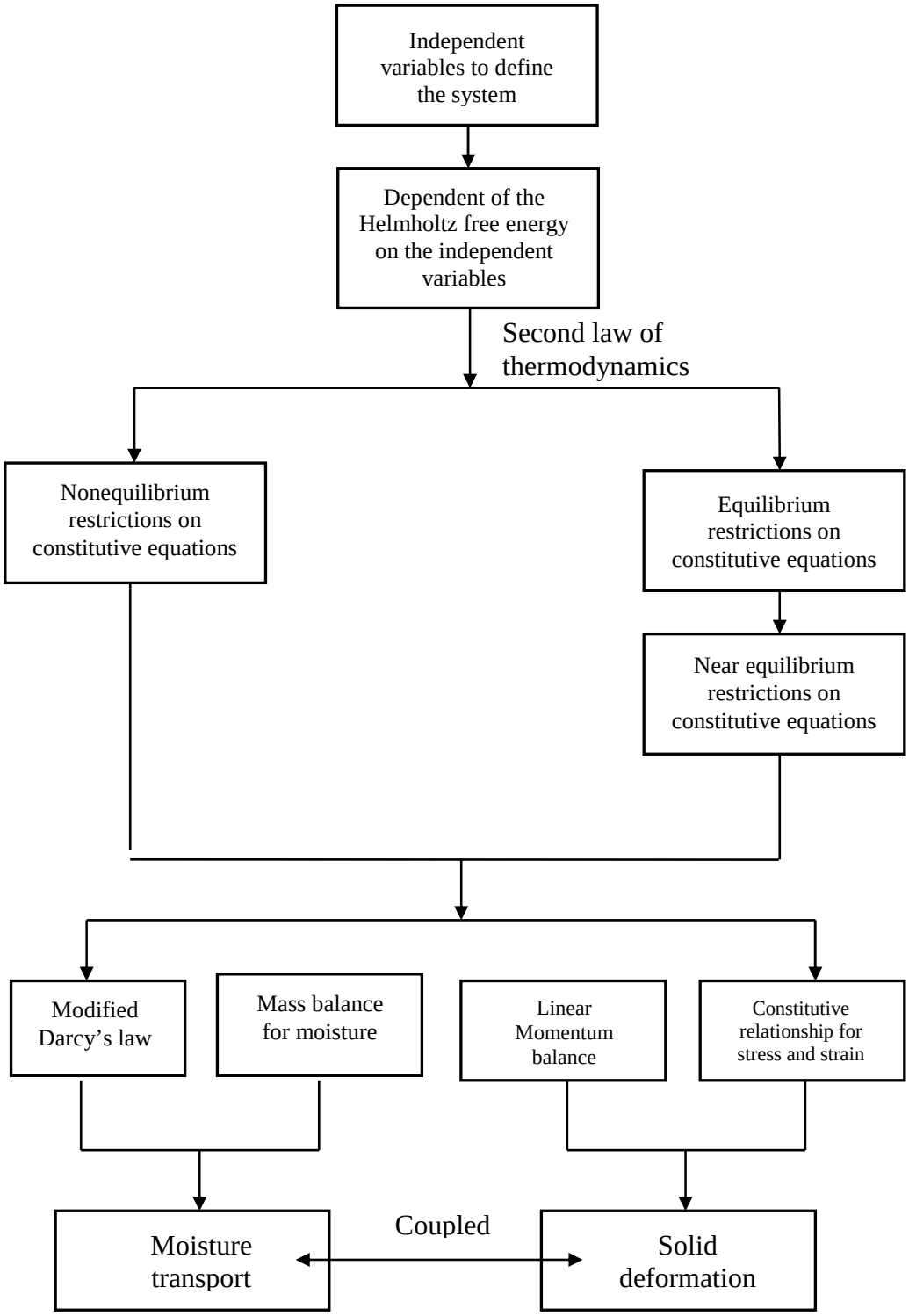

Figure 2.1: Methodology followed to derive the coupled model for an unsaturated swelling porous material.

Some of these restrictions hold only at equilibrium and are thus called equilibrium restrictions; while some others are true regardless of the state of the system and are called non-equilibrium restrictions. New forms of Darcy's law and Cauchy stress-strain relationship are then obtained when a near equilibrium state is considered.

Macroscopic conservation laws for all the three phases: solid, liquid and air, are listed in Appendix A. These conservation laws are obtained from Bennethum and Cushman (1996a) [19]. In this section, we use the Coleman and Noll (1963) [31] procedure to impose restrictions on the constitutive relations.

2.2.1 Development of expressions for free energies and entropy

We consider three phases in the system: the solid phase denoted by *s*, fluid *l*, and air *a* (Figure 2.2). The solid is considered as viscoelastic and both fluids are taken as viscous in nature. We make the following assumptions:

1. Both the solid and the liquid phases are incompressible.

2. All constituents are chemically non-reacting and dissolution of air in the fluid is assumed to be negligible.

3. Local thermodynamic equilibrium exists so that only one temperature and one energy equation is needed.

4. The system is thermodynamically simple following Eringen (1994) [42], which means that the entropy flux is due to heat flux alone and the external supplies (sources) are due to heat alone.

5. There are no interfacial effects.

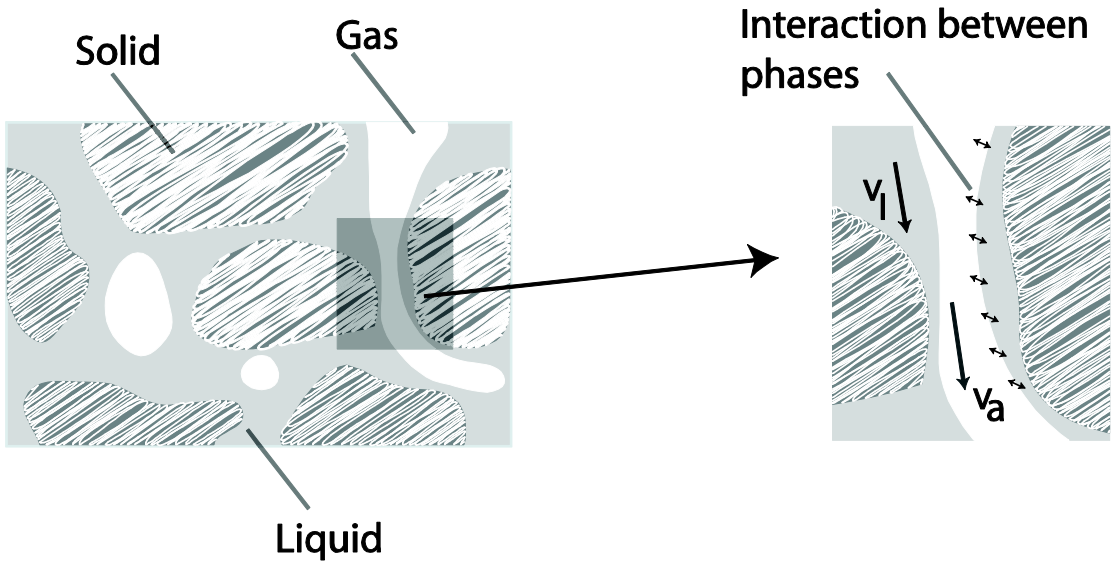

Figure 2.2: Schematic of the porous medium showing the three phases and interactions between the phases.

The starting point of constitutive modeling is the selection of a set of independent variables to describe the system. The choice is based on the nature of the system as well as experience. We choose the following independent variables to define the system:

$$\varepsilon^l, \nabla\varepsilon^l, \overset{(m)}{\varepsilon^l}, \nabla\overset{(m)}{\varepsilon^l}, \varepsilon^s, \nabla\varepsilon^s, J^s, \overline{\boldsymbol{C}}^s, \overset{(n)}{\overline{\boldsymbol{C}}^s}, C^{s_j}, T, \nabla T \tag{2.1}$$

$$\rho^l, \boldsymbol{d}^l, C^{l_j}, \boldsymbol{v}^{\alpha,s}, \boldsymbol{v}^{\alpha_j,s}, \nabla\boldsymbol{v}^{\alpha_j,s}, \rho^a, \boldsymbol{d}^a, C^{a_j}$$

where $m = 1, \ldots, p$ and $n = 1, \ldots, q$ denote the material time derivatives of order *m* and *n*. The complete list of variables along with descriptions is available in the nomenclature.

Here, only ε^l and ε^s, volume fractions of liquid and solid, respectively, are chosen because ε^a, volume fraction of air, is related through

$$\varepsilon^l + \varepsilon^s + \varepsilon^a = 1 \tag{2.2}$$

As is discussed by Weinstein and Bennethum (2006) [126], the Green strain tensor $\boldsymbol{E}^s$, the density ρ^s and the solid phase volume fraction ε^s are related due to mass conservation of the solid phase. So, instead of choosing $\boldsymbol{E}^s$, ρ^s and ε^s as independent variables, we follow Weinstein and Bennethum (2006) [126] and consider the multiplicative decomposition of the deformation gradient $\boldsymbol{F}^s$:

$$\overline{\boldsymbol{F}}^s = J^{s\,-\frac{1}{3}} \boldsymbol{F}^s \tag{2.3}$$

Then we consider a new strain measure given by:

$$\overline{\boldsymbol{C}}^s = (\overline{\boldsymbol{F}}^s)^T \overline{\boldsymbol{F}}^s \tag{2.4}$$

This multiplicative decomposition of the deformation gradient was originally proposed by Flory (1961) [45] and successful applications include Simo et al. (1997) [105] in the context of finite strain viscoelasticity. We use J^s and $\overline{\boldsymbol{C}}^s$ to replace $\boldsymbol{E}^s$ and ρ^s. More discussion on the advantage of this replacement can be found in Weinstein and Bennethum (2008a) [127]. The higher order derivatives of $\overline{\boldsymbol{C}}^s$ and ε^l are also included to ensure that the solid phase is modeled as a Kelvin-Voigt solid. The viscous nature of the two fluids are represented by the rate of deformation tensors, $\boldsymbol{d}^l$ and $\boldsymbol{d}^a$

respectively, which are all macroscopic variables. We choose temperature instead of entropy as an independent variable because entropy could hardly be measured while we could easily measure temperature. And we could perform a Legendre transformation to convert the internal energy into the Helmhotlz free energy (Atkins and de Paula, 2002)[9].

Note that we are taking the solid phase as the reference phase and in what follows the time derivatives follow the velocity of the solid phase:

$$\dot{(\bullet)} = \frac{D^s(\bullet)}{Dt} = \frac{\partial(\bullet)}{\partial t} + \boldsymbol{v}^s \bullet \nabla(\bullet) \tag{2.5}$$

$$\overset{(m)}{(\bullet)} = \frac{D^{sm}(\bullet)}{Dt^m} \tag{2.6}$$

Once the system is described by a set of independent variables, the Helmholtz free energies could be defined as a function of these variables. We postulate the forms of the Helmholtz free energies as being dependent on a subset of the independent variables:

$$A^s = A^s(\boldsymbol{\varepsilon}^s, \overline{\boldsymbol{C}}^s, \overset{(n)}{\overline{\boldsymbol{C}}}^s, \boldsymbol{\varepsilon}^l, \overset{(m)}{\boldsymbol{\varepsilon}}^l, C^{s_j}, T) \tag{2.7}$$

$$A^l = A^l(\boldsymbol{\varepsilon}^s, \overline{\boldsymbol{C}}^s, \overset{(n)}{\overline{\boldsymbol{C}}}^s, \boldsymbol{\varepsilon}^l, \overset{(m)}{\boldsymbol{\varepsilon}}^l, \rho^l, C^{l_j}, T) \tag{2.8}$$

$$A^a = A^a(\boldsymbol{\varepsilon}^s, \boldsymbol{\varepsilon}^l, \rho^a, C^{a_j}, T) \tag{2.9}$$

Here, the liquid and the solid Helmholtz energies are functions of the state of the system (volume fractions, densities, mass fractions of constituents, deformation and temperature) as well as some of their histories (viscoelastic effects). The interactions

between the solid and the liquid are accounted for by the dependence of the solid and liquid Helmholtz energies on cross terms, ε^l, $\overset{(m)l}{\boldsymbol{\varepsilon}}$ and $\overline{\boldsymbol{C}}^s$, $\overset{(n)s}{\overline{\boldsymbol{C}}}$, respectively. Helmholtz energy of air does not have any viscoelastic effects (Table 2.1).

Table 2.1 Dependence of the Helmholz free energies on the independent variables

Helmholtz free energy	Volume fraction	Density	Mass concentration	Deformation	Temperature	Viscoelastic effects
Liquid, A^l	ε^l, ε^s	ρ^l	$C^{l}{}_{j}$	$\overline{\boldsymbol{C}}^s$	T	$\overset{(n)s}{\overline{\boldsymbol{C}}}$, $\overset{(m)l}{\boldsymbol{\varepsilon}}$
Solid, A^s	ε^l, ε^s	None	$C^{s}{}_{j}$	J^s, $\overline{\boldsymbol{C}}^s$	T	$\overset{(n)s}{\overline{\boldsymbol{C}}}$, $\overset{(m)l}{\boldsymbol{\varepsilon}}$
Gas, A^a	ε^l, ε^s	ρ^a	$C^{a}{}_{j}$	None	T	None

Total derivatives of the free energies are involved in the entropy inequality. Therefore, to explore the entropy inequality, we need to calculate the total derivatives of the free energies using the chain rule. We use the following identities to obtain the material derivatives of the free energies:

$$\frac{D^{\alpha}(\bullet)}{Dt} = \frac{D^{s}(\bullet)}{Dt} + \boldsymbol{v}^{\alpha,s} \bullet \nabla(\bullet) \tag{2.10}$$

where

$$\boldsymbol{v}^{\alpha,s} = \boldsymbol{v}^{\alpha} - \boldsymbol{v}^{s} \tag{2.11}$$

denotes the relative velocity of the α phase with respect to the solid phase.

Since C^{α_N} is a dependent variable as listed in Appendix A, this gives rise to the relative chemical potential:

$$\tilde{\mu}^{\alpha,j} \equiv \mu^{\alpha_j} - \mu^{\alpha_N} \tag{2.12}$$

where

$$\mu^{\alpha_j} \equiv \frac{\partial A^{\alpha}}{\partial C^{\alpha_j}} \tag{2.13}$$

Then the material time derivatives of the free energies are given as:

$$\begin{aligned}\frac{D^s A^s}{Dt} &= \frac{\partial A^s}{\partial \varepsilon^l}\dot{\varepsilon}^l + \frac{\partial A^s}{\partial \varepsilon^s}\dot{\varepsilon}^s + \frac{\partial A^s}{\partial T}\dot{T} + \sum_{j=1}^{N}\tilde{\mu}^{s_j}\dot{C}^{s_j} + \sum_{m=1}^{p}\frac{\partial A^s}{\partial \overset{(m)}{\varepsilon^l}}\overset{(m+1)}{\varepsilon^l} \\ &= \frac{\partial A^s}{\partial \overline{\boldsymbol{C}}^s}:\dot{\overline{\boldsymbol{C}}}^s + \sum_{n=1}^{q}\frac{\partial A^s}{\partial \overset{(n)}{\overline{\boldsymbol{C}}^s}}:\overset{(n+1)}{\overline{\boldsymbol{C}}^s}\end{aligned} \tag{2.14}$$

$$\begin{aligned}\frac{D^l A^l}{Dt} &= \frac{\partial A^l}{\partial \varepsilon^l}\dot{\varepsilon}^l + \frac{\partial A^l}{\partial \varepsilon^s}\dot{\varepsilon}^s + \frac{\partial A^l}{\partial T}\dot{T} + \sum_{j=1}^{N}\tilde{\mu}^{l_j}\dot{C}^{l_j} + \sum_{m=1}^{p}\frac{\partial A^l}{\partial \overset{(m)}{\varepsilon^l}}\overset{(m+1)}{\varepsilon^l} \\ &+ \frac{\partial A^l}{\partial \rho^l}\dot{\rho}^l + \frac{\partial A^l}{\partial \overline{\boldsymbol{C}}^s}:\dot{\overline{\boldsymbol{C}}}^s + \sum_{n=1}^{q}\frac{\partial A^l}{\partial \overset{(n)}{\overline{\boldsymbol{C}}^s}}:\overset{(n+1)}{\overline{\boldsymbol{C}}^s} + \frac{\partial A^l}{\partial \varepsilon^l}\boldsymbol{v}^{l,s}\bullet\nabla\varepsilon^l + \frac{\partial A^l}{\partial \varepsilon^s}\boldsymbol{v}^{l,s}\bullet\nabla\varepsilon^s \\ &+ \frac{\partial A^l}{\partial T}\boldsymbol{v}^{l,s}\bullet\nabla T + \frac{\partial A^l}{\partial \rho^l}\boldsymbol{v}^{l,s}\bullet\rho^l + \sum_{j=1}^{N}\tilde{\mu}^{l_j}\boldsymbol{v}^{l,s}\bullet\nabla C^{l_j} + \frac{\partial A^l}{\partial \overline{\boldsymbol{C}}^s}:\nabla\overline{\boldsymbol{C}}^s\bullet\boldsymbol{v}^{l,s} \\ &+ \sum_{n=1}^{q}\frac{\partial A^l}{\partial \overset{(n)}{\overline{\boldsymbol{C}}^s}}:\nabla\overset{(n)}{\overline{\boldsymbol{C}}^s}\bullet\boldsymbol{v}^{l,s} + \sum_{m=1}^{p}\frac{\partial A^l}{\partial \overset{(m)}{\varepsilon^l}}\boldsymbol{v}^{l,s}\bullet\nabla\overset{(m)}{\varepsilon^l}\end{aligned} \tag{2.15}$$

$$\begin{aligned}\frac{D^a A^a}{Dt} &= \frac{\partial A^a}{\partial \varepsilon^l}\dot{\varepsilon}^a + \frac{\partial A^a}{\partial \varepsilon^s}\dot{\varepsilon}^s + \frac{\partial A^a}{\partial T}\dot{T} + \sum_{j=1}^{N}\tilde{\mu}^{a_j}\dot{C}^{a_j} + \frac{\partial A^a}{\partial \rho^a}\dot{\rho}^a + \frac{\partial A^a}{\partial \rho^a}\boldsymbol{v}^{a,s}\bullet\nabla\rho^a \\ &+ \frac{\partial A^a}{\partial \varepsilon^l}\boldsymbol{v}^{a,s}\bullet\nabla\varepsilon^l + \frac{\partial A^a}{\partial \varepsilon^s}\boldsymbol{v}^{a,s}\bullet\nabla\varepsilon^s + \frac{\partial A^a}{\partial T}\boldsymbol{v}^{a,s}\bullet\nabla T + \sum_{j=1}^{N}\tilde{\mu}^{a_j}\boldsymbol{v}^{a,s}\bullet\nabla C^{a_j}\end{aligned} \tag{2.16}$$

The material time derivatives of the free energies are then inserted in the total entropy inequality for the system (given by Equation A. 40). Mass conservation equations are weakly imposed in the entropy inequality using Lagrange multipliers in the sense of Liu (1972) [66]:

$$\begin{aligned}\Lambda_{new} = \Lambda_{old} &+ \sum_{\alpha} \frac{\lambda^{\alpha}}{T}\left[\frac{D^{\alpha}(\varepsilon^{\alpha}\rho^{\alpha})}{Dt} + \varepsilon^{\alpha}\rho^{\alpha}\nabla\bullet\mathbf{v}^{\alpha} - \sum_{\alpha,\alpha\neq\beta}\hat{e}_{\alpha}^{\beta}\right] \\ &+ \sum_{\alpha}\sum_{j=1}^{N}\frac{\lambda^{\alpha_j}}{T}\left[\varepsilon^{\alpha}\rho^{\alpha}\frac{D^{\alpha}C^{\alpha_j}}{Dt} + \nabla\bullet(\varepsilon^{\alpha}\rho^{\alpha_j}\mathbf{v}^{\alpha_j,\alpha})\right] \\ &- \sum_{\alpha}\sum_{j=1}^{N}\frac{\lambda^{\alpha_j}}{T}\left[\sum_{\alpha,\alpha\neq\beta}\hat{e}_{\alpha_j}^{\beta} + \hat{r}^{\alpha_j} - C^{\alpha_j}\sum_{\alpha,\alpha\neq\beta}\hat{e}_{\alpha}^{\beta}\right] \geq 0\end{aligned} \tag{2.17}$$

where Λ_{old} is given in Appendix A.

The entropy inequality is then given as:

$$
\begin{aligned}
\Lambda \quad = & -\frac{1}{T}(\varepsilon^s\rho^s\frac{\partial A^s}{\partial T}+\varepsilon^l\rho^l\frac{\partial A^l}{\partial T}++\varepsilon^a\rho^a\frac{\partial A^a}{\partial T}+\eta^s+\eta^l+\eta^a)\dot{T} \\
& -\frac{1}{T}(\varepsilon^s\rho^s\frac{\partial A^s}{\partial \varepsilon^l}+\varepsilon^l\rho^l\frac{\partial A^l}{\partial \varepsilon^l}+\varepsilon^a\rho^a\frac{\partial A^a}{\partial \varepsilon^l}-\lambda^l\rho^l+\lambda^a\rho^a)\cdot\varepsilon^l \\
& -\frac{1}{T}(\varepsilon^s\rho^s\frac{\partial A^s}{\partial \varepsilon^s}+\varepsilon^l\rho^l\frac{\partial A^l}{\partial \varepsilon^s}+\varepsilon^a\rho^a\frac{\partial A^a}{\partial \varepsilon^s}+\lambda^a\rho^a)\cdot\varepsilon^s \\
& -\frac{1}{T}[\varepsilon^s\rho^s\frac{\partial A^s}{\partial J^s}-\frac{1}{3}\varepsilon^s\frac{1}{J^s}\sum tr(t^{s}{}_j)]\dot{J}^s \\
& -\frac{1}{T}\sum_\alpha\sum_{j=1}^{N}\varepsilon^\alpha\rho^\alpha(\tilde{\mu}^{\alpha}{}_j-\lambda^{\alpha}{}_j)\dot{C}^{\alpha}{}_j \\
& -\frac{1}{T}(\varepsilon^s\rho^s\sum_{m=1}^{p}\frac{\partial A^s}{\partial \overset{(m)l}{\varepsilon}}+\varepsilon^l\rho^l\sum_{m=1}^{p}\frac{\partial A^l}{\partial \overset{(m)l}{\varepsilon}})\overset{(m+1)l}{\varepsilon} \\
& -\frac{1}{T}[\varepsilon^s\rho^s\sum_{n=1}^{q}\frac{\partial A^s}{\partial \overset{(n)s}{\boldsymbol{C}}}+\varepsilon^l\rho^l\sum_{n=1}^{q}\frac{\partial A^l}{\partial \overset{(n)s}{\boldsymbol{C}}}]:\overset{(n+1)s}{\dot{\boldsymbol{C}}} \\
& -\frac{1}{T}(\varepsilon^l\rho^l\frac{\partial A^l}{\partial \rho^l}-\lambda^l\varepsilon^l)\dot{\rho}^l \\
& -\frac{1}{T}(\varepsilon^a\rho^a\frac{\partial A^a}{\partial \rho^a}-\lambda^a\varepsilon^a)\dot{\rho}^a \\
& -\frac{1}{T}(\varepsilon^l\rho^l\frac{\partial A^l}{\partial \varepsilon^l}\nabla\varepsilon^l+\varepsilon^l\rho^l\frac{\partial A^l}{\partial \varepsilon^s}\nabla\varepsilon^s+\varepsilon^l\rho^l\sum_{j=1}^{N-1}\tilde{\mu}^{l}{}_j\nabla C^{l}{}_j+\varepsilon^l\rho^l\frac{\partial A^l}{\partial \overline{\boldsymbol{C}}^s}:\nabla\overline{\boldsymbol{C}}^s \\
& +\varepsilon^l\rho^l\sum_{n=1}^{q}\frac{\partial A^l}{\partial \overset{(n)s}{\boldsymbol{C}}}:\nabla\overset{(n)s}{\boldsymbol{C}} \\
& +\varepsilon^l\rho^l\sum_{m=1}^{p}\frac{\partial A^l}{\partial \overset{(m)l}{\varepsilon}}\nabla\overset{(m)l}{\varepsilon}-\lambda^l\rho^l\nabla\varepsilon^l+\sum_{\beta\neq l}T_l^{\beta}-\lambda^{l}{}_j\varepsilon^l\rho^l\nabla C^{s}{}_j)\boldsymbol{v}^{l,s} \\
& -\frac{1}{T}(\varepsilon^a\rho^a\frac{\partial A^a}{\partial \varepsilon^l}\nabla\varepsilon^l+\varepsilon^a\rho^a\frac{\partial A^a}{\partial \varepsilon^s}\nabla\varepsilon^s-\lambda^a\rho^a\nabla\varepsilon^a+\varepsilon^a\rho^a\sum_{j=1}^{N-1}\tilde{\mu}^{a}{}_j\nabla C^{a}{}_j \\
& +\sum_{\beta\neq a}T_a^{\beta}-\lambda^{a}{}_j\varepsilon^a\rho^a\nabla C^{a}{}_j)\boldsymbol{v}^{a,s} \\
& -\frac{1}{T}(\varepsilon^s\rho^s\frac{\partial A^s}{\partial \overline{\boldsymbol{C}}^s}+\varepsilon^l\rho^l\frac{\partial A^l}{\partial \overline{\boldsymbol{C}}^s}-\frac{\varepsilon^s}{2}(\overline{\boldsymbol{F}}^s)^{-1}\sum_{j=1}^{N}t^{s}{}_j(\overline{\boldsymbol{F}}^s)^{-T}-\frac{\varepsilon^s\rho^s\lambda^s}{2}(\overline{\boldsymbol{F}}^s)^{-1}(\overline{\boldsymbol{F}}^s)^{-T}):\overline{\boldsymbol{C}}^s \\
& +\frac{\varepsilon^l}{T}(\sum_{j=1}^{N}t^{l}{}_j+\lambda^l\rho^l\boldsymbol{I}):\boldsymbol{d}^l \\
& +\frac{\varepsilon^a}{T}(\sum_{j=1}^{N}t^{a}{}_j+\lambda^a\rho^a\boldsymbol{I}):\boldsymbol{d}^a \\
& +\sum_\alpha\frac{\varepsilon^\alpha}{T}(q^\alpha-\sum_{j=1}^{N}[t^{\alpha}{}_j\cdot\boldsymbol{v}^{\alpha}{}_{j,\alpha}-\rho^{\alpha}{}_j\boldsymbol{v}^{\alpha}{}_{j,\alpha}(A^{\alpha}{}_j+\frac{1}{2}(\boldsymbol{v}^{\alpha}{}_{j,\alpha})^2)])\cdot\nabla T \\
& +\sum_\alpha\sum_{j=1}^{N-1}\frac{\varepsilon^\alpha}{T}(\boldsymbol{t}^{\alpha}{}_j-\rho^{\alpha}{}_jA^{\alpha}{}_j\boldsymbol{I}-\frac{\rho^{\alpha}{}_j}{\rho^{\alpha}{}_N}\boldsymbol{t}^{\alpha}{}_N+\rho^{\alpha}{}_jA^{\alpha}{}_N\boldsymbol{I}+\rho^{\alpha}{}_j\lambda^{\alpha}{}_j\boldsymbol{I}-\rho^{\alpha}{}_j\lambda^{\alpha}{}_N\boldsymbol{I})\cdot\nabla\boldsymbol{v}^{\alpha}{}_{j,\alpha} \\
& +\frac{1}{T}\sum_{j=1}^{N-1}[\frac{\rho^{\alpha}{}_j}{\rho^{\alpha}{}_N}(\hat{T}^{\beta}_{\alpha}{}_N+i^{\alpha}{}_N)-(\hat{T}^{\beta}_{\alpha}{}_j+i^{\alpha}{}_j)-\nabla[\varepsilon^\alpha\rho^{\alpha}{}_j(A^{\alpha}{}_N-A^{\alpha}{}_j)] \\
& +(\lambda^{\alpha}{}_j-\lambda^{\alpha}{}_N)\nabla(\varepsilon^\alpha\rho^{\alpha}{}_j)-\varepsilon^\alpha\boldsymbol{t}^{\alpha}{}_N\nabla(\frac{\rho^{\alpha}{}_j}{\rho^{\alpha}{}_N})]\cdot\boldsymbol{v}^{\alpha}{}_{j,\alpha} \\
& -\frac{1}{T}\sum_{j=1}^{N}r^{\alpha}{}_j[\lambda^{\alpha}{}_j+\frac{1}{2}(\boldsymbol{v}^{\alpha}{}_{j,\alpha})^2] \\
& -\frac{1}{T}\sum_\alpha\sum_{\beta\neq\alpha}\hat{e}^{\beta}_{\alpha}[-\sum_{j=1}^{N-1}\lambda^{\alpha}{}_jC^{\alpha}{}_j+\lambda^\alpha+A^\alpha+\frac{1}{2}(v^{a,s})^2+\frac{1}{2}(v^{a,s})^2] \\
& -\frac{1}{T}\sum_\alpha\sum_{j=1}^{N-1}\hat{e}^{\beta}_{\alpha_j}[\lambda^{\alpha}{}_j+\frac{1}{2}(v^{\alpha}{}_{j,\alpha})^2]\geq 0
\end{aligned}
\tag{2.18}
$$

Since ρ^s is not chosen as an independent variable, we have used the determinant of the deformation tensor, J^s:

$$\rho^s \varepsilon^s = \frac{\rho_0^s \varepsilon_0^s}{J^s} \tag{2.19}$$

in the entropy inequality above, to express $\dot{\rho}^s$ in terms of other independent variables:

$$\begin{aligned}
&\frac{\lambda^s}{T}\left[\frac{D^s(\varepsilon^s\rho^s)}{Dt} + \varepsilon^s\rho^s\nabla\bullet\boldsymbol{v}^s - \sum_{\beta\neq s}\hat{e}_s^{\beta}\right] \\
&= \frac{\lambda^s}{T}\left[\frac{D^s(\frac{\varepsilon_0^s\rho_0^s}{J^s})}{Dt} + \varepsilon^s\rho^s\nabla\bullet\boldsymbol{v}^s - \sum_{\beta\neq s}\hat{e}_s^{\beta}\right] \\
&= \frac{\lambda^s}{T}\left[-\frac{\varepsilon_0^s\rho_0^s\dot{J}^s}{J^{s2}} + \varepsilon^s\rho^s\boldsymbol{d}^s:\boldsymbol{I} - \sum_{\beta\neq s}\hat{e}_s^{\beta}\right] \\
&= \frac{\lambda^s}{T}\left[-\frac{\varepsilon^s\rho^s\dot{J}^s}{J^s} + \varepsilon^s\rho^s\frac{1}{2}((\overline{\boldsymbol{F}}^s)^{-1}(\overline{\boldsymbol{F}}^s)^{-t}):\dot{\overline{\boldsymbol{C}}}^s + \frac{\varepsilon^s\rho^s\dot{J}^s}{J^s} - \sum_{\beta\neq s}\hat{e}_s^{\beta}\right] \\
&= \frac{\lambda^s}{T}\left[\varepsilon^s\rho^s\frac{1}{2}((\overline{\boldsymbol{F}}^s)^{-1}(\overline{\boldsymbol{F}}^s)^{-t}):\dot{\overline{\boldsymbol{C}}}^s - \sum_{\beta\neq s}\hat{e}_s^{\beta}\right]
\end{aligned} \tag{2.20}$$

where $\boldsymbol{d}^s:\boldsymbol{I}$ is calculated as:

$$\boldsymbol{d}^s:\boldsymbol{I} = \frac{1}{2}((\overline{\boldsymbol{F}}^s)^{-1}(\overline{\boldsymbol{F}}^s)^{-t}):\dot{\overline{\boldsymbol{C}}}^s + \frac{\dot{J}^s}{J^s} \tag{2.21}$$

The details of this calculation can be found in Weinstein et al. (2008a) [127] where $\boldsymbol{d}^s$ is rewritten in terms of J^s and $\overline{\boldsymbol{C}}^s$.

To remove dependence on velocities of the N^{th} components of the phases (more later), we have used (Holzapfel, 2000) [54]:

$$\sum_{j=1}^{N} \boldsymbol{F}^{\alpha_j} \bullet \boldsymbol{v}^{\alpha_j,\alpha} = \sum_{j=1}^{N-1} (\boldsymbol{F}^{\alpha_j} - \frac{\rho^{\alpha_j}}{\rho^{\alpha_N}} \boldsymbol{F}^{\alpha_N}) \bullet \boldsymbol{v}^{\alpha_j,\alpha} \tag{2.22}$$

$$\sum_{j=1}^{N} \boldsymbol{G}^{\alpha_j} : \nabla \boldsymbol{v}^{\alpha_j,\alpha} = \sum_{j=1}^{N-1} (\boldsymbol{G}^{\alpha_j} - \frac{\rho^{\alpha_j}}{\rho^{\alpha_N}} \boldsymbol{G}^{\alpha_N}) : \nabla \boldsymbol{v}^{\alpha_j,\alpha} - \boldsymbol{G}^{\alpha_N} \sum_{j=1}^{N-1} \nabla (\frac{\rho^{\alpha_j}}{\rho^{\alpha_N}}) \bullet \boldsymbol{v}^{\alpha_j,\alpha} \tag{2.23}$$

2.2.2 Non-equilibrium restrictions

We first consider that the system is in a stationary state far from thermodynamic equilibrium. Following the procedure of Coleman-Noll (1963)[31], the variables $\dot{T}, \dot{J}^s, \nabla \boldsymbol{v}^{s_j,s}, \dot{C}^{\alpha_j}, \dot{\rho}^{\alpha}, \overset{(q+1)s}{\boldsymbol{C}}$ and $\overset{(p+1)l}{\boldsymbol{\varepsilon}}$ in the entropy inequality are neither dependent nor independent. Since they could vary arbitrarily, the coefficients of these variables in the entropy inequality must vanish. Thus, the following non-equilibrium results are obtained:

$$\sum_{\alpha} (\frac{\partial A^{\alpha}}{\partial T} + \eta^{\alpha}) = 0 \tag{2.24}$$

$$\frac{1}{3} \sum_{j=1}^{N} tr(\boldsymbol{t}^{s_j}) = -p^s \tag{2.25}$$

where the physical pressure is given by (Bennethum and Weinstein 2004)[24]:

$$p^s = -\rho^s J^s \left. \frac{\partial A^s}{\partial J^s} \right|_{\varepsilon^s} \tag{2.26}$$

$$\sum_{j=1}^{N} \boldsymbol{t}^{s_j} = \rho^{s_j}(A^{s_j} - A^{s_N} - \tilde{\mu}^{s_j})\boldsymbol{I} + \frac{\rho^{s_j}}{\rho^{s_N}}\boldsymbol{t}^{s_N} \tag{2.27}$$

$$\tilde{\mu}^{\alpha_j} = \lambda^{\alpha_j} \tag{2.28}$$

$$\lambda^{l} = \rho^{l}\frac{\partial A^{l}}{\partial \rho^{l}}\Big|_{\varepsilon^{l}} = \frac{p^{l}}{\rho^{l}} \tag{2.29}$$

$$\lambda^{a} = \rho^{a}\frac{\partial A^{a}}{\partial \rho^{a}}\Big|_{\varepsilon^{a}} = \frac{p^{a}}{\rho^{a}} \tag{2.30}$$

$$\varepsilon^{s}\rho^{s}\frac{\partial A^{s}}{\partial \overset{(q)s}{\boldsymbol{C}}} + \varepsilon^{l}\rho^{l}\frac{\partial A^{l}}{\partial \overset{(q)s}{\boldsymbol{C}}} = 0 \tag{2.31}$$

$$\varepsilon^{s}\rho^{s}\frac{\partial A^{s}}{\partial \overset{(p)l}{\varepsilon}} + \varepsilon^{l}\rho^{l}\frac{\partial A^{l}}{\partial \overset{(p)l}{\varepsilon}} = 0 \tag{2.32}$$

Since temperature and entropy are conjugate thermodynamic variables for a single phase, for Equation (2.24), we further assume that entropy of each phase is related to temperature through:

$$\eta^{\alpha} = -\frac{\partial A^{\alpha}}{\partial T}, \alpha = s, l, a \tag{2.33}$$

If we assume that there is only one species in the solid phase or if we assume that the diffusive velocity in the solid phase is negligible, Equation (2.25) would become:

$$\frac{1}{3}tr(\boldsymbol{t}^{s}) = -p^{s} \tag{2.34}$$

Equations (2.29) and (2.30) will be used throughout this dissertation. In this section and hereafter, not all the relationships are listed as some are not needed in the model development.

2.2.3 Equilibrium restrictions

Next we explore information from the entropy inequality when the system is at an equilibrium state. The total rate of entropy production, Λ, reaches its minimum value at equilibrium. When the system is in thermodynamic equilibrium, the state variables do not change with time and so the following variables are zero at thermodynamic equilibrium:

$$\dot{\varepsilon}^l, \dot{\varepsilon}^s, \overset{(m)l}{\varepsilon}, \overset{(n+1)s}{\overline{\boldsymbol{C}}}, \boldsymbol{v}^{l,s}, \boldsymbol{v}^{a,s}, \boldsymbol{d}^l, \boldsymbol{d}^a, \nabla T, \boldsymbol{v}^{\alpha_j,\alpha}, \nabla \boldsymbol{v}^{l_j,l}, \nabla \boldsymbol{v}^{a_j,a}, \hat{e}^{\beta}_{\alpha_j}, \hat{e}^{\beta}_{\alpha}, \overline{\boldsymbol{C}}^s \tag{2.35}$$

If we denote these variables as x and y, then the necessary and sufficient conditions for Λ to be at a minimum at thermodynamic equilibrium is:

$$\left(\frac{\partial \Lambda}{\partial x}\right)_{eq} = 0 \tag{2.36}$$

and

$$\left(\frac{\partial^2 \Lambda}{\partial x \partial y}\right)_{eq} \text{ be positive semi} - \text{definite} \tag{2.37}$$

Using these conditions, we can obtain the following relations at equilibrium:

$$\varepsilon^s \rho^s \frac{\partial A^s}{\partial \varepsilon^l} + \varepsilon^l \rho^l \frac{\partial A^l}{\partial \varepsilon^l} + \varepsilon^a \rho^a \frac{\partial A^a}{\partial \varepsilon^l} - p^l + p^a = 0 \tag{2.38}$$

$$\varepsilon^s \rho^s \frac{\partial A^s}{\partial \varepsilon^s} + \varepsilon^l \rho^l \frac{\partial A^l}{\partial \varepsilon^s} + \varepsilon^a \rho^a \frac{\partial A^a}{\partial \varepsilon^s} + p^a = 0 \tag{2.39}$$

$$\varepsilon^s \rho^s \frac{\partial A^s}{\partial \overset{(m)l}{\varepsilon}} + \varepsilon^l \rho^l \frac{\partial A^l}{\partial \overset{(m)l}{\varepsilon}} = 0 \tag{2.40}$$

$$\varepsilon^s \rho^s \frac{\partial A^s}{\partial \overset{(n)s}{\overline{\boldsymbol{C}}}} + \varepsilon^l \rho^l \frac{\partial A^l}{\partial \overset{(n)s}{\overline{\boldsymbol{C}}}} = 0 \tag{2.41}$$

$$\boldsymbol{t}^l = -p^l \boldsymbol{I} \tag{2.42}$$

$$\boldsymbol{t}^a = -p^a \boldsymbol{I} \tag{2.43}$$

$$\begin{aligned} &\varepsilon^l \rho^l \frac{\partial A^l}{\partial \varepsilon^l} \nabla \varepsilon^l + \varepsilon^l \rho^l \frac{\partial A^l}{\partial \varepsilon^s} \nabla \varepsilon^s - p^l \nabla \varepsilon^l + \varepsilon^l \rho^l \frac{\partial A^l}{\partial \overline{\boldsymbol{C}}^s} : \nabla \overline{\boldsymbol{C}}^s \\ &+ \varepsilon^l \rho^l \sum_{n=1}^{q} \frac{\partial A^l}{\partial \overset{(n)s}{\overline{\boldsymbol{C}}}} : \nabla \overset{(n)s}{\overline{\boldsymbol{C}}} + \varepsilon^l \rho^l \sum_{m=1}^{p} \frac{\partial A^l}{\partial \overset{(m)l}{\boldsymbol{\varepsilon}}} \nabla \overset{(m)l}{\boldsymbol{\varepsilon}} + \sum_{\beta \neq l} \hat{T}_l^{\beta} = 0 \end{aligned} \tag{2.44}$$

$$\varepsilon^a \rho^a \frac{\partial A^a}{\partial \varepsilon^l} \nabla \varepsilon^l + \varepsilon^a \rho^a \frac{\partial A^a}{\partial \varepsilon^s} \nabla \varepsilon^s - p^a \nabla \varepsilon^a + \sum_{\beta \neq a} \hat{T}_a^{\beta} = 0 \tag{2.45}$$

$$\sum_{\alpha} \varepsilon^{\alpha} \boldsymbol{q}^{\alpha} = 0 \tag{2.46}$$

$$\begin{aligned} &\frac{\rho^{\alpha_j}}{\rho^{\alpha_N}} (\hat{\boldsymbol{T}}_{\alpha_N}^{\beta} + \hat{\boldsymbol{i}}^{\alpha_N}) - (\hat{\boldsymbol{T}}_{\alpha_j}^{\beta} + \hat{\boldsymbol{i}}^{\alpha_j}) - \nabla[\varepsilon^{\alpha} \rho^{\alpha_j} (A^{\alpha_N} - A^{\alpha_j})] \\ &+ (\lambda^{\alpha_j} - \lambda^{\alpha_N}) \nabla(\varepsilon^{\alpha} \rho^{\alpha_j}) - \varepsilon^{\alpha} \boldsymbol{t}^{\alpha_N} \nabla(\frac{\rho^{\alpha_j}}{\rho^{\alpha_N}}) = 0 \end{aligned} \tag{2.47}$$

$$t^{\alpha_j} - \rho^{\alpha_j} A^{\alpha_j} I - \frac{\rho^{\alpha_j}}{\rho^{\alpha_N}} t^{\alpha_N} + \rho^{\alpha_j} A^{\alpha_N} I + \rho^{\alpha_j} \lambda^{\alpha_j} I = 0, \alpha = l, a \tag{2.48}$$

$$-\sum_{j=1}^{N-1} \lambda^{\alpha_j} C^{\alpha_j} + \lambda^{\alpha} + A^{\alpha} + \frac{1}{2} (\boldsymbol{v}^{a,s})^2 + \frac{1}{2} (\boldsymbol{v}^{l,s})^2 = 0 \tag{2.49}$$

$$\tilde{\mu}^{s_j} = \tilde{\mu}^{l_j} = \tilde{\mu}^{a_j} \tag{2.50}$$

$$\boldsymbol{t}^s = -\lambda^s \rho^s \boldsymbol{I} + 2 \frac{\varepsilon^l}{\varepsilon^s} \rho^l \overline{\boldsymbol{F}}^s \frac{\partial A^l}{\partial \overline{\boldsymbol{C}}^s} (\overline{\boldsymbol{F}}^s)^T + 2 \rho^s \overline{\boldsymbol{F}}^s \frac{\partial A^s}{\partial \overline{\boldsymbol{C}}^s} (\overline{\boldsymbol{F}}^s)^T \tag{2.51}$$

$$A^{\alpha} + \lambda^{\alpha} - \sum_{j=1}^{N-1} \tilde{\mu}^{\alpha_j} C^{\alpha_j} = A^{\beta} + \lambda^{\beta} - \sum_{j=1}^{N-1} \tilde{\mu}^{\beta_j} C^{\beta_j}, \alpha \neq \beta \tag{2.52}$$

Since ρ^s is not taken as an independent variable, we have replaced the term involving $\dot{\rho}^s$ in the entropy inequality. Thus, there is no equation for λ^s. We take $\frac{1}{3}$ of the trace of Equation (2.51), use Equation (2.52) and solve for λ^s (Weinstein and Bennethum 2006) [126]:

$$\lambda^s = \frac{p^s}{\rho^s} + \frac{2}{3}\frac{\varepsilon^l \rho^l}{\varepsilon^s \rho^s}\frac{\partial A^l}{\partial \overline{\boldsymbol{C}}^s} : \overline{\boldsymbol{C}}^s + \frac{2}{3}\frac{\partial A^s}{\partial \overline{\boldsymbol{C}}^s} : \overline{\boldsymbol{C}}^s \tag{2.53}$$

Then

$$\begin{aligned} \boldsymbol{t}^s = & -p^s \boldsymbol{I} + 2\frac{\varepsilon^l}{\varepsilon^s}\rho^l \overline{\boldsymbol{F}}^s \frac{\partial A^l}{\partial \overline{\boldsymbol{C}}^s}(\overline{\boldsymbol{F}}^s)^T + 2\rho^s \overline{\boldsymbol{F}}^s \frac{\partial A^s}{\partial \overline{\boldsymbol{C}}^s}(\overline{\boldsymbol{F}}^s)^T \\ & -\frac{2}{3}\frac{\varepsilon^l \rho^l}{\varepsilon^s}\left(\frac{\partial A^l}{\partial \overline{\boldsymbol{C}}^s} : \overline{\boldsymbol{C}}^s\right)\boldsymbol{I} - \frac{2}{3}\rho^s\left(\frac{\partial A^s}{\partial \overline{\boldsymbol{C}}^s} : \overline{\boldsymbol{C}}^s\right)\boldsymbol{I} \end{aligned} \tag{2.54}$$

We write out the Terzaghi stress $\boldsymbol{t}^{se}$ and the hydration stress $\boldsymbol{t}^{sh}$ as:

$$\boldsymbol{t}^{se} = 2\left[\varepsilon^s \rho^s \overline{\boldsymbol{F}}^s \frac{\partial A^s}{\partial \overline{\boldsymbol{C}}^s}(\overline{\boldsymbol{F}}^s)^T - \frac{1}{3}\varepsilon^s \rho^s \left(\frac{\partial A^s}{\partial \overline{\boldsymbol{C}}^s} : \overline{\boldsymbol{C}}^s\right)\boldsymbol{I}\right] \tag{2.55}$$

$$\boldsymbol{t}^{sh} = 2\left[\varepsilon^l \rho^l \overline{\boldsymbol{F}}^s \frac{\partial A^l}{\partial \overline{\boldsymbol{C}}^s}(\overline{\boldsymbol{F}}^s)^T - \frac{1}{3}\varepsilon^l \rho^l \left(\frac{\partial A^l}{\partial \overline{\boldsymbol{C}}^s} : \overline{\boldsymbol{C}}^s\right)\boldsymbol{I}\right] \tag{2.56}$$

Then the equilibrium result for the Cauchy stress is of the following form:

$$\varepsilon^s \boldsymbol{t}^s = -\varepsilon^s p^s \boldsymbol{I} + \boldsymbol{t}^{sh} + \boldsymbol{t}^{se} \tag{2.57}$$

2.2.4 Removing Nth component dependence

The relationships we obtained based on HMT for the species are expressed relative to the N th constituent. In classical Gibbsian thermodynamics, however, since extensive

variables, such as number of molecules of each constituent, rather than intensive variables, such as concentrations, are chosen as independent variables, *N*th components do not appear in the species equations. Here, we follow Bennethum et al. (1996b)[20] and find out results that are in accordance with the classic Gibbsian thermodynamics. To do so, we use the definition of the N th chemical potential μ^{α_N} by Bennethum et al. (1996b) [20] and remove the *N*th component dependence. We take:

$$\mu^{\alpha_N}\boldsymbol{I} = A^{\alpha_N}\boldsymbol{I} - \frac{\boldsymbol{t}^{\alpha_N}}{\rho^{\alpha_N}}, \alpha = l, a \tag{2.58}$$

$$\mu^{s_N}\boldsymbol{I} = A^{s_N}\boldsymbol{I} - \frac{\boldsymbol{t}^{s_N}}{\rho^{s_N}} + \frac{\boldsymbol{t}^{se}}{\rho^{s}} + \frac{\varepsilon^{l}}{\varepsilon^{s}}\frac{\boldsymbol{t}^{sh}}{\rho^{s}} \tag{2.59}$$

Substituting Equations (2.59) and (2.60) into Equations (2.48) and (2.49) respectively, we obtain:

$$\mu^{\alpha_j}\boldsymbol{I} = A^{\alpha_j}\boldsymbol{I} - \frac{\boldsymbol{t}^{\alpha_j}}{\rho^{\alpha_j}}, \alpha = l, a \tag{2.60}$$

$$\mu^{s_j}\boldsymbol{I} = A^{s_j}\boldsymbol{I} - \frac{\boldsymbol{t}^{s_j}}{\rho^{s_j}} + \frac{\boldsymbol{t}^{se}}{\rho^{s}} + \frac{\varepsilon^{l}}{\varepsilon^{s}}\frac{\boldsymbol{t}^{sh}}{\rho^{s}} \tag{2.61}$$

Multiplying Equations (2.60) and (2.61) by C^{α_j} and C^{s_j} respectively, summing over all species and substituting $\boldsymbol{t}^{\alpha}$ with Equations (2.42), (2.43) and (2.44), we obtain the Gibbs free energies:

$$G^{\alpha} = \sum_{j=1}^{N} C^{\alpha_j}\mu^{\alpha_j} = A^{\alpha} + \frac{p^{\alpha}}{\rho^{\alpha}} \tag{2.62}$$

$$G^s = \sum_{j=1}^{N} C^{s_j} \mu^{s_j} = A^s + \frac{p^s}{\rho^s} \tag{2.63}$$

We rewrite Equation (2.52) as:

$$A^\alpha + \lambda^\alpha - \sum_{j=1}^{N} \mu^{\alpha_j} C^{\alpha_j} + \mu^{\alpha_N} = A^\beta + \lambda^\beta - \sum_{j=1}^{N} \mu^{\beta_j} C^{\beta_j} + \mu^{\beta_N} \tag{2.64}$$

Substituting λ^α using Equations (2.29), (2.30) and (2.31) and using Equations (2.62) and (2.63), we obtain:

$$\mu^{\alpha_N} = \mu^{\beta_N}, \alpha \neq \beta \tag{2.65}$$

Therefore, the classical result is obtained as:

$$\mu^{\alpha_j} = \mu^{\beta_j}, \alpha \neq \beta \tag{2.66}$$

To remove *N*th component dependence from Equation (2.47), we sum from $j = 1$ to *N*:

$$\begin{aligned} &\frac{\rho^{\alpha_j}}{\rho^{\alpha_N}} \left(\sum_{\beta \neq \alpha} \hat{\boldsymbol{T}}^{\beta}_{\alpha_N} + \hat{\boldsymbol{i}}^{\alpha_N} \right) - \sum_{\beta \neq \alpha} \hat{\boldsymbol{T}}^{\beta}_{\alpha} + \nabla(\varepsilon^\alpha \rho^\alpha A^{\alpha_N}) - \varepsilon^\alpha \rho^\alpha (\nabla A^\alpha) - A^\alpha \nabla(\varepsilon^\alpha \rho^\alpha) \\ &+ \sum_{j=1}^{N} \tilde{\mu}^{\alpha_j} \nabla(\varepsilon^\alpha \rho^{\alpha_j}) - \varepsilon^\alpha \boldsymbol{t}^{\alpha_N} \nabla\left(\frac{\rho^\alpha}{\rho^{\alpha_N}}\right) = 0, \alpha = l, a \end{aligned} \tag{2.67}$$

Expanding ∇A^α using Equations (2.6)-(2.8) yields:

$$\begin{aligned} \nabla A^s \quad = &\frac{\partial A^s}{\partial \varepsilon^s} \nabla \varepsilon^s + \frac{\partial A^s}{\partial T} \nabla T + \frac{\partial A^s}{\partial J^s} \nabla J^s + \sum_{j=1}^{N-1} \tilde{\mu}^{s_j} \nabla C^{s_j} + \\ &\sum_{m=1}^{p} \frac{\partial A^s}{\partial \overset{(m)l}{\boldsymbol{\varepsilon}}} \nabla \overset{(m)l}{\boldsymbol{\varepsilon}} + \sum_{n=0}^{q} \frac{\partial A^s}{\partial \overset{(n)s}{\boldsymbol{C}}} : \nabla \overset{(n)s}{\boldsymbol{C}} \end{aligned} \tag{2.68}$$

$$\begin{aligned} \nabla A^l \quad = &\frac{\partial A^l}{\partial \varepsilon^l} \nabla \varepsilon^l + \frac{\partial A^l}{\partial \varepsilon^s} \nabla \varepsilon^s + \frac{\partial A^l}{\partial T} \nabla T + \frac{\partial A^l}{\partial \rho^l} \nabla \rho^l + \sum_{j=1}^{N-1} \tilde{\mu}^{l_j} \nabla C^{l_j} + \\ &\sum_{m=1}^{p} \frac{\partial A^l}{\partial \overset{(m)l}{\boldsymbol{\varepsilon}}} \nabla \overset{(m)l}{\boldsymbol{\varepsilon}} + \sum_{n=0}^{q} \frac{\partial A^l}{\partial \overset{(n)s}{\boldsymbol{C}}} : \nabla \overset{(n)s}{\boldsymbol{C}} \end{aligned} \tag{2.69}$$

$$\nabla A^a = \frac{\partial A^a}{\partial \varepsilon^l}\nabla \varepsilon^l + \frac{\partial A^a}{\partial \varepsilon^s}\nabla \varepsilon^s + \frac{\partial A^a}{\partial T}\nabla T + \frac{\partial A^a}{\partial \rho^a}\nabla \rho^a + \sum_{j=1}^{N-1} \tilde{\mu}^{a_j} \nabla C^{a_j} \quad (2.70)$$

Substituting ∇A^α and $\sum_{\beta \neq \alpha} T_\alpha^\beta$ into Equation (2.67), for phase *l*, we get:

$$\begin{aligned} &\frac{\rho^l}{\rho^{l_N}}(\hat{\boldsymbol{T}}^s_{l_N} + \hat{\boldsymbol{T}}^a_{l_N} + \hat{\boldsymbol{i}}^{l_N}) - p^l \nabla \varepsilon^l + \nabla(\varepsilon^l \rho^l A^{l_N}) - \varepsilon^l \rho^l \frac{\partial A^l}{\partial \rho^l}\nabla \rho^l - \varepsilon^l \rho^l \sum_{j=1}^{N-1} \tilde{\mu}^{l_j} \nabla C^{l_j} \\ &- A^l \nabla(\varepsilon^l \rho^l) + \sum_{j=1}^{N} \tilde{\mu}^{l_j} \nabla(\varepsilon^l \rho^{l_j}) - \varepsilon^l t^{l_N} \nabla(\frac{\rho^l}{\rho^{l_N}}) = 0 \end{aligned} \quad (2.71)$$

where we have ignored the term involving ∇T since it is zero at equilibrium. If we write out $\nabla(\varepsilon^l \rho^{l_j}) = \varepsilon^l \rho^l \nabla C^{l_j} + C^{l_j} \nabla \varepsilon^l \rho^l$ and simplify, the above equation becomes:

$$\begin{aligned} &\frac{\rho^l}{\rho^{l_N}}(\hat{\boldsymbol{T}}^s_{l_N} + \hat{\boldsymbol{T}}^a_{l_N} + \hat{\boldsymbol{i}}^{l_N}) - \varepsilon^l t^{l_N} \nabla(\frac{\rho^l}{\rho^{l_N}}) + \nabla(\varepsilon^l \rho^l A^{l_N}) - \mu^{l_N} \nabla(\varepsilon^l \rho^l) \\ &= p^l \nabla \varepsilon^l + A^l \nabla(\varepsilon^l \rho^l) - \sum_{j=1}^{N} \mu^{l_j} C^{l_j} \nabla(\varepsilon^l \rho^l) - \varepsilon^l \rho^l \frac{\partial A^l}{\partial \rho^l}\nabla \rho^l \end{aligned} \quad (2.72)$$

We substitute the third term on the right hand side using Equation (2.62) and use the definition that $p^l = (\rho^l)^2 \frac{\partial A^l}{\partial \rho^l}$ in the above equation to obtain:

$$\frac{\rho^l}{\rho^{l_N}}(\hat{\boldsymbol{T}}^s_{l_N} + \hat{\boldsymbol{T}}^a_{l_N} + \hat{\boldsymbol{i}}^{l_N}) - \varepsilon^l t^{l_N} \nabla(\frac{\rho^l}{\rho^{l_N}}) + \nabla(\varepsilon^l \rho^l A^{l_N}) - \mu^{l_N} \nabla(\varepsilon^l \rho^l) = 0 \quad (2.73)$$

Substituting Equation (2.73) back into Equation (2.67) and undoing the sum yields:

$$\sum_{\beta \neq l} \hat{\boldsymbol{T}}^\beta_{l_j} + \hat{\boldsymbol{i}}^{l_j} = \mu^{l_j} \nabla(\varepsilon^l \rho^{l_j}) - \nabla(\varepsilon^l \rho^l A^{l_j}) \quad (2.74)$$

Following the same procedure, we could find that for phase *a* we obtain exactly the same form as Equation (2.74). Thus, removing the *N*th component dependence from Equation (2.47), we obtain:

$$\sum_{\beta\neq\alpha}\hat{\boldsymbol{T}}^{\beta}_{\alpha_j}+\hat{\boldsymbol{i}}^{\alpha_j}=\mu^{\alpha_j}\nabla(\varepsilon^{\alpha}\rho^{\alpha_j})-\nabla(\varepsilon^{\alpha}\rho^{\alpha}A^{\alpha_j}),\alpha=l,a \tag{2.75}$$

2.2.5 Near-equilibrium results

Other useful information, such as Darcy's and Fick's laws could be obtained when we consider the systems to be at a state near equilibrium. Here, we use Taylor's expansion about variables that become zero at equilibrium (2.35) and truncate all second order and higher order terms to obtain near-equilibrium results. Taking Taylor's expansion of $\boldsymbol{t}^s$ about ∇T and $\overset{(n)s}{\boldsymbol{C}}$ (two of the several variables that go to zero at equilibrium) and retaining only linear terms, we perform a two-term linearization (as discussed in Singh et al. (2003b) [108]) and obtain:

$$\varepsilon^s\boldsymbol{t}^s=-\varepsilon^s p^s\boldsymbol{I}+\boldsymbol{t}^{sh}+\boldsymbol{t}^{se}+\sum_{n=1}^{q}\overline{\boldsymbol{F}}^s A^n:\overset{(n)s}{\boldsymbol{C}}(\overline{\boldsymbol{F}}^s)^T+\boldsymbol{H}^s:\nabla T \tag{2.76}$$

$$\boldsymbol{t}^l=-p^l\boldsymbol{I}-\sum_{j=1}^{N}\rho^{l_j}(\boldsymbol{v}^{l_j,l})^2+\boldsymbol{B}^l:\boldsymbol{d}^l+\boldsymbol{H}^l:\nabla T \tag{2.77}$$

$$\boldsymbol{t}^a=-p^a\boldsymbol{I}-\sum_{j=1}^{N}\rho^{a_j}(\boldsymbol{v}^{a_j,a})^2+\boldsymbol{B}^a:\boldsymbol{d}^a+\boldsymbol{H}^a:\nabla T \tag{2.78}$$

We perform a linearization about $\dot{\varepsilon}^l$ and $\dot{\varepsilon}^s$ and obtain:

$$\varepsilon^s\rho^s\frac{\partial A^s}{\partial\varepsilon^l}+\varepsilon^l\rho^l\frac{\partial A^l}{\partial\varepsilon^l}+\varepsilon^a\rho^a\frac{\partial A^a}{\partial\varepsilon^l}-p^l+p^a=-M^l\dot{\varepsilon}^l \tag{2.79}$$

$$\varepsilon^s\rho^s\frac{\partial A^s}{\partial\varepsilon^s}+\varepsilon^l\rho^l\frac{\partial A^l}{\partial\varepsilon^s}+\varepsilon^a\rho^a\frac{\partial A^a}{\partial\varepsilon^s}+p^a=-M^s\dot{\varepsilon}^s \tag{2.80}$$

The following is obtained by a linearization about $\boldsymbol{v}^{l,s}$:

$$\sum_{\beta\neq l}\hat{\boldsymbol{T}}_l^{\beta} = -\boldsymbol{R}^l\boldsymbol{v}^{l,s} - \varepsilon^l\rho^l\frac{\partial A^l}{\partial \varepsilon^l}\nabla\varepsilon^l - \varepsilon^l\rho^l\frac{\partial A^l}{\partial \varepsilon^s}\nabla\varepsilon^s + p^l\nabla\varepsilon^l$$
$$-\varepsilon^l\rho^l\frac{\partial A^l}{\partial \overline{\boldsymbol{C}}^s}:\nabla\overline{\boldsymbol{C}}^s - \varepsilon^l\rho^l\sum_{n=1}^{q}\frac{\partial A^l}{\partial \overset{(n)s}{\overline{\boldsymbol{C}}}}:\nabla\overset{(n)s}{\overline{\boldsymbol{C}}} - \varepsilon^l\rho^l\sum_{m=1}^{p}\frac{\partial A^l}{\partial \overset{(m)l}{\boldsymbol{\varepsilon}}}\nabla\overset{(m)l}{\boldsymbol{\varepsilon}} \tag{2.81}$$

A linearization about $\boldsymbol{v}^{a,s}$ gives:

$$\sum_{\beta\neq a}\hat{\boldsymbol{T}}_a^{\beta} = -\boldsymbol{R}^a\boldsymbol{v}^{a,s} - \varepsilon^a\rho^a\frac{\partial A^a}{\partial \varepsilon^l}\nabla\varepsilon^l - \varepsilon^a\rho^a\frac{\partial A^a}{\partial \varepsilon^s}\nabla\varepsilon^s + p^a\nabla\varepsilon^a \tag{2.82}$$

Finally, we perform a linearization about ∇T:

$$\boldsymbol{q}^{\alpha} = \sum_{j=1}^{N}[\boldsymbol{t}^{\alpha_j}\cdot\boldsymbol{v}^{\alpha_j,\alpha} - \rho^j\boldsymbol{v}^{\alpha_j,\alpha}(A^{\alpha_j} + \frac{1}{2}(\boldsymbol{v}^{\alpha_j,\alpha})^2)] + \boldsymbol{K}^{\alpha}\cdot\nabla T, \alpha = s,l,a \tag{2.83}$$

In Equation (2.76), $\boldsymbol{A}^n$ is a fourth order positive semi-definite tensor representing dissipation of the viscoelastic solid stress in shear due to relaxation. $\boldsymbol{H}^{\alpha}, \alpha = s,l,a$ in Equations (2.76), (2.77) and (2.78) are third rank tensors and thus the thermal gradient only affects the stress field in an anisotropic solid. The terms involving $\boldsymbol{H}^{\alpha}, \alpha = s,l,a$ vanish when the solid phase is isotropic. $\boldsymbol{A}^n$ and $\boldsymbol{H}^s$ are not functions of $\overset{(n)s}{\overline{\boldsymbol{C}}}$ and ∇T. The quantity $\boldsymbol{B}^{\alpha}, \alpha = l,a$ are fourth rank positive semi-definite tensors accounting for the viscous dissipation in the liquid and air phase. M^s and M^l in Equations (2.79) and (2.80) are material coefficients resulting from the Taylor expansion. In Equations (2.81) and (2.82), $\boldsymbol{R}^l$ and $\boldsymbol{R}^a$ are second rank tensors arising from the Taylor series expansion and represent resistance to the liquid and air flow. $\boldsymbol{K}^{\alpha}$ in Equation (2.83) denotes a second rank tensor.

2.2.6 Darcy's law

We substitute Equation (2.81) into the linear momentum balance equation (A.12) with $\alpha = l$ and we neglect the inertia term. Simplifying, we obtain Darcy's law for the liquid phase as:

$$\begin{aligned}\boldsymbol{R}^l\boldsymbol{v}^{l,s} = &-\varepsilon^l\nabla p^l - \varepsilon^l\rho^l\frac{\partial A^l}{\partial \varepsilon^l}\nabla\varepsilon^l - \varepsilon^l\rho^l\frac{\partial A^l}{\partial \varepsilon^s}\nabla\varepsilon^s - \varepsilon^l\rho^l\frac{\partial A^l}{\partial \overline{\boldsymbol{C}}^s}:\nabla\overline{\boldsymbol{C}}^s - \varepsilon^l\rho^l\sum_{n=1}^{q}\frac{\partial A^l}{\partial \overline{\boldsymbol{C}}^{(n)s}}:\nabla\overline{\boldsymbol{C}}^{(n)s} \\ &-\varepsilon^l\rho^l\sum_{m=1}^{p}\frac{\partial A^l}{\partial \boldsymbol{\varepsilon}^{(m)l}}\nabla\boldsymbol{\varepsilon}^{(m)l} + \nabla\cdot(\varepsilon^l\boldsymbol{B}^l:\boldsymbol{d}^l) + \nabla\cdot(\varepsilon^l\boldsymbol{H}^l:\nabla T) + \varepsilon^l\rho^l\boldsymbol{g}\end{aligned} \tag{2.84}$$

The first term on the right hand side is the primary driving force in classical Darcy's law for non-swelling media. This term represents flow due to a negative pressure gradient. The second and third terms denote flow due to the gradient of the volume fraction of the fluid and solid phases respectively. The fourth term on the right hand side was presented in Weinstein et al. (2008a) [127]. The fourth and fifth terms were also first presented in Weinstein and Bennethum (2006) [126]. These terms are responsible for flow due to the effect of rate of shear on the free energy of the fluid. At moderate to high moisture content, as the solid phase alters the liquid free energy only through the normal component, these terms could be neglected. As ε^l is related to the normal component of the strain of the solid phase, the sixth term on the right hand side represents the effect of the rate of expansion on the free energy of the fluid. The seventh term on the right hand side is Brinkman's correction and is always neglected at

slow velocity flows. The eighth term on the right hand side was first mentioned in Singh et al. (2003b) [108] and it represents flow due to thermal gradient in anisotropic materials. The last term represents gravity as a driving force.

2.3 Conclusions

Unsaturated flow in porous materials with non-linear viscoelastic deformation has a wide range of applications in biomedical and agricultural engineering. Previous studies to incorporate both the physics-transport and non-linear viscoelastic deformation are mostly empirical with “moisture expansion coefficient” or experimentally fitted parameters. In some fundamental theories previously developed, the solid is assumed to be elastic or only short memories are considered. Complexities and difficulties arise when modeling unsaturated swelling systems in a three-scale Hybrid Mixture Theory.

Based on Hybrid Mixture Theory, a two-scale thermomechanical theory is developed here starting from macroscopic conservation equations that are averaged from smaller scales. A set of independent variables are chosen to represent an unsaturated swelling porous material that exhibit viscoelastic large deformation in transport processes. Restrictions on the constitutive relations are investigated from the second law of thermodynamics.

The major contribution of this work is the development of a two-scale mathematical framework to study unsaturated swelling porous systems with coupled effects of moisture transport and non-linear viscoelastic deformation.

CHAPTER 3

A MODEL FOR FLOW AND DEFORMATION IN UNSATURATED SWELLING POROUS SYSTEMS UNDER ISOTHERMAL CONDITIONS

3.1 Introduction

Porous materials consist of a hierarchical of scales. Many phenomena that are observed in higher scales are results of interactions of constituents in different spatial scales. Deformation of the porous matrix causes relaxation of the material, which plays an important role on fluid transport when the time scale of relaxation is of the same order as that of diffusion. The interaction between the solid and the vicinal fluid (See Figure 1.2) at smaller scales affects and lowers the free energy of the vicinal fluid, which in turn causes the flow of fluid between the bulk phase and the vicinal fluid phase. This eventually causes the swelling of the material (Singh 2002) [106]. Fundamental based models that are developed based on the Hybrid Mixture Theory that incorporate these effects include Singh 2002 [106]. In all other works that are based on the Hybrid Mixture Theory, the effect of relaxation on fluid transport is not captured. However, in Singh's work [106], the system is essentially saturated and the deformation of the solid can be assumed to be fully compensated by fluid gain/loss and thus solution of the solid linear momentum balance equation is not necessary. Here, we develop a continuum thermodynamics based approach to include the effect of fluid transport and viscoelastic relaxation on each other for an unsaturated swelling porous system.

In this chapter, a two-scale transport model is developed based on the thermomechanical theory presented in chapter 2 for an unsaturated swelling porous system that exhibits viscoelastic large deformations in a transport process. The model is developed using the conservation laws listed in Appendix A and the constitutive relationships developed in chapter 2. The focus is on the combination of the mass conservation of the fluid phase with the modified Darcy's law, exploitation of the driving force in the linear momentum balance equation by relating the momentum transported from all other phases to the pressures and derivation of an explicit form of the constitutive relationship between the solid stress and strain using a neo-Hookean model. In this model, we assume isothermal conditions. Both the liquid phase and the solid skeleton are assumed to be isotropic and incompressible, while the "smeared-out" solid is compressible due to uptake/release of fluids. The effect of gravity is ignored.

3.2 Model Development: Solid Phase

After ignoring the inertial terms, linear momentum balance (A.12) for the solid phase is given by:

$$\nabla \cdot (\varepsilon^s \boldsymbol{t}^s) = -\sum_{\beta \neq s} \hat{\boldsymbol{T}}_s^{\beta} \tag{3.1}$$

Since there is no mass transfer from other phases to the solid phase, summing over all N species, the restriction (A.18) becomes:

$$-\sum_{\beta \neq s} \hat{\boldsymbol{T}}_s^{\beta} = \sum_{\beta \neq l} \hat{\boldsymbol{T}}_l^{\beta} + \sum_{\beta \neq a} \hat{\boldsymbol{T}}_a^{\beta} \tag{3.2}$$

We substitute Equation (2.84) into Equation (2.81) and obtain:

$$\sum_{\beta \neq l} \hat{\boldsymbol{T}}_l^{\beta} = \nabla(\varepsilon^l p^l) \tag{3.3}$$

And similarly, the following is obtained when the air phase is considered:

$$\sum_{\beta \neq a} \hat{\boldsymbol{T}}_a^{\beta} = \nabla(\varepsilon^a p^a) \tag{3.4}$$

With Equations (3.2), (3.3) and (3.4), linear momentum balance of the solid phase is finally given by:

$$\nabla \cdot (\varepsilon^s \boldsymbol{t}^s) = \nabla(\varepsilon^l p^l) + \nabla(\varepsilon^a p^a) \tag{3.5}$$

The right hand side of the above equation has the linear momentum transported from the liquid and the air phases, to the solid phase, respectively. This indicates that the negative pressure gradient and the negative concentration gradient are the volumetric driving forces of the deformation. Since isotropy is assumed, the last term of Equation (2.76) vanishes and the constitutive relationship between the Cauchy stress tensor and the strain becomes:

$$\varepsilon^s \boldsymbol{t}^s = -\varepsilon^s p^s \boldsymbol{I} + \boldsymbol{t}^{sh} + \boldsymbol{t}^{se} + \sum_{n=1}^{q} \overline{\boldsymbol{F}}^s A^n : \overline{\overline{\boldsymbol{C}}}^{(n)s} (\overline{\boldsymbol{F}}^s)^T \tag{3.6}$$

Since the solid phase is assumed to be isotropic, the energy is a function of the strain invariants (Ogden 1984) [84].

$$A(I_1, I_2, I_3) = A(\bar{I}_1, \bar{I}_2, J^s) \tag{3.7}$$

where $I_k, k = 1,2,3$ are the principal invariants of $\boldsymbol{C}^s$ and the ones with bars denote the principal invariants of $\overline{\boldsymbol{C}}^s$. They are related by:

$$\bar{I}_k = (J^s)^{-\frac{2}{3}} I_k, k = 1,2 \tag{3.8}$$

For simplicity, we assume that the material is of the Neo-Hookean type. The modified form of the free energy to account for compressibility is given by (Treloar 1943a, b; Holzapfel 2000) [117-118,54]:

$$\varepsilon^\alpha \rho^\alpha A^\alpha = \varepsilon_0^\alpha \rho^\alpha A_0^\alpha + \frac{\mu_\alpha}{2}(\bar{I}_1 - 3) + \frac{1}{d_\alpha}(J^s - 1)^2, \alpha = s, l \tag{3.9}$$

where we only list terms related to $\overline{\boldsymbol{C}}^s$. $A_0^\alpha = A^\alpha(\varepsilon_0^\alpha)$ is the free energy evaluated at the initial volume fraction. μ_α is the initial shear modulus of the α phase while d_α is related to the initial bulk modulus of the α phase K^α by:

$$\frac{2}{d_\alpha} = K^\alpha, \alpha = s, l \tag{3.10}$$

To express (3.6) and write out the Cauchy stress as an explicit function of the strain, we take the partial derivative of A^α with respect to $\overline{\boldsymbol{C}}^s$ using the chain rule:

$$\frac{\partial A^\alpha}{\partial \overline{\boldsymbol{C}}^s} = \frac{\partial A^\alpha}{\partial \bar{I}_1}\frac{\partial \bar{I}_1}{\partial \overline{\boldsymbol{C}}^s} + \frac{\partial A^\alpha}{\partial J^s}\frac{\partial J^s}{\partial \overline{\boldsymbol{C}}^s} = \frac{\mu_\alpha}{2}\boldsymbol{I} + \frac{2}{d_\alpha}(J^s - 1)\frac{\partial J^s}{\partial \overline{\boldsymbol{C}}^s} \tag{3.11}$$

where

$$\frac{\partial J^s}{\partial \overline{\boldsymbol{C}}^s} = \frac{\partial J^s}{\partial \overline{\boldsymbol{C}}^s}\frac{\partial \overline{\boldsymbol{C}}^s}{\partial \overline{\boldsymbol{C}}^s} = \frac{1}{2} J^s (\overline{\boldsymbol{C}}^s)^{-1} : \boldsymbol{L} \tag{3.12}$$

where we have used the identity:

$$\frac{\partial det(\cdot)}{\partial(\cdot)} = det(\cdot)(\cdot)^{-1} \tag{3.13}$$

and the fact that:

$$J^s = \sqrt{det\boldsymbol{C}^s} \tag{3.14}$$

In Equation (3.12), $\boldsymbol{L}$ is a fourth rank tensor and its inverse is given by (Simo and Hughes 1997) [105]:

$$\frac{\partial \overline{\boldsymbol{C}}^s}{\partial \boldsymbol{C}^s} = (J^s)^{-\frac{2}{3}}[\boldsymbol{I} - \frac{1}{3}\boldsymbol{C}^s \otimes (\boldsymbol{C}^s)^{-1}] \tag{3.15}$$

The Terzaghi and hydration stresses become:

$$\begin{aligned} \boldsymbol{t}^{se} = \quad & 2\{\frac{\mu_s}{2}\overline{\boldsymbol{F}}^s(\overline{\boldsymbol{F}}^s)^T + \frac{K^s}{2}J^s(J^s-1)\overline{\boldsymbol{F}}^s[(\boldsymbol{C}^s)^{-1}:\boldsymbol{L}](\overline{\boldsymbol{F}}^s)^T \\ & -\frac{1}{3}\frac{\mu_s}{2}tr(\overline{\boldsymbol{C}}^s)\boldsymbol{I} - \frac{K^s}{6}J^s(J^s-1)[(\boldsymbol{C}^s)^{-1}:\boldsymbol{L}:\overline{\boldsymbol{C}}^s]\boldsymbol{I}\} \end{aligned} \tag{3.16}$$

$$\begin{aligned} \boldsymbol{t}^{sh} = \quad & 2\{\frac{\mu_l}{2}\overline{\boldsymbol{F}}^s(\overline{\boldsymbol{F}}^s)^T + \frac{K^l}{2}J^s(J^s-1)\overline{\boldsymbol{F}}^s[(\boldsymbol{C}^s)^{-1}:\boldsymbol{L}](\overline{\boldsymbol{F}}^s)^T \\ & -\frac{1}{3}\frac{\mu_l}{2}tr(\overline{\boldsymbol{C}}^s)\boldsymbol{I} - \frac{K^l}{6}J^s(J^s-1)[(\boldsymbol{C}^s)^{-1}:\boldsymbol{L}:\overline{\boldsymbol{C}}^s]\boldsymbol{I}\} \end{aligned} \tag{3.17}$$

The pressure p^s is given by:

$$p^s = -\rho^s J^s \frac{\partial A^s}{\partial J^s} = -\frac{K^s}{\varepsilon_0^s}(J^{s^3} - J^{s^2}) \tag{3.18}$$

Finally, the Cauchy stress tensor is given by:

$$
\begin{aligned}
\boldsymbol{\varepsilon}^s \boldsymbol{t}^s = \; & \frac{K^s}{\varepsilon_0^s}(J^{s3} - J^{s2})\boldsymbol{I} \\
& + \mu_s \overline{\boldsymbol{F}}^s (\overline{\boldsymbol{F}}^s)^T + K^s (J^{s2} - J^s)\overline{\boldsymbol{F}}^s [(\boldsymbol{C}^s)^{-1} : L](\overline{\boldsymbol{F}}^s)^T \\
& - \frac{\mu_s}{3} tr(\overline{\boldsymbol{C}}^s)\boldsymbol{I} - \frac{K^l}{3}(J^{s2} - J^s)[(\boldsymbol{C}^s)^{-1} : \boldsymbol{L} : \overline{\boldsymbol{C}}^s]I \\
& + \mu_l \overline{\boldsymbol{F}}^s (\overline{\boldsymbol{F}}^s)^T + K^l (J^{s2} - J^s)\overline{\boldsymbol{F}}^s [(\boldsymbol{C}^s)^{-1} : \boldsymbol{L}](\overline{\boldsymbol{F}}^s)^T \\
& - \frac{\mu_l}{3} tr(\overline{\boldsymbol{C}}^s)\boldsymbol{I} - \frac{K^l}{3}(J^{s2} - J^s)[(\boldsymbol{C}^s)^{-1} : \boldsymbol{L} : \overline{\boldsymbol{C}}^s]I \\
& + \overline{\boldsymbol{F}}^s \int_0^t \boldsymbol{G}(t-\tau) : \overline{\boldsymbol{C}}^s d\tau (\overline{\boldsymbol{F}}^s)^T
\end{aligned}
\tag{3.19}
$$

where the last term is obtained by using the Laplace transform technique on the last term in Equation (3.6). This procedure is explained below.

We first note that the relationship between the Cauchy stress tensor $\boldsymbol{t}^s$ and the second Piola-Kirchhoff stress tensor $\boldsymbol{S}^s$ is given by:

$$
\boldsymbol{S}^s = J^s \boldsymbol{F}^{s-1} \boldsymbol{t}^s \boldsymbol{F}^{s-T} \tag{3.20}
$$

Using Equation (3.20) and Equation (2.3), we convert the last term in Equation (3.6), $\sum_{n=1}^{q} \overline{\boldsymbol{F}}^s \boldsymbol{A}^n : \overset{(n)s}{\overline{\boldsymbol{C}}} (\overline{\boldsymbol{F}}^s)^T$, into the corresponding second Piola-Kirchhoff counterpart:

$$
J^{s-1/3} \boldsymbol{\varepsilon}^s \boldsymbol{S}^{vs} = \sum_{n=1}^{q} \boldsymbol{A}^n : \overset{(n)s}{\overline{\boldsymbol{C}}} \tag{3.21}
$$

Then as $\boldsymbol{A}^n$ is not a function of $\overset{(n)s}{\overline{\boldsymbol{C}}}$, it is possible that we take the Laplace transform of the above equation:

$$
L(J^{s-1/3} \boldsymbol{\varepsilon}^s \boldsymbol{S}^{vs}) = \sum_{n=1}^{q} s^{n-1} \boldsymbol{A}^n : \overline{\boldsymbol{C}}^s s \tag{3.22}
$$

The inverse transform of the above is then given by:

$$J^{s-1/3}\boldsymbol{\varepsilon}^s \boldsymbol{S}^{vs} = \int_0^t \sum_{n=1}^{q} \frac{d^{n-1}}{dt^{n-1}} \delta(t-\tau)\boldsymbol{A}^n : \overline{\boldsymbol{C}}^s d\tau \tag{3.23}$$

where $\delta(t)$ is the Dirac's delta function. Let

$$\boldsymbol{G}(t) \equiv \sum_{n=1}^{q} \boldsymbol{A}^n \frac{d^{n-1}}{dt^{n-1}} \delta(t) \tag{3.24}$$

where $\boldsymbol{G}$ is the relaxation function in shear. Equation (3.23) becomes:

$$J^{s-1/3}\boldsymbol{\varepsilon}^s \boldsymbol{S}^{vs} = \int_0^t \boldsymbol{G}(t-\tau) : \overline{\boldsymbol{C}}^s d\tau \tag{3.25}$$

The above is then converted back to the Cauchy form and the last term in Equation (3.19) is obtained.

3.3 Model Development: Liquid Phase

Mass conservation of the liquid phase is given by Equation (A.2). We assume there is no exchange of mass with other phases, so that the right hand side of this equation vanishes and the equation becomes:

$$\frac{D^l(\varepsilon^l \rho^l)}{Dt} + \varepsilon^l \rho^l (\nabla \cdot \boldsymbol{v}^l) = 0 \tag{3.26}$$

Since relative velocity appears in Darcy's law, we rewrite Equation (3.26) as:

$$\dot{\varepsilon}^l + \nabla \cdot (\varepsilon^l \boldsymbol{v}^{l,s}) + \varepsilon^l \nabla \cdot \boldsymbol{v}^s = 0 \tag{3.27}$$

We rewrite Darcy's law (2.84) as:

$$\begin{aligned}\boldsymbol{v}^{l,s} = \quad & (\boldsymbol{R}^l)^{-1}[-\varepsilon^l \nabla p^l - \varepsilon^l \rho^l \frac{\partial A^l}{\partial \varepsilon^l} \nabla \varepsilon^l - \varepsilon^l \rho^l \frac{\partial A^l}{\partial \varepsilon^s} \nabla \varepsilon^s - \varepsilon^l \rho^l \frac{\partial A^l}{\partial \overline{\boldsymbol{C}}^s} : \nabla \overline{\boldsymbol{C}}^s \\ & -\varepsilon^l \rho^l \sum_{n=1}^{q} \frac{\partial A^l}{\partial \overset{(n)s}{\overline{\boldsymbol{C}}}} : \nabla \overset{(n)s}{\overline{\boldsymbol{C}}} - \varepsilon^l \rho^l \sum_{m=1}^{p} \frac{\partial A^l}{\partial \overset{(m)l}{\varepsilon}} \nabla \overset{(m)l}{\varepsilon}]\end{aligned} \tag{3.28}$$

We assume that the term $\varepsilon^s \rho^s \frac{\partial A^s}{\partial \varepsilon^l}$ and the term $\varepsilon^a \rho^a \frac{\partial A^a}{\partial \varepsilon^l}$ can be neglected in the capillary pressure result (2.79). The first term is neglected since layers of fluid molecules do not exert stress on molecules of the solid phase when the moisture content is not very low, i.e., when the moisture content is larger than that occupied by 10 fluid monolayers (Bennethum et al. 1997) [22]. The second term is ignored if we assume that the free energy of the air phase does not depend on the volume fraction of the liquid phase since the two phases interact only through the boundaries. Then:

$$-\pi^l - p^l + p^a = -M^l \dot{\varepsilon}^l \tag{3.29}$$

where

$$\pi^l = -\varepsilon^l \rho^l \frac{\partial A^l}{\partial \varepsilon^l} \tag{3.30}$$

is the swelling pressure. This definition is consistent with that in Achanta and Cushman (1994) [3]. The negative sign takes into account the fact that fluid flows from regions of high swelling pressure to regions of low swelling pressure. Then Equation (3.28) can be written as:

$$\begin{aligned}\boldsymbol{v}^{l,s} = \quad & (\boldsymbol{R}^l)^{-1}[-\varepsilon^l \nabla(-\pi^l + p^a + M^l \dot{\varepsilon}^l) + \pi^l \nabla \varepsilon^l - \varepsilon^l \rho^l \frac{\partial A^l}{\partial \varepsilon^s} \nabla \varepsilon^s \\ & -\varepsilon^l \rho^l \frac{\partial A^l}{\partial \overline{\boldsymbol{C}}^s} : \nabla \overline{\boldsymbol{C}}^s - \varepsilon^l \rho^l \sum_{n=1}^{q} \frac{\partial A^l}{\partial \overset{(n)s}{\overline{\boldsymbol{C}}}} : \nabla \overset{(n)s}{\overline{\boldsymbol{C}}} - \varepsilon^l \rho^l \sum_{m=1}^{p} \frac{\partial A^l}{\partial \overset{(m)l}{\varepsilon}} \nabla \overset{(m)l}{\varepsilon}]\end{aligned} \tag{3.31}$$

Simplifying Equation (3.31), we obtain:

$$\begin{aligned}\boldsymbol{v}^{l,s} = \quad & (\boldsymbol{R}^l)^{-1}[-\nabla(p^a-\pi^l)\varepsilon^l-\varepsilon^l\nabla(M^l\dot{\varepsilon}^l)-p^a\nabla\varepsilon^a-\varepsilon^l\rho^l\frac{\partial A^l}{\partial\overline{\boldsymbol{C}}^s}:\nabla\overline{\boldsymbol{C}}^s \\ & -\varepsilon^l\rho^l\sum_{n=1}^{q}\frac{\partial A^l}{\partial\overset{(n)s}{\overline{\boldsymbol{C}}}}:\nabla\overset{(n)s}{\overline{\boldsymbol{C}}}-\varepsilon^l\rho^l\sum_{m=1}^{p}\frac{\partial A^l}{\partial\overset{(m)l}{\varepsilon}}\nabla\overset{(m)l}{\varepsilon}\,]\end{aligned} \tag{3.32}$$

Here we have used Equation (2.80). We assumed that M^s is zero since it denotes the viscosity. In this case, the swelling pressure reduces to capillary pressure considering the relationship between swelling pressure and capillary pressure in Achanta and Cushman (1994) [3]. Substituting Equation (3.32) into (3.27), we obtain:

$$\begin{aligned}&\dot{\varepsilon}^l+\nabla\cdot\{\varepsilon^l(\boldsymbol{R}^l)^{-1}[-\nabla(p^a-\pi^l)\varepsilon^l-\varepsilon^l\nabla(M^l\dot{\varepsilon}^l)-p^a\nabla\varepsilon^a-\varepsilon^l\rho^l\frac{\partial A^l}{\partial\overline{\boldsymbol{C}}^s}:\nabla\overline{\boldsymbol{C}}^s \\ &-\varepsilon^l\rho^l\sum_{n=1}^{q}\frac{\partial A^l}{\partial\overset{(n)s}{\overline{\boldsymbol{C}}}}:\nabla\overset{(n)s}{\overline{\boldsymbol{C}}}-\varepsilon^l\rho^l\sum_{m=1}^{p}\frac{\partial A^l}{\partial\overset{(m)l}{\varepsilon}}\nabla\overset{(m)l}{\varepsilon}\,]\}+\varepsilon^l\nabla\cdot\boldsymbol{v}^s=0\end{aligned} \tag{3.33}$$

We assume that the resistivity tensor $\boldsymbol{R}^l$ is isotropic. The above equation can then be written as:

$$\begin{aligned}&\dot{\varepsilon}^l+\nabla\cdot\{\varepsilon^l\frac{k^l}{\mu^l}\boldsymbol{I}[-E^l\nabla\varepsilon^l-\varepsilon^l\nabla(M^l\dot{\varepsilon}^l)-p^a\nabla\varepsilon^a-\varepsilon^l\rho^l\frac{\partial A^l}{\partial\overline{\boldsymbol{C}}^s}:\nabla\overline{\boldsymbol{C}}^s \\ &-\varepsilon^l\rho^l\sum_{n=1}^{q}\frac{\partial A^l}{\partial\overset{(n)s}{\overline{\boldsymbol{C}}}}:\nabla\overset{(n)s}{\overline{\boldsymbol{C}}}-\varepsilon^l\rho^l\sum_{m=1}^{p}\frac{\partial A^l}{\partial\overset{(m)l}{\varepsilon}}\nabla\overset{(m)l}{\varepsilon}\,]\}+\varepsilon^l\nabla\cdot\boldsymbol{v}^s=0\end{aligned} \tag{3.34}$$

where

$$\frac{k^l}{\mu^l}\boldsymbol{I}=(\boldsymbol{R}^l)^{-1} \tag{3.35}$$

with k^l the permeability and μ^l the viscosity of the liquid phase. We have defined

$$E^l\equiv-\frac{\partial(\pi^l\varepsilon^l)}{\partial\varepsilon^l} \tag{3.36}$$

Notice here that the gradient of the air pressure vanishes. We also define

$$D \equiv \frac{\varepsilon^l k^l}{\mu^l} E^l \tag{3.37}$$

which is the Darcian diffusion coefficient. Equation (3.34) is further simplified to:

$$\begin{aligned} &\dot{\varepsilon}^l - \nabla \cdot (D \nabla \varepsilon^l) - \nabla \cdot \{ \varepsilon^l \frac{k^l}{\mu^l} \boldsymbol{I} [\varepsilon^l \nabla (M^l \dot{\varepsilon}^l) + p^a \nabla \varepsilon^a - \varepsilon^l \rho^l \frac{\partial A^l}{\partial \overline{\boldsymbol{C}}^s} : \nabla \overline{\boldsymbol{C}}^s \\ &+ \varepsilon^l \rho^l \sum_{n=1}^{q} \frac{\partial A^l}{\partial \overset{(n)s}{\underline{\boldsymbol{C}}}} : \nabla \overset{(n)s}{\underline{\boldsymbol{C}}} + \varepsilon^l \rho^l \sum_{m=1}^{p} \frac{\partial A^l}{\partial \overset{(m)l}{\varepsilon}} \nabla \overset{(m)l}{\varepsilon}] \} + \varepsilon^l \nabla \cdot \boldsymbol{v}^s = 0 \end{aligned} \tag{3.38}$$

We assume that the free energy of the liquid phase A^l is linear in both $\overset{(m)l}{\varepsilon}, m = 1,..., p$ and $\overset{(n)s}{\underline{\boldsymbol{C}}}$,n=1,...,q, and initially the material is free of strain and all its material time derivatives. We use the Laplace transform method and merge the term $\nabla(M^l \dot{\varepsilon}^l)$ into the term $\varepsilon^l \rho^l \frac{\partial A^l}{\partial \overset{(m)l}{\varepsilon}} \nabla \overset{(m)l}{\varepsilon}$. The details of the discussion can be found in Singh et al. (2003b) [108]. Here we also assume that the air pressure is constant. We thus obtain a differential-integral form of the fluid transport equation:

$$\begin{aligned} &\dot{\varepsilon}^l - \nabla \cdot (D \nabla \varepsilon^l) - \nabla \cdot [\varepsilon^l \frac{k^l}{\mu^l} p^a \nabla \varepsilon^a + \varepsilon^l \frac{k^l}{\mu^l} \varepsilon^l \rho^l \frac{\partial A^l}{\partial \overline{\boldsymbol{C}}^s} : \nabla \overline{\boldsymbol{C}}^s \\ &+ \int_0^t \boldsymbol{B}(t-\tau) (\nabla \dot{\varepsilon}^l) d\tau + \int_0^t \boldsymbol{S}(t-\tau) : \nabla \overline{\boldsymbol{C}}^s d\tau] + \varepsilon^l \nabla \cdot \boldsymbol{v}^s = 0 \end{aligned} \tag{3.39}$$

where we follow Singh et al. (2003b) [108] and postulate that $\boldsymbol{B}(t)$ and $\boldsymbol{S}(t)$ are related to the bulk and shear relaxation functions respectively. According to Equation (3.9), we work on the third term and obtain the transport equation:

$$\begin{aligned} &\dot{\varepsilon}^l - \nabla \cdot (D \nabla \varepsilon^l) - \nabla \cdot \{ \varepsilon^l \frac{k^l}{\mu^l} p^a \nabla \varepsilon^a + \varepsilon^l \frac{k^l}{\mu^l} [\frac{\mu_l}{2} \boldsymbol{I} + \frac{K_l}{2} J^s (J^s - 1) \overline{\boldsymbol{C}}^{s-1} : \boldsymbol{L}] : \nabla \overline{\boldsymbol{C}}^s \\ &+ \int_0^t \boldsymbol{B}(t-\tau) (\nabla \dot{\varepsilon}^l) d\tau + \int_0^t \boldsymbol{S}(t-\tau) : \nabla \overline{\boldsymbol{C}}^s d\tau \} + \varepsilon^l \nabla \cdot \boldsymbol{v}^s = 0 \end{aligned} \tag{3.40}$$

When the moisture content is moderate to high, namely, when the moisture content is larger than that occupied by 10 fluid monolayers (Bennethum et al. 1997) [22], the above is simplified to:

$$\dot{\varepsilon}^l - \nabla \cdot (D \nabla \varepsilon^l) - \nabla \cdot [\varepsilon^l \frac{k^l}{\mu^l} p^a \nabla \varepsilon^a + \int_0^t \boldsymbol{B}(t-\tau)(\nabla \dot{\varepsilon}^l) d\tau] + \varepsilon^l \nabla \cdot \boldsymbol{v}^s = 0 \qquad (3.41)$$

The transport equation is found to be coupled with the other two phases.

3.4 Summary of the Model

The unknowns of the unsaturated problem include ε^l, ε^s, $\boldsymbol{u}^s(\boldsymbol{v}^s)$, which are the volume fractions of the liquid and solid phase respectively and the displacement of the solid phase. The initial-boundary value problem is composed of the transport equation (3.40) or (3.41) for ε^l, the mass conservation for the solid phase given by (2.19) for ε^s, the linear momentum balance of the solid phase given as (3.5) for $\boldsymbol{t}^s$, and appropriate boundary and initial conditions. We also need the constitutive relationship for the Cauchy stress and the strain given by (3.19) and the nonlinear strain-displacement relationship:

$$\boldsymbol{E}^s = \frac{1}{2}(\nabla \boldsymbol{u}^s + \nabla \boldsymbol{u}^{sT} + \nabla \boldsymbol{u}^s \nabla \boldsymbol{u}^{sT}) \qquad (3.42)$$

For a saturated system, with $\varepsilon^a = 0$, the volume fraction of the solid becomes:

$$\varepsilon^s = 1 - \varepsilon^l \qquad (3.43)$$

and J^s becomes dependent. Therefore, linear momentum balance for the solid is not needed. For such a case, only ε^l is independent, and the transport equation (3.40) or (3.41) alone, with the air phase volume fraction ε^a being zero, is sufficient to describe the behavior of the system. A material that has both saturated and unsaturated regions can potentially be more challenging, as the saturated region and the unsaturated region will have different number of independent unknowns. Possible methods to model such systems are 1) to prevent air phase volume fraction ε^a from going to zero (i.e. have non-zero residual air fraction); or 2) to track the interface between fully saturated and unsaturated regions, and have two sets of unknowns for the two regions. Both the methods have been successfully implemented to tackle corresponding phase disappearance/appearance issues in rigid porous media (Perre and Moyne 1991; Pruess 1991) [88,91].

3.5 Conclusions

By applying HMT on a two-scale system and based on the thermomechanical theory developed in chapter 2, a novel model for unsaturated swelling porous systems, with a generalized Kelvin-Voigt viscoelastic solid undergoing large deformation, has been developed in this chapter. Based on the Neo-Hookean model, we have exploited the stress-strain relationship in detail and obtained a new explicit form of the constitutive law for the solid phase. By manipulating the mass conservation equation for the liquid phase and the modified Darcy's law obtained from HMT, we have developed a

differential-integral form of the transport equation. The transport equation for the liquid is coupled with the linear momentum balance for the solid, and the momentum transported from the liquid and the air phases plays the role of the body force for the solid phase.

The model developed thus can be applied to a whole class of problems where viscoelastic large deformation occurs in a porous medium due to liquid transport. Phenomena such as transport in saturated and unsaturated systems, stresses generated, large deformation due to transport and effect of viscoelasticity of the solid on fluid transport, for example drying of gels, stress-crack predictions, soaking of foodstuffs, consolidation of clays, drug delivery, etc, hitherto either studied empirically or studied in detail individually only for simpler systems, can all be brought together under one unified framework.

CHAPTER 4

NUMERICAL IMPLEMENTATION: A FINITE ELEMENT ANALYSIS OF COUPLING BETWEEN WATER ABSORPTION AND SWELLING OF FOODSTUFFS DURING SOAKING

4.1 Introduction and Objectives

Water absorption in a porous material is an important transport phenomenon in many fields including agriculture, soil science, tissue engineering, pharmaceutical engineering and food engineering. In terms of foodstuffs, water absorption of foods involves mass transport of a liquid, e.g. water, milk or fruit juice, into them. Pasta, an important part of people's diet around the world and a major source for carbohydrates, is an example of traditional food where water absorption is of great importance before it can be consumed. For transportation and storage purposes and for longer shelf life, pasta is usually dehydrated and then rehydrated for consumption. It is important to understand the mechanism of water movement in pasta and thus investigate the quality and structure changes of pasta. Extensive research has been conducted to study soaking of foodstuffs (Sanjuan et al. 1999; Krokida et al. 2003; Marabi et al. 2003; Bilbao-Sainz et al. 2005; Meda and Ratti 2005; Saguy et al. 2005; Weerts et al. 2005; Cunningham et al. 2007, 2008; Markowski et al. 2009; Bakalis et al. 2009, etc) [101,61,73,25,75,100,124,64,32-33,70,14]. However, some of the models are empirical, i.e., the Peleg equation (Peleg 1988) [86] or the Weibull distribution

function (Weibull 1951) [125] are used to describe the sorption curves (Sopade et al. 1992; Abu-Ghannam and Mckenna 1997; Machado et al. 1999; Maskan 2001; Ruiz Diaz et al. 2003; Garcia-Pascual et al. 2005; Planinic et al. 2005) [111,1,69,72,99,46,89]. And in some studies, empirical factors are brought into the mathematical models. For example, in some models, Fick's Second Law of Diffusion is used to describe the sorption behavior where an experimentally fitted effective diffusivity is normally used. This is either constant or dependent on the moisture content. In addition, in most of the studies, another important phenomenon, swelling that takes place simultaneously with water absorption in foodstuffs, is often not taken care of appropriately. For example, the influence of swelling and the viscoelastic nature of the food matrix on the liquid transport is often lumped into experimentally fitted parameters, or, the food matrix is assumed to be rigid. As most food materials are porous in nature, with a solid food skeleton with fluid or gas filled pores, it is necessary to consider a porous medium approach to study soaking of food as fluid transport in a porous material that can swell during the soaking process. In addition, in many applications, products to be soaked have been dehydrated. Thus, in a soaking process, the food material can be unsaturated initially, i.e., the pores of the porous food matrix are only partially filled with fluids. In order to capture the unsaturated characteristic of the soaking process, a theoretical model, which describes appropriately the kinetics of liquid transport in a viscoelastic food material that is unsaturated/saturated during soaking, and investigations on the swelling behavior of the food matrix during soaking, is needed for understanding of the fundamental

characteristics of the soaking processes of a food material. Thus, the objectives of this study are the following:

1. To apply the mathematical model developed in chapter 3 (Zhu et al. 2010) [133] and study non-empirically the two way coupled moisture transport in plane sheet pasta and swelling of the pasta sample during soaking.

2. To develop a finite element based model and investigate the effect of viscoelasticity on the moisture transport during soaking of pasta; and predict the stresses and size change of a pasta sample after soaking.

4.2 Problem Description and the Mathematical Model

In this section, the problem is described and a mathematical model based on the thermomechanical theory presented in chapter 2 as well as the model developed in chapter 3 is also introduced.

4.2.1 Problem description

Soaking tests for pasta have been conducted by Cafieri et al. (2008) [27]. Several different shapes of dehydrated pasta samples were used in their study. They were cooked and overcooked in boiling distilled water (100 ± 0.6^0 C). Sample weights were measured at various times during the cooking process (Cafieri et al. 2008) [27]. Here we only consider pasta with plane sheet shape ("lasagna"). The samples were 40 mm

long and 6 mm wide with a thickness of 0.5 mm (Cafieri et al. 2008) [27]. Here we use the mathematical model presented in chapter 3 to study this moisture transport process into plane sheet pasta across its thickness and the swelling behavior of the material. One dimensional geometry is considered. It is assumed that there are three phases in the system: water as a liquid phase, the solid phase and air phase. Phase transition of water is not considered in this study.

4.2.2 Governing Equations

Here we assume that the moisture content is moderate to high and thus for transport, Equation (3.41) is used:

$$\dot{\varepsilon}^l - \nabla_x \cdot (D\nabla_x \varepsilon^l) - \nabla_x \cdot \left[-\varepsilon^l \frac{k^l}{\mu} p^a \nabla_x \varepsilon^s + \int_0^t \boldsymbol{B}(t-\tau)(\nabla_x \dot{\varepsilon}^l) d\tau \right] + \varepsilon^l \nabla_x \cdot \boldsymbol{v}^s = 0 \qquad (4.1)$$

where ε^l denotes the volume fraction of water, D is the coefficient of diffusion, k^l is permeability, μ is viscosity of water, p^a is the pressure in the air phase, ε^s is the volume fraction of the solid phase, $\boldsymbol{B}$ is a function of time and is related to the viscoelastic parameters of the material as was discussed in Zhu et al. (2010) [133], $\boldsymbol{v}^s$ is the velocity of the solid phase. Time derivatives in Equation (4.1) follow the velocity of the solid phase:

$$\dot{(\cdot)} = \frac{D^s(\cdot)}{Dt} = \frac{\partial(\cdot)}{\partial t} + \boldsymbol{v}^s \cdot \nabla(\cdot) \qquad (4.2)$$

For the solid phase, linear momentum balance is given as (Equation (3.90) in Zhu et al. 2010) [133]:

$$\nabla_x \cdot (\varepsilon^s \boldsymbol{t}^s) = \nabla_x (\varepsilon^l p^l) + \nabla_x (\varepsilon^a p^a) \tag{4.3}$$

where $\boldsymbol{t}^s$ is the Cauchy stress of the solid phase, p^l is the liquid pressure and ε^a denotes the volume fraction of the air phase. Here, to consider this problem in 1 dimension, plane stress condition is assumed. The primary variables in the governing Equations (4.1) and (4.3) include the volume fraction of water ε^l and the displacement vector of the solid phase $\boldsymbol{u}^s$, where the displacement vector of the solid phase $\boldsymbol{u}^s$ is related to the velocity of the solid phase $\boldsymbol{v}^s$ through the following:

$$\boldsymbol{v}^s = \frac{\partial \boldsymbol{u}^s}{\partial t} \tag{4.4}$$

These two equations, i.e., Equations (4.1) and (4.3), are supplemented by several relationships. The first supplemental relationship is the mass conservation of the solid phase which relates the volume fraction of the solid to the deformation:

$$\rho^s \varepsilon^s = \frac{\rho_0^s \varepsilon_0^s}{J} \tag{4.5}$$

where J is the determinant of the deformation gradient $\boldsymbol{F}$, defined by:

$$\boldsymbol{F} = \frac{\partial \boldsymbol{x}}{\partial \boldsymbol{X}} \tag{4.6}$$

with $\boldsymbol{x}$ and $\boldsymbol{X}$ being the position vectors from the deformed and undeformed configurations respectively. Please note that for simplicity, from here on we drop the superscript s and use J instead of J^s to denote the determinant of the deformation gradient. ρ^s is the true density of the solid phase and the ones with subscript 0 denote

the quantities at the initial state. With the assumption that the solid phase is incompressible, Equation (4.5) becomes:

$$\varepsilon^s = \frac{\varepsilon_0^s}{J} \tag{4.7}$$

The second supplemental relationship is the dependence of the volume fraction of air ε^a on the volume fractions of the other two phases:

$$\varepsilon^l + \varepsilon^s + \varepsilon^a = 1 \tag{4.8}$$

And the third supplemental relationship is the constitutive relationship which relates the stress tensor $\boldsymbol{t}^s$ of the solid to the deformation. This relationship is discussed in detail in the following section.

4.2.3 Constitutive relationship for the solid phase

The constitutive relationship presented in chapter 3 is general for any two dimensional or three dimensional body. When only one dimension is considered, however, the assumption that the body is elastic in dilation and viscoelastic in shear is not appropriate anymore. The reason is shown as follows.

Let the energy be written as:

$$W(\boldsymbol{C}) = \bar{W}(\bar{\boldsymbol{C}}) + U(J) \tag{4.9}$$

where *U(J)* is the volumetric contribution to the energy function while $\bar{W}(\bar{\boldsymbol{C}})$ defines the volume-preserving contribution to the energy function. We show below that the first term on the right hand side of the following relationship vanishes for one dimension:

$$\frac{\partial W}{\partial \boldsymbol{C}} = \frac{\partial \bar{W}(\bar{\boldsymbol{C}})}{\partial \bar{\boldsymbol{C}}} \frac{\partial \bar{\boldsymbol{C}}}{\partial \boldsymbol{C}} + \frac{dU(J)}{dJ} \frac{\partial J}{\partial \boldsymbol{C}} \tag{4.10}$$

When one dimensional geometry is considered, the multiplicative decomposition of the deformation gradient $\bar{\boldsymbol{F}}$ is modified as:

$$\bar{\boldsymbol{F}} = J^{-1}\boldsymbol{F} \tag{4.11}$$

since it denotes the volume-preserving part of the deformation gradient. Thus, the corresponding strain measure $\bar{\boldsymbol{C}}$ is given by:

$$\bar{\boldsymbol{C}} = J^{-2}\boldsymbol{C} \tag{4.12}$$

Then, it can be shown that:

$$\frac{\partial \bar{\boldsymbol{C}}}{\partial \boldsymbol{C}} = 0 \tag{4.13}$$

which means that the first term on the right hand side of Equation (4.10) vanishes. This leads us to make modifications to the constitutive relationship Equation (3.19). We use the following definitions to rewrite the linear momentum balance of the solid phase

$$\varepsilon^s = 1 - \phi \tag{4.14}$$

$$\varepsilon^l = S^l \phi \tag{4.15}$$

$$\varepsilon^a = S^a \phi \tag{4.16}$$

where ϕ is the porosity, and S^l and S^a are the degrees of saturation of the water and air phase, respectively. Then Equation (4.3) is written as

$$\nabla_x \cdot [(1-\phi)(\boldsymbol{t}^s + S^l p^l \boldsymbol{I} + S^a p^a \boldsymbol{I})] = \nabla_x (S^l p^l + S^a p^a) \tag{4.17}$$

Follow Gray et al. (2009) [47] and define

$$(1-\phi)(\boldsymbol{t}^s + S^l p^l \boldsymbol{I} + S^a p^a \boldsymbol{I}) = \boldsymbol{t}' \tag{4.18}$$

as the effective Cauchy stress, then Equation (4.17) becomes

$$\nabla_x \cdot \boldsymbol{t}' = \nabla_x (S^l p^l + S^a p^a) \tag{4.19}$$

This expression is equivalent to the conservation of linear momentum in terms of the total stress $\boldsymbol{t}$ as a weighted sum of the stresses in all the three phases

$$\boldsymbol{t} = \varepsilon^s \boldsymbol{t}^s + \varepsilon^l \boldsymbol{t}^l + \varepsilon^a \boldsymbol{t}^a \tag{4.20}$$

with the stress for the water and air phases being, respectively

$$\boldsymbol{t}^l = -p^l \boldsymbol{I} \tag{4.21}$$

and

$$\boldsymbol{t}^a = -p^a \boldsymbol{I} \tag{4.22}$$

Then,

$$\nabla_x \cdot \boldsymbol{t} = 0 \tag{4.23}$$

Here we postulate a constitutive relationship for the 2nd effective Piola-Kirchhoff stress tensor. We make the assumption that the viscoelastic response is in dilation and follow Simo and Hughes (1997) [105] to obtain a constitutive relationship for $\boldsymbol{S}'$, the 2nd Piola-Kirchhoff effective stress:

$$\boldsymbol{S}' = \int_0^t g(t-\tau)\frac{d}{d\tau}\left[J\frac{dU(J)}{dJ}\boldsymbol{C}^{-1} \right] d\tau \tag{4.24}$$

where $g(t)$ is the relaxation function. Let the energy function be of the form:

$$U(J) = \frac{1}{2}\kappa\left[\frac{1}{2}(J^2-1) - ln(J) \right] \tag{4.25}$$

Then Equation (4.24) can be written as:

$$\boldsymbol{S}' = \int_0^t g(t-\tau)\frac{d}{d\tau}\left[\frac{1}{2}\kappa(J^2-1)\boldsymbol{C}^{-1} \right] d\tau \tag{4.26}$$

4.2.4 Initial and boundary conditions

A schematic of the geometry under consideration is shown in Figure 4.1.

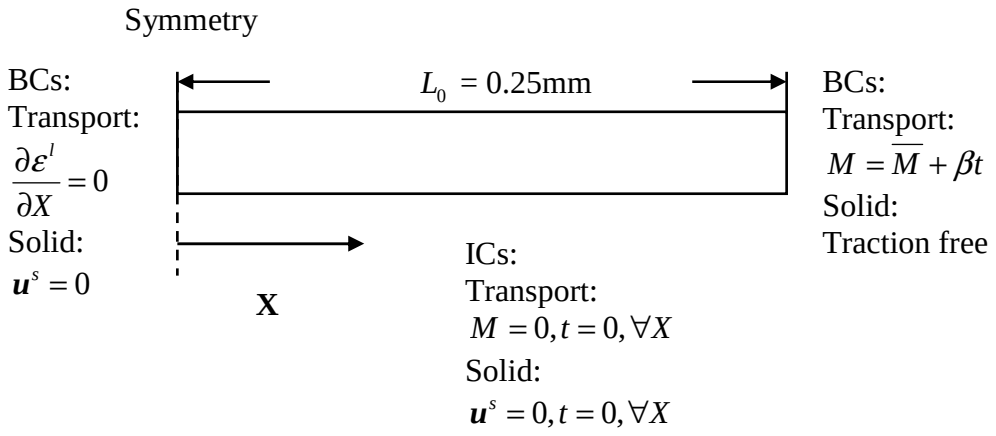

Figure 4.1: Schematic of the geometry showing symmetry, with intial and boundary conditions.

Because of symmetry, only half of the domain is considered here. The same initial and boundary conditions are used for the transport equation (4.1) in this mathematical model as were described in Cafieri et al. (2008) [27]. These conditions are:

$$M = 0, 0 \le x \le L, t = 0 \tag{4.27}$$

$$M = \overline{M} + \beta t, x = L, \forall t \tag{4.28}$$

$$\frac{\partial \varepsilon^l}{\partial x} = 0, x = 0, \forall t \tag{4.29}$$

where M is the moisture content on a dry basis and is related to the volume fraction of water ε^l through the following relationship:

$$M = \frac{\rho^l \varepsilon^l}{\rho^s \varepsilon^s} \tag{4.30}$$

Note that for the saturated case, there is no air, i.e., $\varepsilon^a = 0$.

For Equation (4.19), first we note that the effective Cauchy stress can be expressed by:

$$\boldsymbol{t}' = \boldsymbol{t} - S^l p^l \boldsymbol{I} - S^a p^a \boldsymbol{I} \tag{4.31}$$

and the surface at $X = L_0$ (Figure 4.1) is traction free in terms of the total stress, so

$$\boldsymbol{t}'|_{boundary} = -(S^l p^l \boldsymbol{I} + S^a p^a \boldsymbol{I})|_{boundary} \tag{4.32}$$

The initial condition is given by:

$$\boldsymbol{u}^s = 0, \forall x, t = 0 \tag{4.33}$$

4.3 Material Properties

All the material properties used in the simulation are discussed and listed in this section.

4.3.1 Relaxation properties

Pasta exhibits viscoelastic properties and this is mainly due to the rheological properties of gluten (Bloksma and Bushuk 1988) [26]. The viscoelastic properties of pasta has been studied by several authors in the past. For example, Lee et al. (1983) [65] used creep tests and investigated the viscoelastic behavior of Korean noodles prepared from both wheat flour and wheat flour-sweet potato starch. Dynamic viscoelastic properties of cooked white salted noodles were determined for various amylose contents by Sasaki et al. (2004) [102]. Takhar et al. (2006) [116] obtained the dynamical viscoelastic properties of pasta at different temperatures and moisture contents and observed glass transition temperatures at several moisture contents. Sozer and Dalgic (2007) [112] measured the relaxation and creep data of spaghetti of various types, including control pasta, pasta enriched with resistant starch and Bran pasta, when boiled, and expressed the relaxation data in both a one-term and a three-term Prony series. Since the temperature under which the experiments were performed in Sozer's study is the same as in our study, and the relaxation modulus as a function of moisture content was measured by them, we use their data for control pasta in this study (What they call “force” (order of (MPa)) is interpreted here as the Young's modulus. This is because the Young's modulus of pasta, from other publications, is of

the order of MPa (Stamatopoulos 1986) [114]). A constant Poisson's ratio 0.45 is assumed and it is assumed that it does not vary with different moisture contents. In the following, we calculate the bulk modulus from the Young's modulus and the Poisson's ratio, and investigate the moisture dependence of the properties.

The Laplace transform of the bulk modulus is obtained as (Christensen 2003) [30]:

$$\overline{K}(s) = \frac{\overline{E}(s)}{3(1-2s\overline{\nu})} \tag{4.34}$$

An inverse Laplace transform is performed and the bulk modulus of pasta at different moisture contents is obtained. In order to deal with the effects of moisture content on the viscoelastic properties, we use the shifting technique to obtain a master curve. $M_0 = 1.9170$ is chosen as the reference moisture content. Then the bulk modulus plotted against $ln(t)$ at an arbitrary moisture content is expressed as:

$$K(ln(t), M) = K[ln(t) + ln(a_M), M_0] \tag{4.35}$$

where a_M is the time-moisture shift factor as a function of the moisture content. We denote the “shifted time” as:

$$\xi_M = t \cdot a_M \tag{4.36}$$

Then, the bulk modulus of pasta at an arbitrary moisture content at time t is equivalent to that at the reference moisture content at the “shifted time” ξ_M. The time-moisture shift factor is found to be (Figure 4.2):

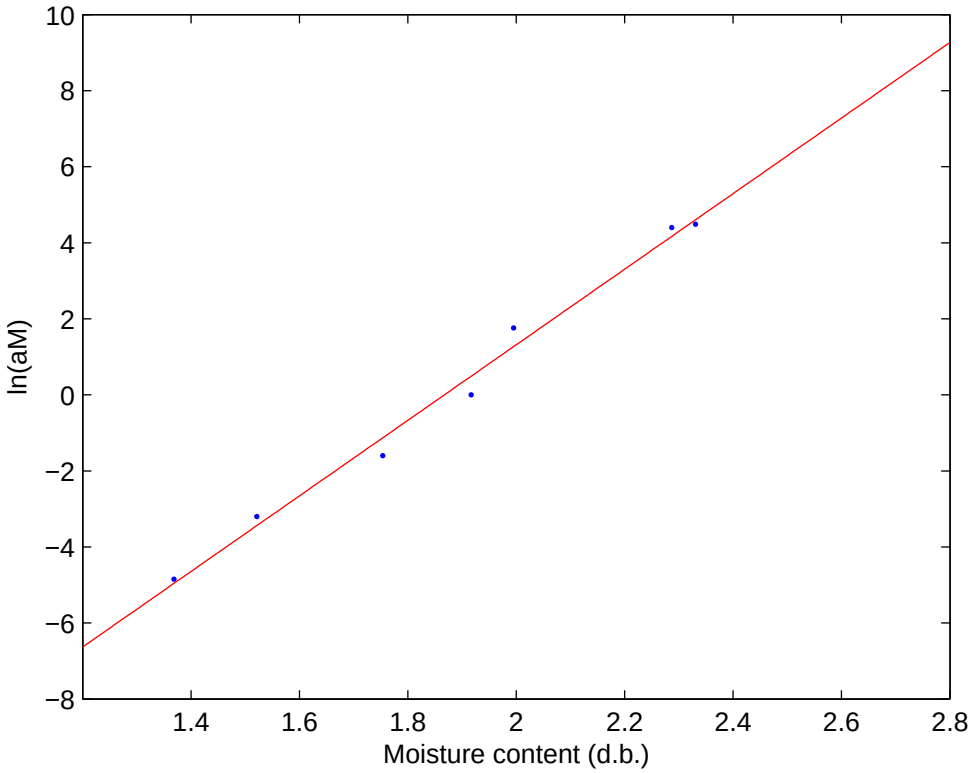

Figure 4.2: Time-moisture shift factor for pasta as analogous to time-temperature shift factor.

$$a_M = exp(9.7577M - 18.1866) \tag{4.37}$$

and the master curve is obtained as (Figure 4.3):

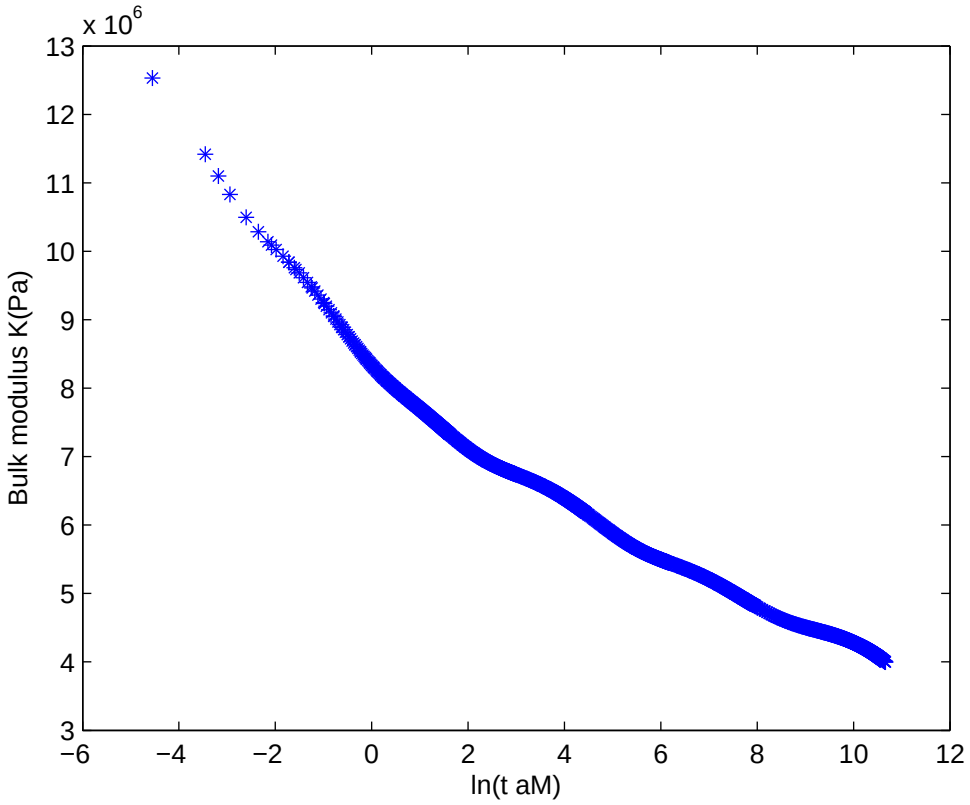

Figure 4.3: Bulk modulus of pasta as a hydro-rheologically simple material: master curve.

$$K(t,M) = \sum_{i=1}^{n_k} K_i exp(-t \cdot a_M / \tau_i) \tag{4.38}$$

where $n_k = 6$ is the number of terms in the Prony series. K_i and τ_i are listed in Table 4.1. Pasta can be considered a hydro-rheologically simple material, analogous to the concept of thermal-rheologically simple materials (Zhu et al. 2011) [134].

Table 4.1: Constants in the six-term Prony series for the bulk modulus.

K_i (Pa)	τ_i (Second)
0.6709e6	0.03
0.5312e6	0.422
0.3694e6	3.9
0.3216e6	98
0.2613e6	2000
1.1322e6	299990

4.3.2 Diffusivity coefficient D

In chapter 2, a theoretically based formulation for the diffusivity coefficient D is presented. The result is:

$$D = -\frac{\varepsilon^l k^l}{\mu}\frac{\partial(\pi^l \varepsilon^l)}{\partial \varepsilon^l} \tag{4.39}$$

where π^l is the swelling pressure defined by:

$$\pi^l = -\varepsilon^l \rho^l \frac{\partial A^l}{\partial \varepsilon^l} \tag{4.40}$$

where A^l is the Helmholtz free energy of the liquid phase. Since in this model the viscoelastic effect has been separated from the other mechanisms of the transport process, using an empirically based model for the diffusion coefficient (where all this

effect is lumped into the coefficient) is not appropriate. We use Kelvin's equation to calculate the swelling pressure and use the definition Equation (4.39) to calculate the diffusion coefficient. Kelvin's equation has been successfully used to model hydration behavior of foodstuff by Weerts et al. (2005) [124]. Here we note that, in the relationship Equation (3.114) in Zhu et al. (2010) [133]:

$$-\pi^l - p^l + p^a = -M^l \dot{\varepsilon}^l \tag{4.41}$$

the right hand side resulted from a linearization about $\dot{\varepsilon}^l$ for a state near equilibrium. In the present work, this relationship is modified to the following:

$$-\pi^l - p^l + p^a = 0 \tag{4.42}$$

There are two reasons for this modification. The first is that the right hand side in the relationship Equation (4.41) has been merged into the viscoelastic term in the derivation of the transport equation (Zhu et al. 2010) [133]. Secondly, since the Kelvin's equation is for equilibrium state, there will be a discrepancy if a near equilibrium relationship is used. Thus, the swelling pressure in this case is reduced to the capillary pressure:

$$\pi^l = p^a - p^l \equiv p^c \tag{4.43}$$

Now using Kelvin's equation (Baggio et al. 1997) [12], we obtain:

$$\pi^l = -\frac{RT}{v_l} ln(a_w) \tag{4.44}$$

Thus, D is calculated as:

$$D = \frac{\varepsilon^l k^l}{\mu} \frac{RT}{v_l} \left[ln(a_w) + \frac{\varepsilon^l}{a_w} \frac{\partial a_w}{\partial \varepsilon^l} \right] \tag{4.45}$$

where a_w is the water activity.

4.3.3 Sorption isotherms

Sorption isotherms for pasta has been obtained by several authors for different temperature and relative humidity range. For example, Lagoudaki et al. (1993) [63] obtained sorption isotherms of semolina and diet spaghetti at $22, 30, 37$ and 45^0 C. Dincer and Esin (1996) [40] obtained sorption isotherms of thin spaghetti at $30, 40, 50, 60$ and $70\ ^0$C. Arslan and Togrul (2005) [8] modelled the water sorption isotherms of macaroni stored in a chamber for temperatures $25, 35$ and 45^0 C. Erbas et al. (2005) [41] determined moisture absorption isotherms of semolina and farina at $20, 35, 50$ and 60^0 C. However, the moisture range, temperatures or pasta types in those studies are not comparable with the conditions in this study. De Temmerman et al. (2008) [37] measured desorption isotherms for pasta and expressed the water activity in the Oswin equation as a function of both moisture content and temperature. The temperature range in their work is closest to this study and thus we assume that an extrapolation in temperature can be performed and that hysteresis can be neglected. The water activity is given as (De Temmerman et al. 2008) [37]:

$$a_w = \frac{\left[\dfrac{M}{0.138-10.4\times10^{-4}T}\right]^{\frac{1}{0.396+11.6\times10^{-4}T}}}{1+\left[\dfrac{M}{0.138-10.4\times10^{-4}T}\right]^{\frac{1}{0.396+11.6\times10^{-4}T}}} \tag{4.46}$$

4.3.4 Permeability

Permeability k^l in Equation (4.39) can be expressed as a product of the intrinsic permeability k^i and the relative permeability k^r given by:

$$k^l = k^i k^r \tag{4.47}$$

The intrinsic permeability represents the permeability of water in a fully saturated state, i.e., when the pores are completely filled with water. It represents the sole effect of the matrix property via:

$$k^i = \frac{1}{8\tau}\sum_i \Delta\beta_i r_i^2 \tag{4.48}$$

where τ represents the tortuosity and $\Delta\beta_i$ is the volume fraction of pores with radius r_i (Datta 2006) [35]. Measurement of the intrinsic permeability is difficult as the dry sample is fragile. In this study, we use the value $1\times10^{-18}\,\mathrm{m}^2$ for the intrinsic permeability of pasta. This value is in the range estimated from the relationship Equation 4.48 using the information on the pore size, porosity and the tortuosity obtained by Fardet et al. (1998) [44]. The relative permeability is unity when the material is saturated. However, in this study, the material is allowed to be unsaturated, i.e., water and gas can both exist in the pores. Here we follow the widely used expression that relates the relative permeability and the degree of saturation of water:

$$k^r = (S^l)^3 \tag{4.49}$$

4.3.5 The parameter B(t)

$B(t)$ is a relaxation parameter that arises from the Laplace transform described in Zhu et al. (2010) [133]. Here we follow Singh et al. (2003b) [108] and postulate that $\boldsymbol{B}(t)$ is related to the bulk modulus of pasta through:

$$B(t) = B_c K(t) \tag{4.50}$$

Details of the discussion on this postulate can be found in Singh et al. (2003b) [108]. Here $B(t)$ is postulated to be related to the bulk modulus because it results from a term that represents the visocleastic effect in dilation on transport. Thus, $B(t)$ can be written as:

$$B(t) = B_c \sum_{i=1}^{n_k} K_i exp(-t \cdot a_M / \tau_i) \tag{4.51}$$

The constant B_c obtained by Singh et al. (2004) [110] is used in this study.

4.3.6 Other parameters

True density of the solid was measured by Porous Materials, Inc[1]. Semolina pasta samples ("lasagne") produced by Barilla (Barilla, Parma, Italy) were purchased from a local grocery store. % porosity, cumulative pore volume and % total pore volume as functions of pore diameter were measured and shown in Figures 4.4, 4.5 and 4.6. Total volume and the porosity were measured and then the initial volume fraction of the

[1]A company at Ithaca NY, USA

solid was calculated. The total porosity is found to be 11.4509% and the average pore diameter is 0.0225μ m. All the parameters used in this study are summarized in Table 4.2.

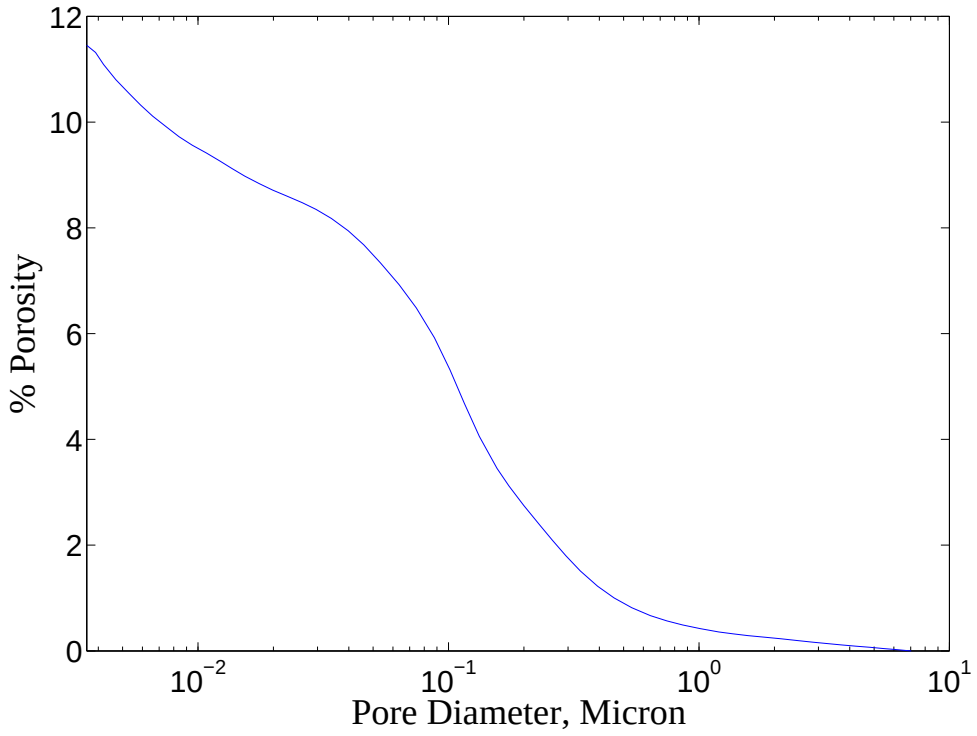

Figure 4.4: Measured % porosity as a function of pore diameter.

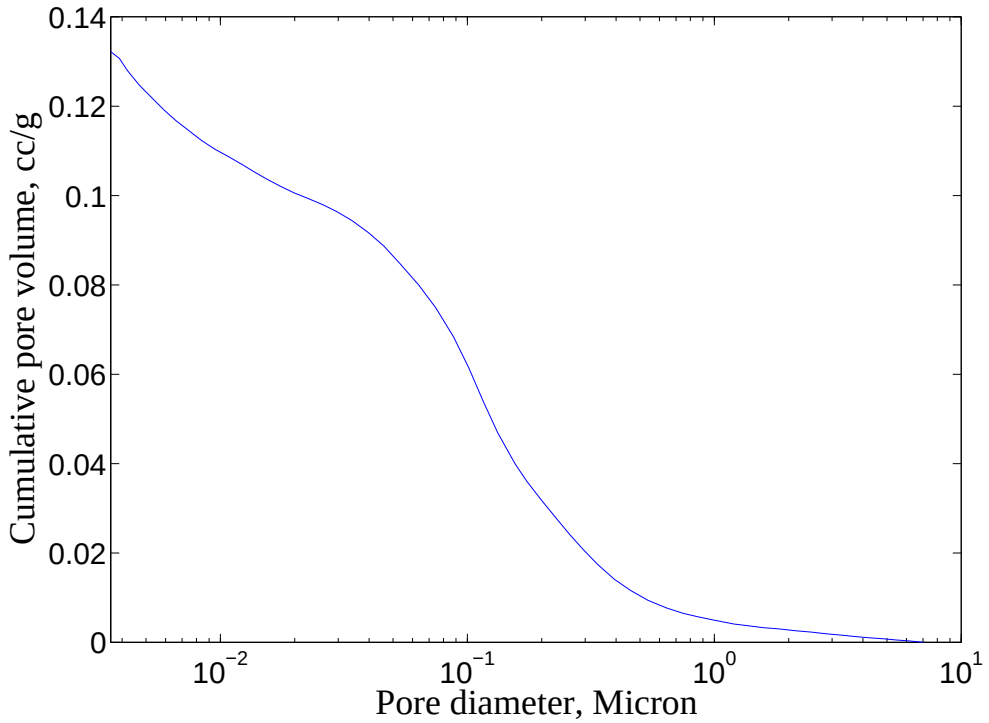

Figure 4.5: Measured cumulative pore volume as a function of pore diameter.

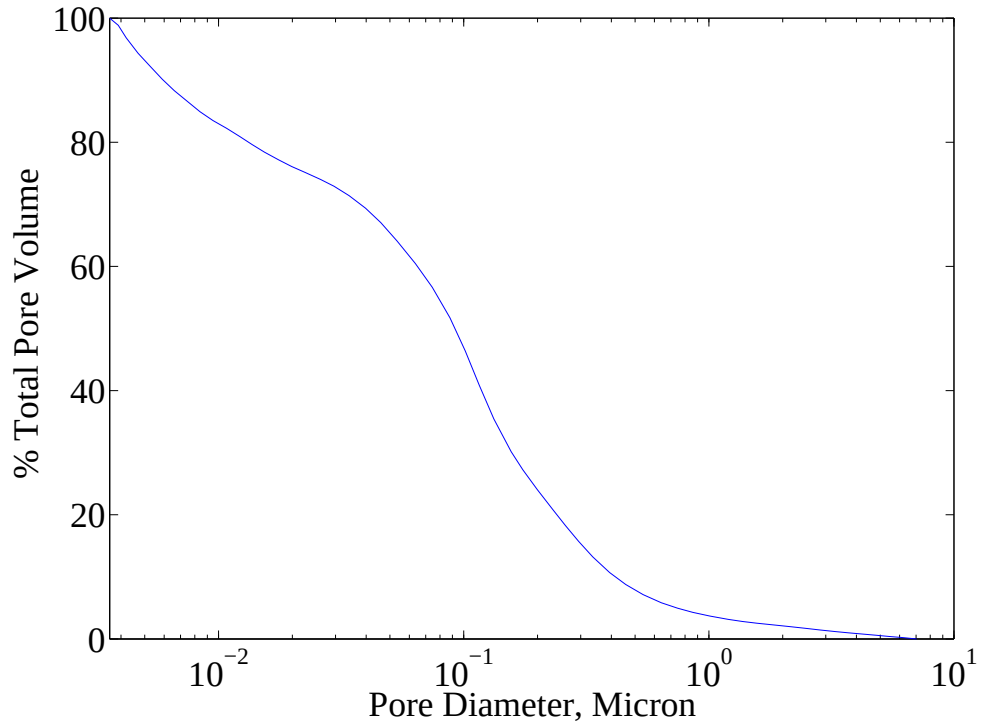

Figure 4.6: Measured %total pore volume as a function of pore diameter.

Table 4.2: Parameters for numerical implementation of the model for flow and viscoelastic large deformation in unsaturated swelling porous materials under isothermal conditions.

Item	Value	Unit	Source
The gas constant R	8.31432	$J/K/mol$	
The atmospheric pressure p^a	101325	Pa	134
Initial volume fraction of the solid ε_0^s	0.148		134
True density of the solid ρ^s	1.29×10^3	kg/m^3	134
True density of water ρ^l at 100^0 C	0.95805×10^3	kg/m^3	134
Viscosity of water at 100^0 C	0.282×10^{-3}	Ns/m^2	Web Source [1]
Molar volume of water v_l	$\frac{18.01528\times10^{-3}}{\rho^l}$	m^3/mol	Web source [2]
Intrinsic permeability k^i	1×10^{-18}	m^2	134
Material constant B_c	8.2×10^{-14}	(m^3s/kg)	110
$\overline{M}$	$1.7\pm8.7e-3$		27
β	$5.78e-8\pm1.1e-2$		27

[1] http://www.engineeringtoolbox.com/water-dynamic-viscosity-d_596.html

[2] http://www.chemistrydaily.com/chemistry/Molecular_mass

4.4 The Finite Element Model

The two-way coupled problem consisting of Equations (4.1) and (4.19), together with initial and boundary conditions, are solved using the finite element method. The primary variables are the volume fraction of the water phase, ε^l and the displacement of the solid "smeared-out" matrix, $\boldsymbol{u}^s$. We use the Total Lagrangian approach and formulate the weak forms in the reference configuration. The solutions are transformed back to the Eulerian (current) configuration.

4.4.1 Time integration

The backward Euler method is an implicit time integration method. Here we use this method to integrate the terms which involve the first order time derivative of any quantity, for example:

$$\frac{\partial \varepsilon^l}{\partial t} = \frac{\varepsilon^l(t) - \varepsilon^l(t-\Delta t)}{\Delta t} \tag{4.52}$$

where Δt is the time step size.

4.4.2 Weak forms of the governing equations: transport equation

We present the weak forms of the governing equations based on the Lagrangian description. We first transform the governing equations from the Eulerian frame to the Lagrangian frame using the deformation gradient $\boldsymbol{F}$ and its determinant J in a one dimensional setting. Then the equations are multiplied by independent weighting functions, respectively, and are then integrated over the domain. The weighting functions vanish on the boundary where the Dirichlet boundary condition is applied (Belytschko et al. 2000) [17]. To carry out the transformation, we make use of the deformation gradient and its determinant in a one dimensional setting.

$$F = \frac{\partial x}{\partial X} \tag{4.53}$$

and

$$J = \det(F) = \frac{\partial x}{\partial X} \tag{4.54}$$

Thus, the transport equation (4.1) in a Lagrangian description is given by:

$$J\frac{\partial \varepsilon^l}{\partial t} - \nabla_X \cdot D(\frac{1}{J}\nabla_X \varepsilon^l) - \nabla_X \cdot \left[-\varepsilon^l \frac{k^l}{\mu} p^a \frac{1}{J}\nabla_X \varepsilon^s + \int_0^t B(t-\tau)\frac{\partial(\frac{1}{J}\nabla_X \varepsilon^l)}{\partial \tau} d\tau \right] + \varepsilon^l \nabla_X \cdot \boldsymbol{v}^s = 0 \tag{4.55}$$

where ∇_X denotes the gradient with respect to the undeformed configuration X. Then, the weak form of the transport equation is given by:

$$\int_0^{L_0}\omega\left[J\frac{\partial\varepsilon^l}{\partial t}-\nabla_X\cdot(D\frac{1}{J}\nabla_X\varepsilon^l)-\nabla_X\cdot[-\varepsilon^l\frac{k^l}{\mu}p^a\frac{1}{J}\nabla_X\varepsilon^s+\int_0^t B(t-\tau)\frac{\partial(\frac{1}{J}\nabla_X\varepsilon^l)}{\partial\tau}d\tau]+\varepsilon^l\nabla_X\cdot\boldsymbol{v}^s\right]dX=0 \tag{4.56}$$

where ω is the weighting function and L_0 is the total length of the domain under consideration (half of the thickness of the pasta sample, see Figure 4.1). Using integration by parts, we obtain:

$$\begin{aligned}
&\int_0^{L_0}\omega J\frac{\partial\varepsilon^l}{\partial t}dX-[\int_0^{L_0}\nabla_X\cdot\omega(D\frac{1}{J}\nabla_X\varepsilon^l)dX-\int_0^{L_0}(\nabla_X\omega)\cdot D\frac{1}{J}\nabla_X\varepsilon^l dX]\\
&-[\int_0^{L_0}\nabla_X\cdot\omega(-\frac{\varepsilon^l k^l}{\mu}p^a\frac{1}{J}\nabla_X\varepsilon^s)dX-\int_0^{L_0}(\nabla_X\omega)\cdot(-\frac{\varepsilon^l k^l}{\mu}p^a\frac{1}{J}\nabla_X\varepsilon^s)dX]\\
&-[\int_0^{L_0}\nabla_X\cdot\omega\int_0^t B(t-\tau)\frac{\partial(\frac{1}{J}\nabla_X\varepsilon^l)}{\partial\tau}d\tau dX-\int_0^{L_0}(\nabla_X\omega)\cdot\int_0^t B(t-\tau)\frac{\partial(\frac{1}{J}\nabla_X\varepsilon^l)}{\partial\tau}d\tau dX]\\
&+\int_0^{L_0}\omega\varepsilon^l\nabla_X\cdot\boldsymbol{v}^s dX=0
\end{aligned} \tag{4.57}$$

Then we use the divergence theorem to obtain:

$$\begin{aligned}
&\int_0^{L_0}\omega J\frac{\partial\varepsilon^l}{\partial t}dX-\int_0^{L_0}\omega D\frac{1}{J}\nabla_X\varepsilon^l\cdot n dX+\int_0^{L_0}(\nabla_X\omega)\cdot D\frac{1}{J}\nabla_X\varepsilon^l dX-\int_0^{L_0}\omega(-\frac{\varepsilon^l k^l}{\mu}p^a\frac{1}{J}\nabla_X\varepsilon^s)\cdot n dX\\
&+\int_0^{L_0}(\nabla_X\omega)\cdot(-\frac{\varepsilon^l k^l}{\mu}p^a\frac{1}{J}\nabla_X\varepsilon^s)dX-\int_0^{L_0}\omega\int_0^t B(t-\tau)\frac{\partial(\frac{1}{J}\nabla_X\varepsilon^l)}{\partial\tau}d\tau\cdot n dX\\
&+\int_0^{L_0}(\nabla_X\omega)\cdot\int_0^t B(t-\tau)\frac{\partial(\frac{1}{J}\nabla_X\varepsilon^l)}{\partial\tau}d\tau dX+\int_0^{L_0}\omega\varepsilon^l\nabla_X\cdot\boldsymbol{v}^s dX=0
\end{aligned} \tag{4.58}$$

Since we have the Dirichlet boundary condition for one end and symmetry for the other (Figure 4.1), the above is simplified to:

$$\int_0^{L_0}\omega J\frac{\partial\varepsilon^l}{\partial t}dX+\int_0^{L_0}(\nabla_X\omega)\cdot D\frac{1}{J}\nabla_X\varepsilon^l dX+\int_0^{L_0}(\nabla_X\omega)\cdot(-\frac{\varepsilon^l k^l}{\mu}p^a\frac{1}{J}\nabla_X\varepsilon^s)dX$$
$$+\int_0^{L_0}(\nabla_X\omega)\cdot\int_0^t B(t-\tau)\frac{\partial(\frac{1}{J}\nabla_X\varepsilon^l)}{\partial\tau}d\tau dX+\int_0^{L_0}\omega\varepsilon^l\nabla_X\cdot\boldsymbol{v}^s dX=0 \quad (4.59)$$

where the inner integral in the fourth term is given by:

$$\int_0^t B(t-\tau)\frac{\partial(\frac{1}{J}\nabla_X\varepsilon^l)}{\partial\tau}d\tau=\int_0^t\sum_{i=1}^{n_k}B_c K_i exp[-(t-\tau)a_M/\tau_i]\frac{\partial(\frac{1}{J}\nabla_X\varepsilon^l)}{\partial\tau}d\tau\equiv\sum_{i=1}^{n_k}B_c K_i H^{(i)} \quad (4.60)$$

We use a one-step, unconditionally stable second-order recurrence formula to calculate $H^{(i)}$ at the $(n+1)^{th}$ time step (Simo and Hughes 1997) [105]:

$$H_{n+1}^{(i)}=exp[-\Delta t\cdot a_M/\tau_i]H_n^{(i)}+exp[-\Delta t\cdot a_M/2\tau_i][(\frac{1}{J}\nabla_X\varepsilon^l)|_{n+1}-(\frac{1}{J}\nabla_X\varepsilon^l)|_n] \quad (4.61)$$

Finally, we denote, at the $(n+1)^{th}$ time step:

$$A_{n+1}\equiv\sum_{i=1}^{n_k}B_c K_i H_{n+1}^{(i)} \quad (4.62)$$

Then the weak form of the transport equation becomes:

$$\int_0^{L_0}\omega J\frac{\partial\varepsilon^l}{\partial t}dX+\int_0^{L_0}\frac{1}{J}(\nabla_X\omega)\cdot D\nabla_X\varepsilon^l dX+\int_0^{L_0}\frac{1}{J}(\nabla_X\omega)\cdot(-\frac{\varepsilon^l k^l}{\mu}p^a)\nabla_X\varepsilon^s dX$$
$$+\int_0^{L_0}(\nabla_X\omega)\cdot A dX+\int_0^{L_0}\omega\varepsilon^l\nabla_X\cdot\boldsymbol{v}^s dX=0 \quad (4.63)$$

4.4.3 Weak forms of the governing equations: linear momentum balance

We follow the same procedure as has been used to obtain the weak form for the transport equation and derive the weak form for the linear momentum balance equation for the solid phase:

$$\int_0^{L_0} \delta \boldsymbol{E} : \boldsymbol{S}' dX - \omega \boldsymbol{S}'|_{X=L_0} = \int_0^{L_0} (\nabla_X \omega)(S^l p^l + S^a p^a) dX \tag{4.64}$$

where

$$\delta \boldsymbol{E} = \frac{1}{2}(\boldsymbol{F}^T \nabla_X \omega + (\nabla_X \omega)^T \boldsymbol{F}) \tag{4.65}$$

and ω is the weighting function. We manipulate the right hand side of Equation (4.64) as follows:

$$\int_0^{L_0} (\nabla_X \omega)(S^l p^l + (1 - S^l) p^a) dX = \int_0^{L_0} (\nabla_X \omega)(-S^l p^c + p^a) dX \tag{4.66}$$

where the degree of saturation of water is calculated as

$$S^l = \frac{V^l}{V^P} = \frac{\varepsilon^l}{1 - \varepsilon^s} \tag{4.67}$$

with V^l the volume of the liquid phase and V^P the volume of the pores. Using Kelvin's equation, the weak form Equation (4.64) becomes:

$$\int_0^{L_0} \delta \boldsymbol{E} : \boldsymbol{S}' dX - \omega \boldsymbol{S}'|_{X=L_0} = \int_0^{L_0} (\nabla_X \omega)(\frac{\varepsilon^l}{1 - \varepsilon^s} \frac{RT}{v_l} ln(a_w) + p^a) dX \tag{4.68}$$

4.4.4 Method of solution

Newton's method is used to solve the coupled problem. This is an iterative root finding algorithm obtained by using the first few terms of the Taylor series of a function $f(x)$ in the vicinity of an approximation of the root. For the one dimensional case, it starts with finding an initial rough estimate to the root and then using the iterative equation:

$$x_{n+1} = x_n + \frac{f(x_n)}{f'(x_n)}, n \geq 0 \tag{4.69}$$

4.4.5 Residuals and their gradients

Three node one dimensional quadratic elements are used to discritize space. The shape functions for the parent element are:

$$[N(\xi)] = [\frac{1}{2}\xi(\xi-1) \quad \frac{1}{2}(1+\xi)(1-\xi) \quad \frac{1}{2}\xi(\xi+1)] \tag{4.70}$$

where ξ, which varies from -1 to 1, is the coordinate for the parent element. Then, the weighting function, volume fraction of water, the displacement of the solid and the positions are discritized as:

$$\begin{aligned} &\omega^{(I)} = [N(\xi)^{(I)}]\{\omega^{(I)}\}, \varepsilon^{l(I)} = [N(\xi)^{(I)}]\{\varepsilon^{l(I)}\}, u^{s(I)} = [N(\xi)^{(I)}]\{u^{s(I)}\}, \\ &X^{(I)} = [N(\xi)^{(I)}]\{X^{(I)}\}, x^{(I)} = [N(\xi)^{(I)}]\{x^{(I)}\} \end{aligned} \tag{4.80}$$

Here, the superscript (I) denotes the I^{th} element. We define:

$$\{\varepsilon^l\} = \begin{Bmatrix} \{\varepsilon^{l(1)}\} \\ \vdots \\ \{\varepsilon^{l(N)}\} \end{Bmatrix}, \{u\} = \begin{Bmatrix} \{u^{s(1)}\} \\ \vdots \\ \{u^{s(N)}\} \end{Bmatrix}, [N] = \begin{bmatrix} [N(\xi)^{(1)}] \\ \vdots \\ [N(\xi)^{(N)}] \end{bmatrix}, [B] = [N_{,X}] \tag{4.90}$$

where the superscript $1, \cdots, N$ are the numbers of the elements. Then the residuals are expressed as:

$$R_\varepsilon(\{\varepsilon^l\},\{u\}) = \int_{-1}^{1}[N]^T \frac{[N]\{\varepsilon^l\}-[N]\{\varepsilon^l\}_{n-1}}{dt} J \frac{dX}{d\xi} d\xi + \int_{-1}^{1}[B]^T D[B]\{\varepsilon^l\}\frac{1}{J}\frac{dX}{d\xi} d\xi$$
$$+ \int_{-1}^{1}[B]^T(-\frac{[N]\{\varepsilon^l\}k^l}{\mu} p^a)(grad\varepsilon^s)\frac{1}{J}\frac{dX}{d\xi} d\xi + \int_{-1}^{1}[B]^T A\frac{dX}{d\xi} d\xi \quad (4.91)$$
$$+ \int_{-1}^{1}[N]^T[N]\{\varepsilon^l\}\frac{[B]\{u\}-[B]\{u\}_{n-1}}{dt}\frac{dX}{d\xi} d\xi$$

where for simplicity, $\{\varepsilon^l\}$ and $\{u\}$ without a subscript n are assumed to be the quantities at the current time step $t_n = t_{n-1} + \Delta t$, while those with a subscript $n-1$ are the quantities at the previous time step t_{n-1}. And we have defined

$$grad\varepsilon^s = \frac{\partial \varepsilon^s}{\partial X} \quad (4.92)$$

Similarly we have

$$R_u(\{\varepsilon^l\},\{u\}) = \int_{-1}^{1}[B_0]^T\{S'\}\frac{dX}{d\xi} d\xi - \int_{-1}^{1}[B]^T[\frac{[N]\{\varepsilon^l\}}{1-\varepsilon^s}\frac{RT}{v_l} ln(a_w) + p^a]\frac{dX}{d\xi} d\xi - \{P\} \quad (4.93)$$

where

$$[B_0] = \left[\frac{\partial x}{\partial X}\frac{\partial N(\xi)^{(1)}}{\partial X} \quad \cdots \quad \frac{\partial x}{\partial X}\frac{\partial N(\xi)^{(N)}}{\partial X}\right] \quad (4.94)$$

$\{S'\}$ denotes the nodal values of the effective 2nd Piola-Kirchhoff stress tensor. To calculate $\{S'\}$ via the constitutive relationship given by Equation (4.26), we first define the following quantity:

$$\{Q\}^{(i)} = \int_0^t exp[-(t-\tau)\cdot a_M/\tau_i]\frac{\partial}{\partial \tau}\left[\frac{1}{2}\kappa(J^2-1)\{C^{-1}\}\right] d\tau \quad (4.95)$$

$\{Q\}$ at the $(n+1)^{th}$ time step can be expressed by a one-step, unconditionally stable second order recurrence formula (Simo and Hughes 1997) [105] similar to Equation (4.61):

$$\{Q\}_{n+1}^{(i)} = exp[-\Delta t \cdot a_M/\tau_i]\{Q\}_n^{(i)} + exp[-\Delta t \cdot a_M/\tau_i][(\frac{1}{2}(J^2-1)\{C^{-1}\})|_{n+1} - (\frac{1}{2}(J^2-1)\{C^{-1}\})|_n] \quad (4.96)$$

The derivatives of the residuals are calculated as follows:

$$\begin{aligned}\frac{\partial\{R_\varepsilon\}}{\partial\{\varepsilon^l\}} \equiv [K_{\varepsilon\varepsilon}] \quad &= \int_{-1}^{1}\frac{[N]^T[N]}{dt}J\frac{dX}{d\xi}d\xi + \int_{-1}^{1}[B]^T D[B]\frac{1}{J}\frac{dX}{d\xi}d\xi \\ &+ \int_{-1}^{1}[B]^T\frac{\partial D}{\partial\{\varepsilon^l\}}([B]\{\varepsilon^l\})\frac{1}{J}\frac{dX}{d\xi}d\xi - \int_{-1}^{1}[B]^T[N]\frac{k^l p^a}{\mu}(grad\varepsilon^s)\frac{1}{J}\frac{dX}{d\xi}d\xi \\ &- \int_{-1}^{1}[B]^T[N]\{\varepsilon^l\}\frac{p^a}{\mu}\frac{\partial k^l}{\partial\{\varepsilon^l\}}(grad\varepsilon^s)\frac{1}{J}\frac{dX}{d\xi}d\xi + \int_{-1}^{1}[B]^T\frac{dA}{d\{\varepsilon^l\}}\frac{dX}{d\xi}d\xi \\ &+ \int_{-1}^{1}[N]^T[N]\frac{[B]\{u\}-[B]\{u\}_{n-1}}{dt}\frac{dX}{d\xi}d\xi\end{aligned} \quad (4.97)$$

$$\begin{aligned}\frac{\partial\{R_\varepsilon\}}{\partial\{u\}} \equiv [K_{\varepsilon u}] \quad &= \int_{-1}^{1}[N]^T\frac{[N]\{\varepsilon^l\}-[N]\{\varepsilon^l\}_{n-1}}{dt}\frac{dJ}{d\{u\}}\frac{dX}{d\xi}d\xi + \int_{-1}^{1}[B]^T\frac{\partial D}{\partial\{u\}}([B]\{\varepsilon^l\})\frac{1}{J}\frac{dX}{d\xi}d\xi \\ &+ \int_{-1}^{1}[B]^T D([B]\{\varepsilon^l\})(-\frac{1}{J^2})\frac{dJ}{d\{u\}}\frac{dX}{d\xi}d\xi - \int_{-1}^{1}[B]^T[N]\{\varepsilon^l\}\frac{\partial k^l}{\partial\{u\}}\frac{p^a}{\mu}\frac{\partial(grad\varepsilon^s)}{\partial\{u\}}\frac{1}{J}\frac{dX}{d\xi}d\xi \\ &- \int_{-1}^{1}[B]^T\frac{[N]\{\varepsilon^l\}k^l p^a}{\mu}(grad\varepsilon^s)(-\frac{1}{J^2})\frac{dJ}{d\{u\}}\frac{dX}{d\xi}d\xi + \int_{-1}^{1}[B]^T\frac{\partial A}{\partial\{u\}}\frac{dX}{d\xi}d\xi \\ &+ \int_{-1}^{1}[N]^T([N]\{\varepsilon^l\})[B]\frac{1}{dt}\frac{dX}{d\xi}d\xi\end{aligned} \quad (4.98)$$

$$\begin{aligned}\frac{\partial\{R_u\}}{\partial\{u\}} \equiv [K_{uu}] \quad &= \int_{-1}^{1}[B_0]^T[C^{SE}][B_0]\frac{dX}{d\xi}d\xi + \int_{-1}^{1}[B]^T\{S'\}[B]\frac{dX}{d\xi}d\xi \\ &+ \int_{-1}^{1}[B]^T\frac{RT}{v_l}[N]\varepsilon^l\frac{\varepsilon_0^s}{J^2(1-\varepsilon^s)^2}ln(a_w)\frac{\partial J}{\partial\{u\}}\frac{dX}{d\xi}d\xi\end{aligned} \quad (4.99)$$

where $[C^{SE}]$ is the algorithmic tangent modulus given by:

$$[C^{SE}] = 2\frac{\partial\{S'\}}{\partial\{C\}} \quad (4.100)$$

with $\{C\}$ being the nodal values of the right Cauchy Green deformation tensor. Finally:

$$\frac{\partial\{R_u\}}{\partial\{\varepsilon^l\}} \equiv [K_{u\varepsilon}] = \int_{-1}^{1}[B_0]^T \frac{\partial\{S'\}}{\partial\{\varepsilon^l\}}\frac{dX}{d\xi}d\xi - \int_{-1}^{1}[B]^T[\frac{[N]\{\varepsilon^l\}}{1-\varepsilon^s}\frac{RT}{v_l}\frac{1}{a_w}\frac{\partial a_w}{\partial\{\varepsilon^l\}}]\frac{dX}{d\xi}d\xi - \int_{-1}^{1}[B]^T[\frac{[N]}{1-\varepsilon^s}\frac{RT}{v_l}ln(a_w)]\frac{dX}{d\xi}d\xi \quad (4.101)$$

Details of the calculation of some quantities and the derivatives can be found in Appendix C.

4.4.6 Solution procedure

The solution method for the coupled problem follows closely from Belytschko et al. (2000) [17]. The Newton iterative scheme is expressed as:

$$\begin{pmatrix}[K_{\varepsilon\varepsilon}] & [K_{\varepsilon u}]\\ [K_{u\varepsilon}] & [K_{uu}]\end{pmatrix}^{(k)} \cdot \begin{pmatrix}\{\Delta\varepsilon^l\}\\ \{\Delta u\}\end{pmatrix}^{(k)} = -\begin{pmatrix}\{R_\varepsilon\}\\ \{R_u\}\end{pmatrix}^{(k)} \quad (4.102)$$

$$\{\varepsilon^l\}^{(k+1)} = \{\varepsilon^l\}^{(k)} + \{\Delta\varepsilon^l\}^{(k)}, \{u\}^{(k+1)} = \{u\}^{(k)} + \{\Delta u\}^{(k)} \quad (4.103)$$

Superscripts are used to denote the iteration steps within each time step. Equation (4.102) is iterated until convergence. The tolerance used here to check convergence is 10^{-3}. The algorithm for the coupled scheme is described below:

1. Set initial values of displacement $\{u\}$ and initial values of the volume fraction $\{\varepsilon^l\}$.

2. Update time $t = t + \Delta t$.

3. Set initial variables for Newton Iterations $\{u\}_{n+1}^{0} = \{u\}_n$, $\{\varepsilon^l\}_{n+1}^{0} = \{\varepsilon^l\}_n$.

Here subscripts are for the time steps.

4. Set $k = 1$ for Newton Iteration at time step $n+1$.

5. Compute the residuals using Equations (4.91) and (4.93).

6. Compute the four residual gradients according to Equations (4.97), (4.98), (4.99) and (4.101).

7. Use Equation (4.103) and solve for the increments.

8. Update the primary variables using Equation (4.103).

9. Update parameters.

10. Compute the error and check for convergence.

11. If the error exceeds the tolerance, set $k = k+1$ and repeat from step 5.

12. $\{u\}_{n+1} = \{u\}_{n+1}^{k}$, $\{\varepsilon^l\}_{n+1} = \{\varepsilon^l\}_{n+1}^{k}$.

13. Repeat from step 3 until time limit is reached.

It is worth noting that the four gradients of the residuals defined in Equations (4.97), (4.98), (4.99) and (4.101) are not of the same order. In order that the resulting matrix in Equation (4.102) is not ill-conditioned, all the units of the quantities in meter are scaled to 10^{-4} m.

4.5 Results

The primary variables: volume fraction of water ε^l and the displacement of the matrix $\boldsymbol{u}$, as functions of position and time, are computed. To compare with the experimental data obtained by Cafieri et al. (2008) [27], the moisture content on a dry basis, M, is calculated using the expression (4.30). Then M is averaged over the domain at each time step. Figure 4.7 shows the sorption curve predicted by the model and a comparison with the experimental data obtained by Cafieri et al. (2008) [27]. They are in good agreement considering that no experimentally fitted parameters are used in this model. The small fluctuations in the experimental and numerical results appear to be opposite to each other. This result requires further investigation.

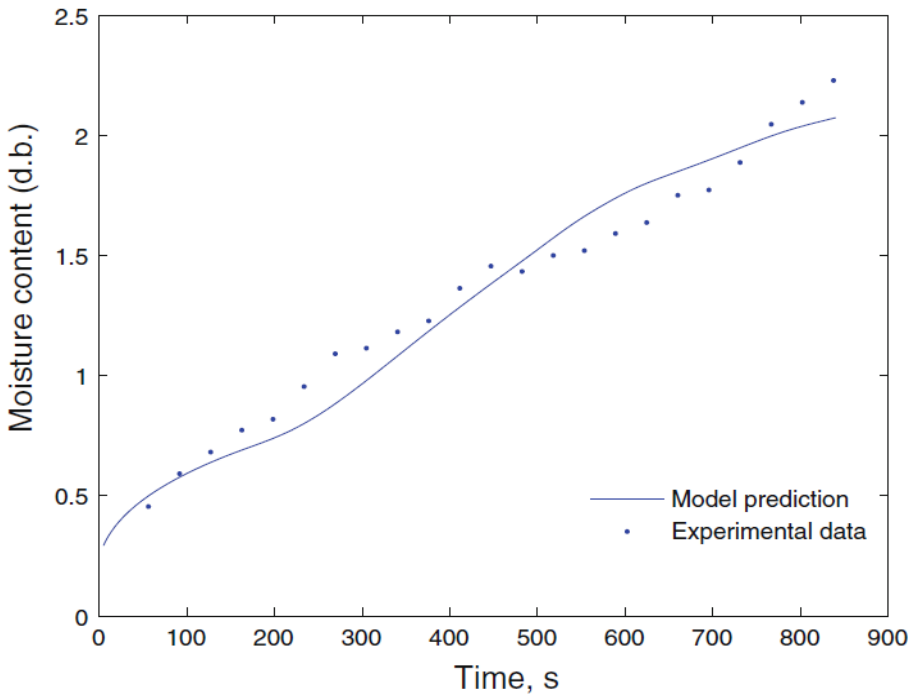

Figure 4.7: Quantity of water absorbed at time t with respect to the initial weight (T=100 $\pm 0.6^{0}C$).

Volume fraction of water as a function of position is shown in Figure 4.8. It is noted that here ε^l is the volume fraction of water relative to the total volume, rather than to the pore volume. It is worth mentioning that the symmetry boundary condition, $\frac{\partial \varepsilon^l}{\partial X} = 0$ at $X = 0$, is implicitly imposed in the FEM formulation. This caused some numerical errors at $X = 0$, at times $t = 10s$ and $t = 200s$, in Figure 4.8. These errors have been corrected by simulating the full sample at these times.

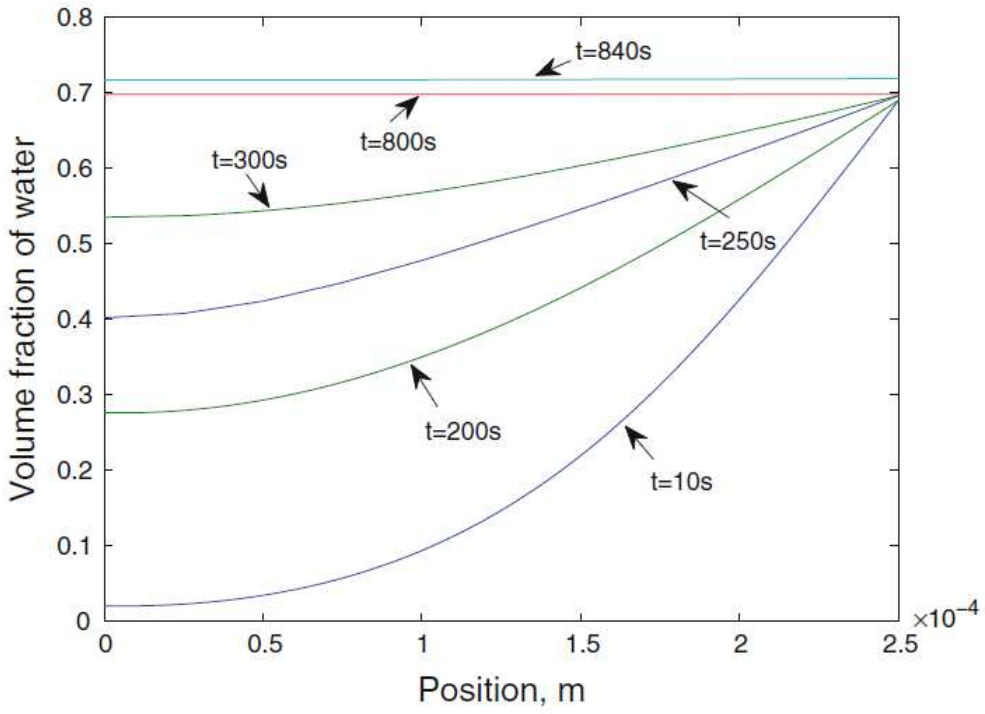

Figure 4.8: Volume fraction of water as a function of position at different times.

The effective stress is predicted and shown in Figure 4.9. Here, we have defined the initial state to be the dehydrated state. As water migrates into the material, the solid

particles are compressed and thus compressive stresses are found in the solid. On the right boundary, it can be seen that the stress is equal to the negative of the atmospheric pressure. The compressive stresses relax with time and their magnitudes become smaller as time becomes larger. Eventually, the compressive stress in the body is equal to the negative of the atmospheric pressure, making the total stress in the body zero.

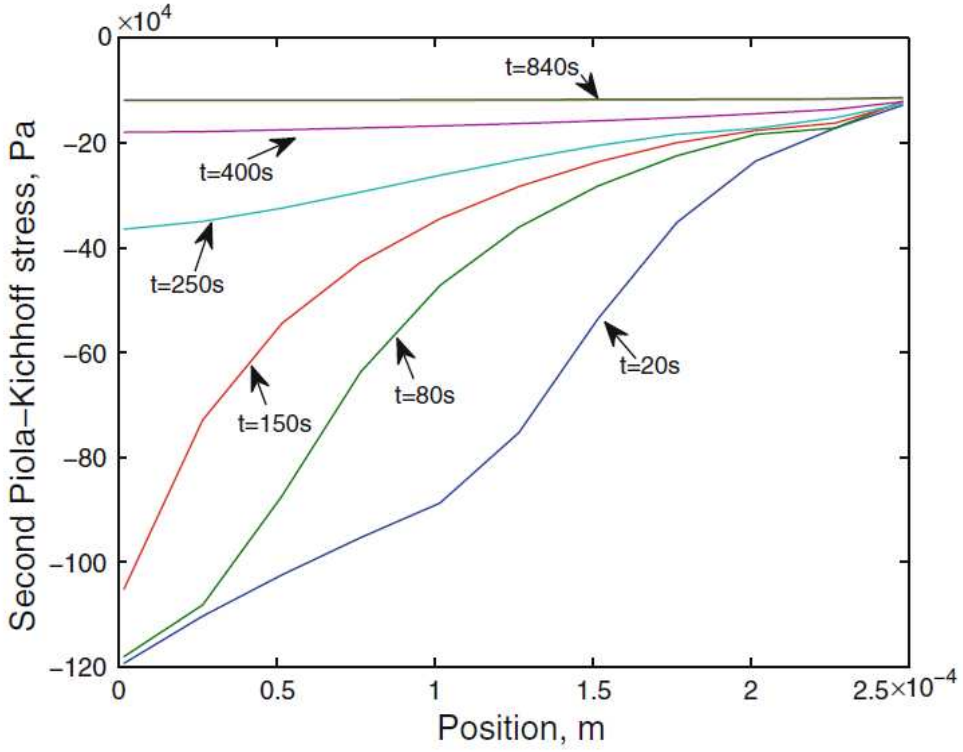

Figure 4.9: The second Piola-Kirchhoff stress.

The displacement of each point across the thickness of the sample is calculated and given in Figure 4.10. It is clearly seen that dimensions change as time increases and eventually the sample is predicted to have a toal thickness change of 84% . Sung and Stone (2005) [115] found from experiments that the diameter of cooked pasta doubled after cooking of 20min. Considering that the cooking time in this study is shorter, the

predicted total length change is reasonable. The closer a material point is to the boundary where moisture is transported in, the more the material is stretched.

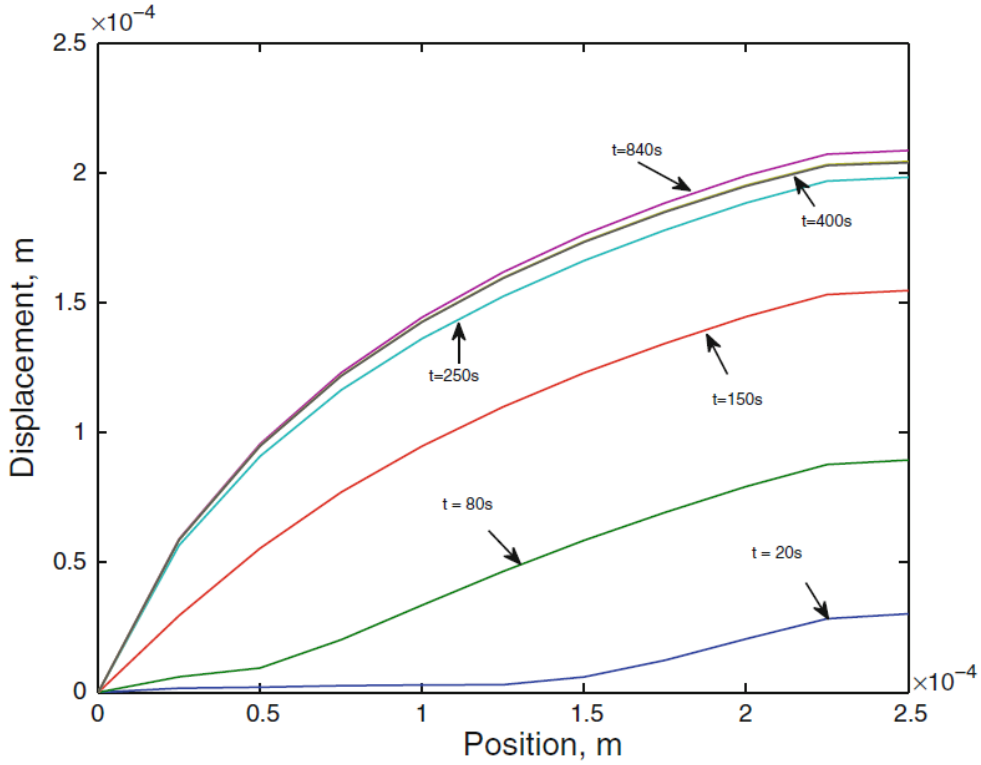

Figure 4.10: Displacement field as a function of time.

A sensitivity analysis is also performed to gain insight on the importance of including the viscoelastic effect on the transport process. Bc is a constant multiplying the term representing the viscoelastic effect on the transport in the transport equation Equation (4.1) (see Equation (4.50)). Different values of Bc represent the extent to which including the viscoelastic effect on the transport is important. This can be related to the Deborah number, which represents the ratio of the characteristic relaxation time to the characteristic diffusion time, for example, defined by Achanta et al. (1997) [5].

When the Deborah number is very low, similar to the case of Bc approaching zero in this study, the relaxation process is very fast and the effect of viscoelastic relaxation on the transport can be neglected (provided that the time t is sufficiently large compared to the relaxation time). But when the Deborah number is high, similar to the case of large Bc in this study, the viscoelastic effect is important. However, when the relaxation time approaches infinity, it can be easily shown that the fourth term in Equation (4.1) reduces to a term representing diffusion which can then be merged to the second term in that equation. In this case, the viscoelastic effect on transport can also be neglected (Please note, however, that the precise material response for the two cases, the Deborah number approaching zero and infinity, are different.). To investigate the importance of including the effect of viscoelasticity on the transport in the process of soaking of pasta at 100^{0}C, the moisture content on a dry basis with different values of Bc are obtained and can be found in Figures 4.11 and 4.12. These can be compared to the moisture content profile obtained using Bc listed in Table 4.2 in Figure 4.7.

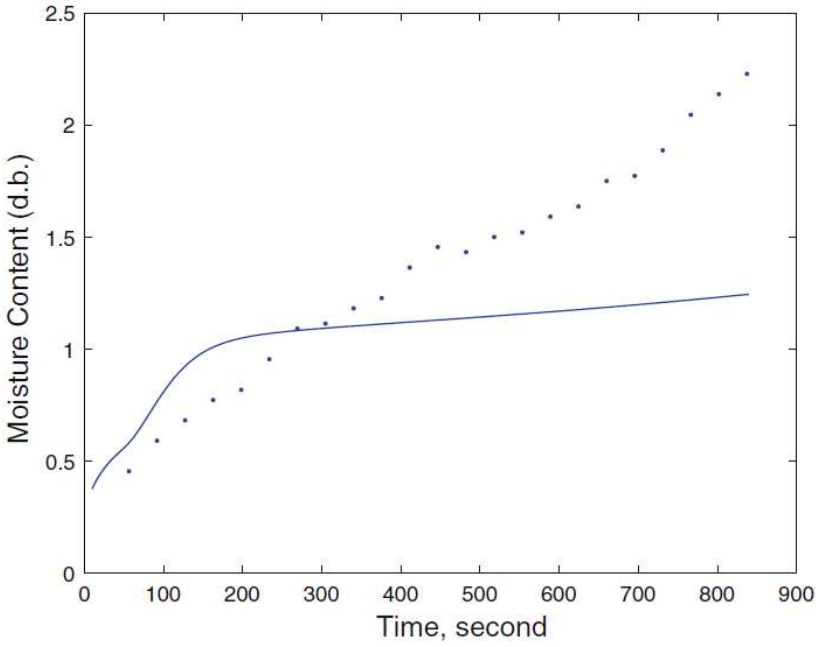

Figure 4.11: Quantity of water absorbed at time t with respect to the initial weight, with Bc = $8.2\times10^{-5} m^3 s/kg$, ' – ' is predicted profile and ' · ' is experimental data

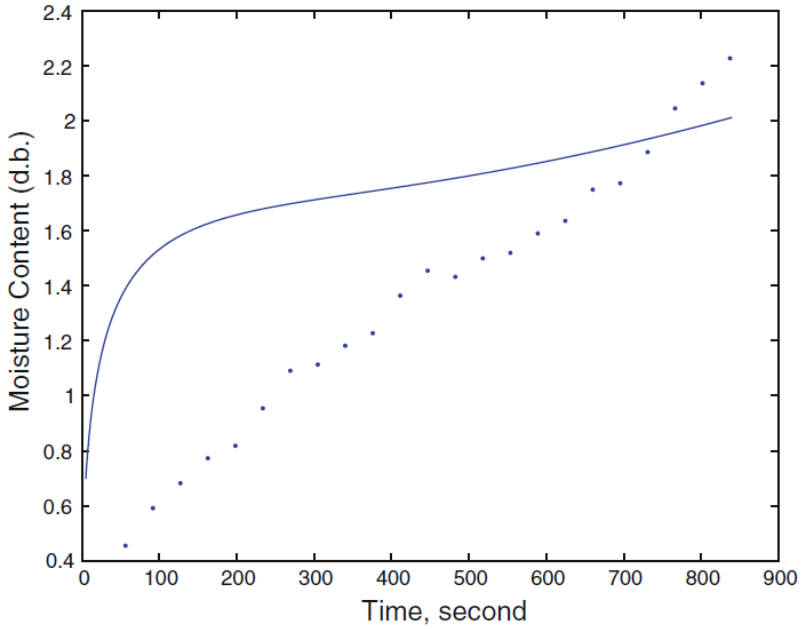

Figure 4.12: Quantity of water absorbed at time t with respect to the initial weight, with Bc = $8.2\times10^{-17} m^3 s/kg$, ' – ' is predicted profile and ' · ' is experimental data

Volume fractions of water corresponding to the different values of Bc are also plotted and can be found in Figures 4.13 and 4.14. It is seen that when Bc is very large, i.e., the effect of the relaxation on the rate of moisture migration is great, the predicted moisture uptake is smaller than that obtained by the experiment. On the other hand, when Bc approaches zero, i.e., the moisture transport process is completely captured by Fickian diffusion, the predicted moisture uptake is greater than that from the experiment. It can be concluded that in the process of soaking of pasta at 100^0C, though the domination of the relaxation on the rate of moisture transport is not great, including the effect of viscoelasticity is very necessary and both diffusion and the viscoelastic effect are important in the transport process.

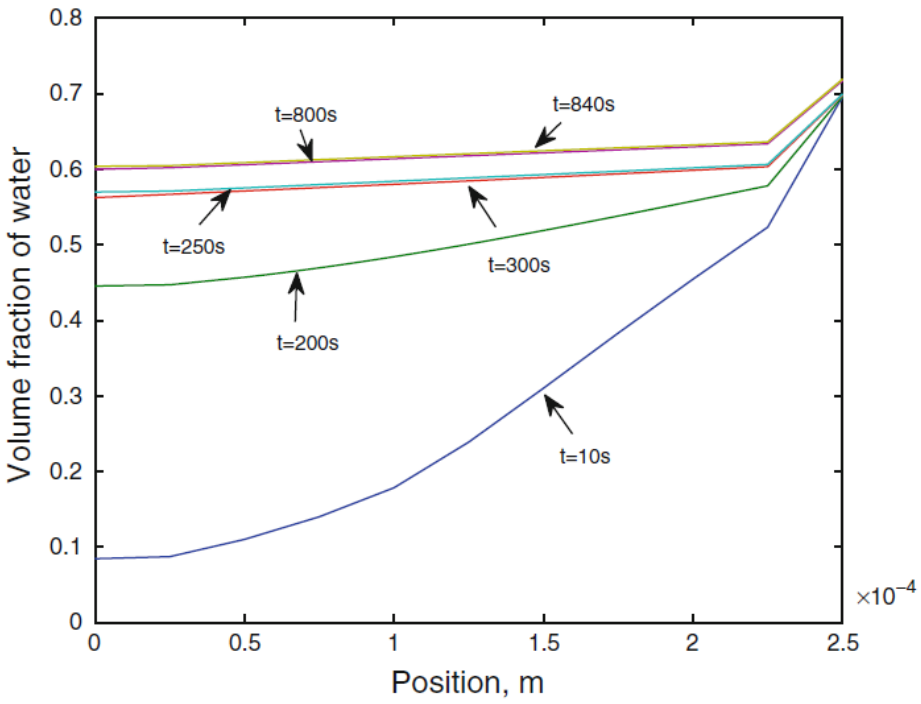

Figure 4.13: Volume fraction of water as a function of position at different times, with $\mathrm{Bc} = 8.2\times10^{-5} m^3 s/kg$

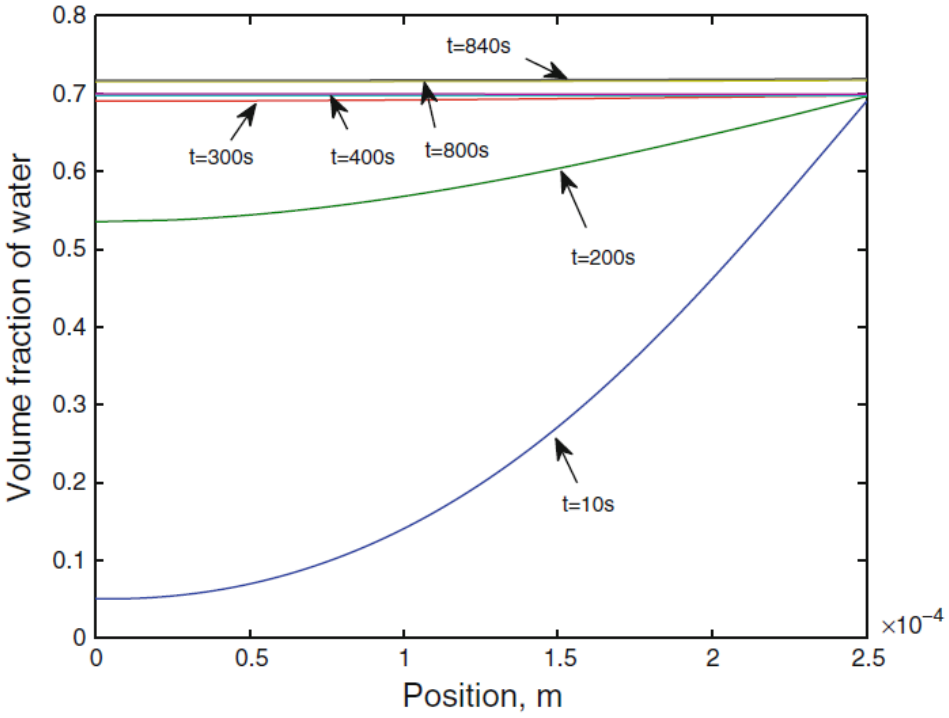

Figure 4.14: Volume fraction of water as a function of position at different times, with $\mathrm{Bc} = 8.2\times10^{-17}\, m^3 s/kg$

4.6 Conclusions

Soaking is an important process which involves water migration and swelling of the material due to water absorption. In particular, for most foodstuffs, soaking can be modelled as coupled fluid flow through a viscoelastic porous material that consists of two or more phases, together with viscoelastic deformation of the solid matrix.

The mathematical model involves a novel integro-differential equation that governs the transport phenomenon, and linear momentum balance for the solid phase, with constitutive relationships for isothermal conditions presented by Zhu et al. (2010) [133]. This model is applied to study simultaneous moisture transport and viscoelastic large deformation of pasta, which is a porous food material, in a soaking process. The dependence of viscoelastic behavior of pasta on moisture content is investigated and pasta is found to be hydro-rheologically simple. The viscoelastic effect on transport has been separated from the commonly used “effective diffusivity” coefficient. A non-empirical model for the diffusivity coefficient has been proposed and successfully utilized to predict moisture tranport in the porous material.

The coupled nonlinear problem is solved using the finite element method based on a Lagrangian description, and the resulting nonlinear system of equations is solved using the Newton scheme. Sorption curves are computed and good agreement is observed with experimental data. Size change of pasta and stresses generated during soaking have been predicted.

A sensitivity analysis is also performed to investigate the importance of including the effect of viscoelasticity on the moisture transport. It is found that both diffusion and the viscoelastic effect are important mechanisms in the study of moisture tranport in a soaking process of pasta, i.e., the transport process is captured by non-Fickian diffusion.

The major contribution of this study is that soaking of porous materials, for example, foodstuffs that exhibit viscoelastic behavior, is studied based on a fundamental porous media theory that is different from models commonly used by authors where either empirical or semi-empirical equations are used, or the swelling behavior associated with soaking is not studied appropriately. Using the model presented in this study, soaking in a food material is considered to be a coupled fluid tranport process with viscoelastic large deformation of the porous matrix. With some modifications, the numerical model developed here can be used to study fluid transport and swelling in many other applications include drying of porous materials, and water absorption in dipers, to name a few.

CHAPTER 5

DRYING OF FOODSTUFFS

5.1 Introduction

5.1.1 Drying models for foodstuffs with shrinkage

There are many models presented in the literature for drying of agricultural products, foodstuffs, and building materials (wood, ceramics, etc), some include and others neglect shrinkage. Removal of fluid and heating of the materials causes stresses in the materials, change of structure and the reduction of volume. For foodstuffs, semi-empirical models that neglect shrinkage during drying utilize balance laws that are suitable for corresponding non-shrinkage situations and experimentally fitted parameters (Maroulis et al. 1995; Aversa et al. 2007; Singh and Gupta 2007; Srikiatden and Roberts 2008) [71,10,109,113]. Many studies that include one way coupling of shrinkage during drying use numerical artifices, for example, modification of the domain of the governing equations, and the regular transport problem is turned into a moving boundary problem. In this approach, a common assumption is that shrinkage occurs solely due to water removal and expressions are formulated that relate moisture content and the dimensions of the bodies (Misra and Young 1980; Ratti 1994; Park 1998; Akiyama et al. 1997; Vazquez et al. 1999; Mayor and Sereno 2004) [76,97,85,7,120,74]. Other studies that include consideration of shrinkage are

more fundamentally based, for example, they focus more on prediction of dimension changes from conservation laws of mass and momentum (Ponsart et al. 2003; Tsukada et al. 1991; Izumi and Hayakawa 1995; Akiyama and Hayakawa 2000; Yang et al. 2001; Itaya et al. 1995) [90,119,57,6,131,56]. However, generally only small strains are considered. Also, the facts that multiple phases exist and that the transport of mass and momentum of these phases are fully coupled, are not usually adequately addressed in these models.

5.1.2 Case hardening during drying

An important phenomenon is observed during drying of some foodstuffs – shrinkage of the material deviates from the volume of removed water. This can happen during the entire drying period (Fang et al. 2009) [43] (Figure 5.1) or during the final stages of drying (Rahman and Potluri 1990; Rahman et al. 1996; Lozano et al. 1983; Wang and Brennan 1995; Krokida and Maroulis 1997; Lozano et al. 1980; Moreira et al. 2000) [94,93,68,123,60,69,77]. This phenomenon can be explained by the fact that at low moisture contents, the mobility of the solid matrix decreases (Mayor and Sereno 2004) [74] and the rigidity of the matrix slows down or stops shrinkage of the material, and this is usually referred to as case hardening (Bai et al. 2002) [13]. Case hardening occurs under appropriate drying conditions, for example, higher drying rate, appropriate temperature, higher velocity of air, and lower relative humidity of air. At higher drying rates, sharp moisture gradients through the material occur and a glass

transition may happen, causing the formation of a rigid shell in the outer surface of the material which fixes the volume of the material. When the drying temperature is appropriate (generally higher), which allows for a glass transition in the material, shell formation is more prone to occur (for example, refer to Willis et al. 1999 [129]). More discussions on the effect of drying conditions on shrinkage can be found in Mayor and Sereno 2004 [74].

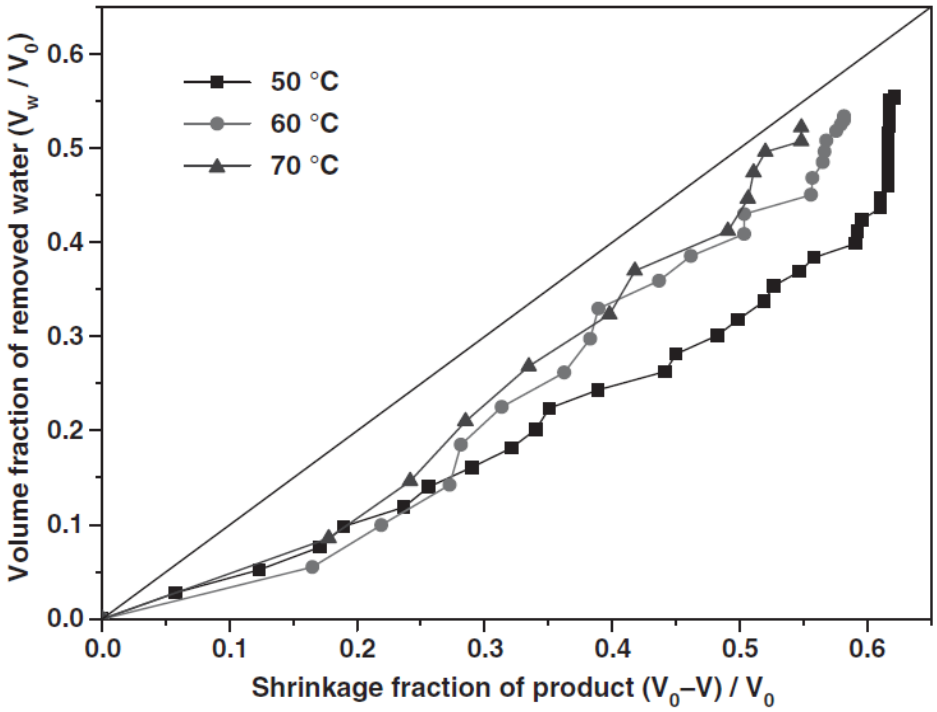

Figure 5.1: Comparison of shrinkage to the amount of water removed, in hot-air drying of Chinese jujube. V_w/V_0 represents the ratio of removed water volume, V_w to the initial fruit volume, V_0. Volume of fruit at any moisture content is given by V. (Fang et al. 2009) [43] (Percentage of shrinkage is $1-(V_0-V)/V$, thus, shrinkage is less than volume fraction of removed water)

5.1.3 Approaches

Modeling of case hardening effect during drying of foodstuffs involves a fundamental based multiphase approach that involves fully coupled multiphase transport with the solid viscoelastic deformation.

As is discussed earlier, one example of such an approach is multiscale modeling based on the Hybrid Mixture Theory which provides marcroscopic equations that are averaged from smaller scales with appropriate constitutive relations. To explore the restrictions on the constitutive relations at the macro-scale from the second law of thermodynamics, we consider a three phase porous material: solid phase *s*, water phase *w*, and gas phase, *g*. The gas phase consists of two components: air *a* and water vapor, *v*. The difference between this system and the one outlined in chapter 2 is that, both air and vapor need to be considered as components of the gas phase in this case due to evaporation. There is mass transfer between phase *w* and the water vapor component in the gas phase, *v*. Thus, the first term on the right hand side of Equation (A.1) does not vanish for component *v* and of Equation (A.2) for phase *w*. This also leads to a non-vanishing first term in Equation (A.12) and second term in Equation (A.11). An example of a system involving mass transfer between phases can be found in Weinstein et al. 2008b [128]. The resultant model in Weinstein et al. 2008b [128] is rather complicated for numerical implementation. Moreover, since two components are considered in the gas phase, exploiting the entropy inequality to obtain the

restrictions on the constitutive relations based on HMT requires that the Helmholtz free energies for both air and vapor be written separately and the number of independent variables introduced to such a system is generally more than the one described in chapter 2. An example of a system involving four phases/components can be found in Singh et al. 2003a [107]. The simplification of the resulting model is rather difficult without making many assumptions, some of which may not be physically realistic, as is discussed in detail in Appendix B. Therefore, for this swelling porous system, which is unsaturated and non-isothermal, using HMT, the modeling involves many parameters, and the implementation of the model requires more information about the system than what is available from experiments. Also, the complexity of the model makes it impossible to carry out numerical implementation in commercial packages and extremely inefficient using a user developed code.

Another approach is to consider the heat, mass and momentum transport of each phase and the constituents in each phase from the macroscopic level by taking into consideration different modes of transport based on the nature of the process under consideration. Discussion of this approach can be found in Datta (2007) [36]. It has been successfully used by several authors to study coupled transport and deformation during food processing (Zhang et al. 2005; Rakesh 2010; Dhall 2011) [132,95,39]. In this chapter, we use the multiphase porous media approach with viscoelastic large deformation and develop a fundamental based model for drying of foodstuffs with capabilities of predicting stresses generated in the material during drying, volume

reduction, (which may or may not deviate from the amount of water removal-case hardening effect in the former case), and final size of the drying sample.

5.2 Mathematical Model

The drying process is modelled based on two-way coupling of multiphase transport and solid mechanics (large strain viscoelasticity). The model describes heat and mass transfer inside a potato cylinder during convective hot air drying as well as the simultaneous large viscoelastic deformation of the solid matrix. Here, drying of potato is considered as an example because case hardening is found during the final stage of drying in Yadollahinia et al. 2009 [130] and the parameters of potato are more readily available in the literature. In the following section, the problem is described, and governing equations with boundary and initial conditions are discussed.

5.2.1 Problem description

A schematic of the geometry is shown in Figure 5.2. A cylindrical sample of potato is considered during drying with air temperatures at 60^0C, 70^0C and 80^0C and air velocity of $1\,m/s$. The sample is considered porous with three phases: solid, liquid water and gas (mixture of air and water-vapor). The problem is considered 2D axisymmetric.

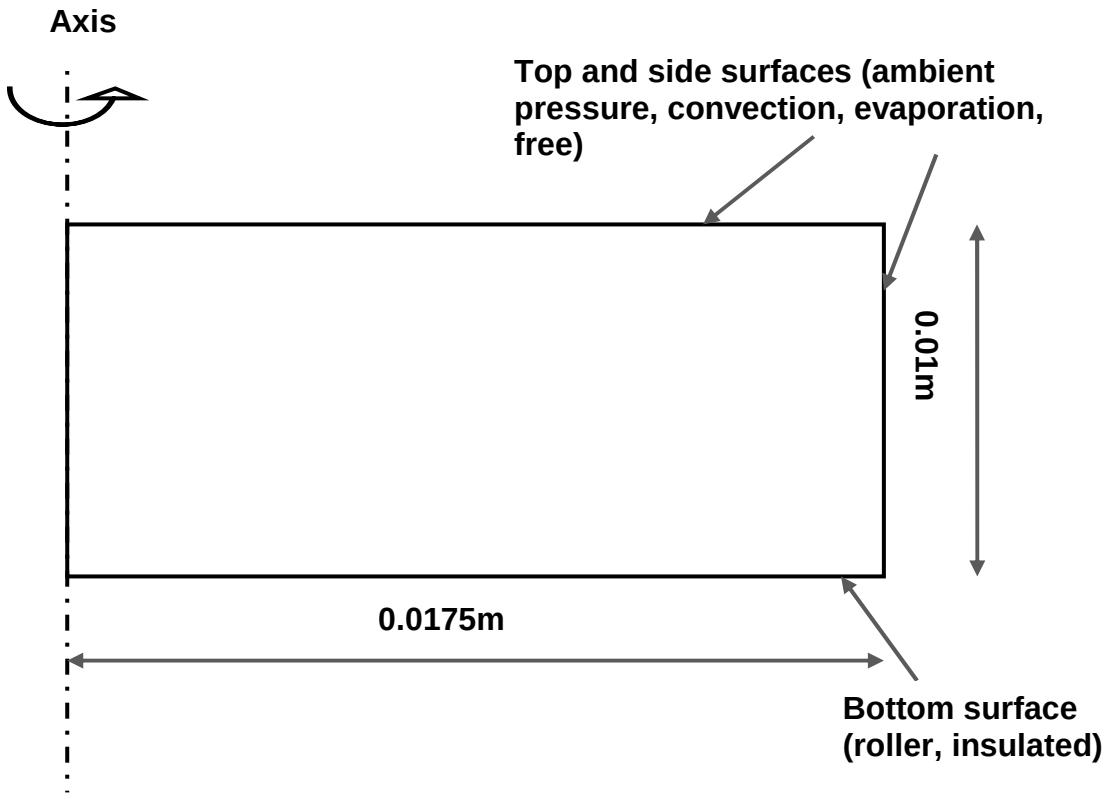

Figure 5.2: A schematic of the potato sample showing axisymmetry.

Conservation equations are developed for liquid water and gas phase and components inside the gas phase. Engergy equation and Darcy flow for the system is also developed. The solid deformation is described using Linear Momentum Balance. The constitutive relationship is also described.

5.2.2 Mass balance equations

The schematic of a representative elementary volume (REV) of the material is shown in Figure 5.3. Porosity, ϕ is used to denote the volume fraction of pores in a representative elementary volume of the material.

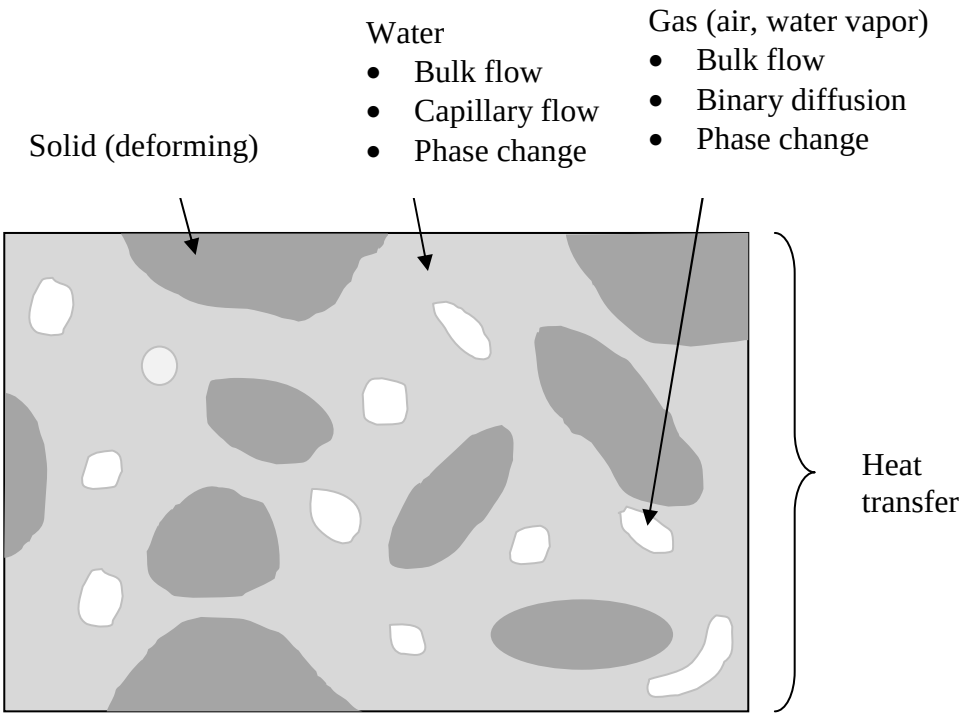

Figure 5.3: Representative elementary volume (REV) of the porous system showing different phases and modes of transport.

$$\phi = \frac{\Delta V_p}{\Delta V} = \frac{\sum_{i=w,g} \Delta V_i}{\Delta V} \tag{5.1}$$

where ΔV is the elemental volume and ΔV_i is the volume occupied by the $i-th$ phase. As the solid matrix deforms, the porosity changes. Volume of the solid phase does not change under the assumption that the solid phase is incompressible. The

porosity at any time t in a deforming porous material can thus be determined using the following relationship:

$$(1-\phi)\Delta V = (1-\phi_0)\Delta V_0 \tag{5.2}$$

The quantities with a subscript 0 represent their initial values.

The mass balance equation of the liquid water phase includes the effects of bulk flow, capillary flow and phase change.

$$\frac{\partial c_w}{\partial t} + \nabla \cdot (\boldsymbol{v}_w \rho_w) = \nabla \cdot [D_{w,cap} \nabla c_w] - \dot{I} \tag{5.3}$$

This equation is rewritten using the ALE description with mesh moving with the solid matrix velocity $\boldsymbol{v}_s$

$$\frac{\partial c_w}{\partial t} + (\boldsymbol{v}_w - \boldsymbol{v}_s) \cdot \nabla c_w + c_w \nabla \cdot \boldsymbol{v}_w = \nabla \cdot [D_{w,cap} \nabla c_w] - \dot{I} \tag{5.4}$$

The total flux of liquid water is due to the fluid pressure, $P_w = P - P_c$, with P being the total pressure and P_c denoting the capillary pressure.

$$\begin{aligned} \boldsymbol{n}_w &= -\rho_w \frac{k_w}{\mu_w} \nabla (P - P_c) \\ &= -\rho_w \frac{k_w}{\mu_w} \nabla P + \rho_w \frac{k_w}{\mu_w} \frac{\partial P_c}{\partial S_w} \nabla S_w \end{aligned} \tag{5.5}$$

where k_w is the permeability of liquid water, μ_w is the dynamic viscosity, and S_w is the liquid water saturation, which denotes the volume fraction of the liquid water with respect to the pore volume

$$S_w = \frac{\Delta V_i}{\Delta V_p} = \frac{\Delta V_i}{\phi \Delta V} \tag{5.6}$$

The first term in Equation (5.5) is rewritten in terms of velocity using Darcy's equation and the second term is written in terms of capillary diffusivity

$$D_{w,cap} = -\frac{k_w}{\phi\mu_w}\frac{\partial p_c}{\partial S_w} \tag{5.7}$$

The gas phase is a mixture of air and water-vapor. Mass balance equation for the gas phase is given by:

$$\frac{\partial c_g}{\partial t} + \nabla\cdot[-\rho_g \frac{k_g}{\mu_g}\nabla P] = \dot{I} \tag{5.8}$$

Using ALE description, the above equation becomes

$$\frac{\partial c_g}{\partial t} + (\boldsymbol{v}_g - \boldsymbol{v}_s)\cdot\nabla c_g + c_g\nabla\cdot\boldsymbol{v}_g = \dot{I} \tag{5.9}$$

Concentration of vapor component in the gas phase is related to the concentration of the gas phase in terms of its mass fraction ω_v, through $c_v = c_g\omega_v$. The mass balance equation of the vapor component includes phase change, bulk flow and binary diffusion:

$$\frac{\partial c_v}{\partial t} + \nabla\cdot(\boldsymbol{v}_g\rho_g\omega_v) = \nabla\cdot(\phi S_g \frac{C_g^2}{\rho_g} M_a M_v D_g \nabla x_v) + \dot{I} \tag{5.10}$$

With ALE, the equation is rewritten as:

$$\frac{\partial c_v}{\partial t} + (\boldsymbol{v}_g - \boldsymbol{v}_s)\cdot\nabla c_g + c_g\nabla\cdot\boldsymbol{v}_g = \nabla\cdot\left(\phi S_g \frac{C_g^2}{\rho_g} M_a M_v D_g \nabla x_v\right) + \dot{I} \tag{5.11}$$

where M_a and M_v are the molecular weights of air and vapor, respectively, D_g is the effective gas diffusivity, C_g is the molar density of gas, S_g is gas saturation defined by $S_g = \frac{\Delta V_g}{\phi\Delta V}$ and is related to the liquid water saturation through $S_w + S_g = 1$,

and x_v is mole fraction of vapor. The mass fraction of the air component in the gas phase, ω_a (with concentration of air being $c_a = \omega_a c_g$) can be obtained by

$$\omega_v + \omega_a = 1 \tag{5.12}$$

In the above equations, velocity of the gaseous and liquid phases with respect to the solid velocity are written using Darcy's law (which replaces the standard momentum conservation equation – Navier-Stokes equation.)

$$\boldsymbol{v}_{i,s} = -\frac{k_i}{\mu_i}\nabla P \tag{5.13}$$

where *i* equals w and g for the liquid water phase and gas phase, respectively.

5.2.3 Energy balance equation

Thermal equilibrium is assumed to exist between all phases. The energy balance equation for the mixture is given as:

$$\rho_{eff} c_{p,eff} \frac{\partial T}{\partial t} + \nabla[(\rho c_p v)_{fluid} T] = \nabla \cdot (K_{eff} \nabla T) - \lambda \dot{I} \tag{5.14}$$

Energy conservation is due to moving phases, phase change and conduction. The properties of the mixture are expressed as averages of phase properties weighted by their mass or volume fractions

$$\rho_{eff} = (1-\phi)\rho_s + \phi(S_w \rho_w + S_g \rho_g) \tag{5.15}$$

$$c_{p,eff} = m_g(\omega_v c_{p,v} + \omega_a c_{p,a}) + m_w c_{p,w} + m_s c_{p,s} \tag{5.16}$$

$$(\rho c_p v)_{fluid} = [\rho_w v_w - D_{w,cap}\nabla c_w]c_{p,w} + \rho_g v_g(\omega_v c_{p,v} + \omega_a c_{p,a}) \tag{5.17}$$

$$K_{eff} = (1-\phi)K_s + \phi[S_w K_w + S_g(\omega_a K_a + \omega_v K_v)] \tag{5.18}$$

5.2.4 Evaporation/Condensation

Phase change between liquid water and water vapor in the gas phase is incorporated using the following expression:

$$\dot{I} = k_{evap}\frac{M_v}{RT}(p_{v,eq} - p_v) \tag{5.19}$$

Where $p_{v,eq}$ is the equilibrium vapor pressure and it is a function of both temperature and moisture content. Detailed discussion about expression (5.19) can be found in Halder et al. (2007) [48].

5.2.5 Solid mechanics

The motion of the solid matrix is governed by linear momentum balance, which is written in terms of the effective stress tensor $\boldsymbol{\sigma}'$:

$$\nabla \cdot (\boldsymbol{\sigma}') = \nabla P_f \tag{5.20}$$

where the effective stress on the solid skeleton $\boldsymbol{\sigma}'$, is related to the pore pressure P_f $(= S_w P_w + S_g P_g)$ and the total stress tensor $\boldsymbol{\sigma}$ via the following relationship:

$$\boldsymbol{\sigma} = \boldsymbol{\sigma}' - P_f \boldsymbol{I} \tag{5.20}$$

Gravity and inertial effect is ignored in this case. The gradient of the pore pressure is acting as the body force in Equation (5.20). When gas pressure gradient is zero (gas is at atmospheric pressure), the right hand side of Equation (5.20) can be rewritten as $-\nabla(S_w P_c)$. Equation (5.20) is written in the current configuration and can be transferred to the reference configuration (see Figure 5.4). The linear momentum balance equation is supplemented by the strain-displacement relationship as well as the constitutive relation that relates the stress and the strain. The strain-displacement relationship is given by:

$$\boldsymbol{E} = \frac{1}{2}[\nabla \boldsymbol{u} + (\nabla \boldsymbol{u})^T + \nabla \boldsymbol{u}(\nabla \boldsymbol{u})^T] \tag{5.21}$$

where $\boldsymbol{E}$ is the green strain tensor and $\boldsymbol{u}$ is the displacement of the solid phase. The constitutive relationship is presented in the next section.

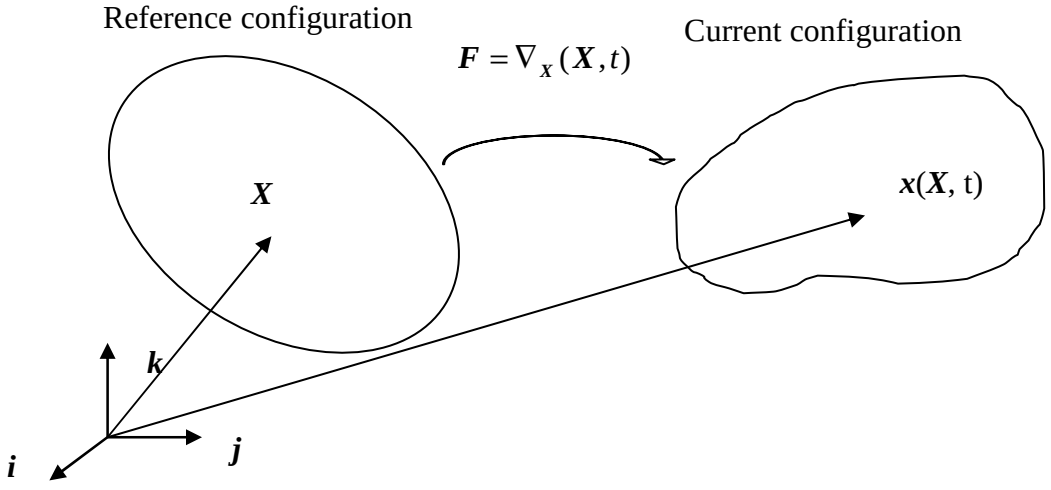

Figure 5.4: The reference and current configuration of a REV during deformation.

5.2.6 Constitutive relationship

As is mentioned earlier, case hardening occurs due to a fast loss of moisture content, causing the increase of rigidity of the porous materials and formation of a shell on the outer surface of the material and a reduced volume decrease. Thus, to correctly model this effect, the material is assumed to be viscoelastic. We consider the finite strain viscoelastic constitutive model presented by Simo and Hughes (1997) [105]. This model is a generalized version of the linear viscoelastic model and it decouples volumetric effects, which are assumed to be elastic, from the volume-preserving effects that are viscoelastic.

We consider the multiplicative decomposition of the mechanical deformation gradient $\boldsymbol{F}$ (total strain is composed of moisture, thermal as well as mechanical strains, for detailed discussion on this, please refer to Perre and Turner (1999) [88] and Dhall (2011) [39]) following Simo and Hughes (1997) [105]:

$$\overline{\boldsymbol{F}} = J^{-1/3}\boldsymbol{F} \tag{5.22}$$

where J is the determinant of the deformation gradient. It can easily be shown that $\overline{\boldsymbol{F}}$ is the volume-preserving part of the deformation gradient. To consider the formulation of a finite strain nonlinear constitutive relationship, we also consider a stored energy function of the following form:

$$W(\boldsymbol{C}) = U(J) + \overline{W}(\overline{\boldsymbol{C}}) \tag{5.23}$$

where the functions U and $\overline{W}$ define the volumetric and volume-preserving contributions of the stored energy function. We choose a Neo-Hookean material model and thus W is written as:

$$W = \frac{K_0}{2}(J-1)^2 - \frac{G_0}{2}(\bar{I}_1 - 3) \tag{5.24}$$

where K_0 and G_0 are the initial bulk and shear modulus, respectively and $\bar{I}_1$ is the first invariant of the right Cauchy-Green strain tensor $\overline{\boldsymbol{C}}$ associated with $\overline{\boldsymbol{F}}$.

The second Piola-Kirchhoff stress tensor is given by (Simo and Hughes 1997) [105]:

$$\boldsymbol{S}^{'}(t) = \boldsymbol{S}^{0}(t) - J^{-2/3} DEV[\sum_{i}^{N} \boldsymbol{Q}_i(t)] \tag{5.25}$$

where $\boldsymbol{S}^{0}(t)$ is defined as

$$\begin{aligned} \boldsymbol{S}^{0}(t) &= 2\frac{\partial W(\boldsymbol{C})}{\partial \boldsymbol{C}} \\ &= JU'(J)\boldsymbol{C}^{-1} + J^{-2/3} DEV\left[2\frac{\partial \overline{W}(\overline{\boldsymbol{C}})}{\partial \overline{\boldsymbol{C}}} \right] \end{aligned} \tag{5.26}$$

and

$$DEV(\bullet) = (\bullet) - \frac{1}{3}[(\bullet) : \boldsymbol{C}]\boldsymbol{C}^{-1} \tag{5.27}$$

In equation (5.25), $\boldsymbol{Q}_i$ are internal variables of stress type. Their evolution is governed by the following rate equation

$$\dot{\boldsymbol{Q}}_i(t) + \frac{1}{\tau_i}\boldsymbol{Q}_i(t) = \frac{\gamma_i}{\tau_i} DEV\left(2\frac{\partial \overline{W}(\overline{\boldsymbol{C}})}{\partial \overline{\boldsymbol{C}}} \right) \tag{5.28}$$

$$lim_{t\to\infty} \boldsymbol{Q}_i(t) = 0 \tag{5.29}$$

where γ_i are the non-dimensional modulus.

5.2.7 Boundary and initial conditions

For solid mechanics, as is illustrated in Figure 5.2, the normal displacement is zero on the left boundary where symmetry is imposed. On the bottom boundary, vertical displacement is zero because the sample is placed on the tray for drying. The other two surfaces are free to move and are traction free.

The boundary conditions for the transport problem are now listed and explained. Liquid water moves out of the top and side surface as water vapor after evaporation.

$$n_{w,surf} = h_m \phi S_w (\rho_{g,surf} \omega_{v,surf} - \rho_{v,amb}) \tag{5.30}$$

Water vapor is convected away on the top and side surfaces.

$$n_{v,surf} = h_m \phi S_g (\rho_{g,surf} \omega_{v,surf} - \rho_{v,amb}) \tag{5.31}$$

The forced convection heat transfer boundary condition is applied to the energy equation. The loss of heat due to evaporation of water and removal of other fluids from the surface are also included in the boundary condition for the energy equation.

$$q_{surf} = h(T_{amb} - T_{surf}) - \lambda n_{w,surf} - \sum n_i c_{p,i} T \tag{5.32}$$

Total pressure on the top and side surfaces equals the ambient pressure and remains constant throughout the drying process.

$$P_{surf} = P_{amb} \tag{5.33}$$

Initial conditions are listed in Table 5.1.

5.2.8 Summary of the model

The independent variables of the two-way coupled model include concentration of water c_w (Equation (5.4)), mass fraction of water vapor ω_v (Equation (5.11)), temperature T (Equation (5.14)), pressure P (Equation (5.9)) and displacement $\boldsymbol{u}$ (Equation (5.20)). These equations are supplemented by Equation (5.12), which is used to determine the dependent variable ω_a, Equation (5.19) for the evaporation rate, Equation (5.21) from the kinematics and Equation (5.25) as a constitutive relation. These equations are fully coupled and need to be solved simultaneously with boundary and initial conditions discussed in the previous section. At each time step, the input parameters, most of which are functions of the independent or dependent variables, are updated. Input parameters are discussed in the following section.

5.3 Input parameters

Input parameters of the problem are listed in Table 5.1. Some of the input parameters are discussed here.

5.3.1 Permeabilities of water and gas

As is discussed in chapter 4, permeabilities of water and gas are products of the intrinsic permeability and the relative permeability. The relative permeabilities of liquid water and gas are given by Bear (1972) [15]:

$$k_{r,w} = \begin{cases} \left(\frac{S_w - S_r}{1 - S_r} \right)^3 f(\phi), & S_w > S_r \\ 0, & S_w < S_r \end{cases} \tag{5.34}$$

$$k_{r,g} = \begin{cases} (1 - 1.1 S_w) f(\phi), & S_w < 1/1.1 \\ 0, & S_w > 1/1.1 \end{cases} \tag{5.35}$$

In Equations (5.34) and (5.35), $f(\phi)$ is the porosity factor that relates the permeabilities of water and gas to the porosity. It represents the effect of porosity change on the permeabilities. Porosity changes following Equation (5.2) for a swelling porous material as has been discussed earlier. The porosity factor is given as (Bear 1972) [15]

$$f(\phi) = \left(\frac{\phi}{\phi_0} \right)^3 \left(\frac{1 - \phi_0}{1 - \phi} \right)^2 \tag{5.36}$$

5.3.2 Viscoelastic parameters

It is reported by Dejmek and Miyawaki (2002) [38] and Ramana and Taylor (1992) [96] that a significant decrease of bending and shear modulus occurs in the

temperature range 60-65 ^0C, indicating a glass transition for potato. Krokida et al. (1998) [62] measured viscoelastic properties for potato using stress relaxation tests and investigated the dependence of the properties on moisture content. In Krokida et al. (1998) [62], it is found that structrual change of potato occurs at a critical moisture content of 1.9 kg/kg d.b. (dimensionless moisture content (M / M_0) of 0.417). This is close to the dimensionless moisture content (0.3) reported in Yadollahinia et al. (2009) [130]. Below this criticle value, the structure of potato becomes more rigid and its area shrinkage decreases. Thus, here we use the properties measured by Krokida et al. (1998) [62]. The force is measured and fitted in a two term Prony Series as a function of moisture content:

$$F(t) = (96.58 - 46.08M) + 68.35exp(-\frac{t}{61.65M^{-0.041}}) + 45.06exp(-\frac{t}{6.07}), M < 1.9 \quad (5.37)$$

$$F(t) = (-42.03 + 30.05M) + 68.35exp(-\frac{t}{49.23M^{0.270}}) + 45.06exp(-\frac{t}{6.07}), M > 1.9 \quad (5.38)$$

Following the approach used in chapter 4 and using the shifting technique, it is found that potato is not hydro-rheologically simple because the relaxation data at different moisture content are not related by a moisture dependent rescaling of time. Thus, we use the data in the form of Equations (5.37) and (5.38).

Table 5.1: Parameters for numerical implementation.

Parameter	**Value**	**Source**
Sample size (m)	0.035(d)×0.01(h)	130
Viscosity		
Water, μ_w (Pa s)	0.988e-3	
Vapor and air, μ_g (Pa s)	1.8e-5	
Intrinsic permeability		

Water, $k_{i,w}$ (m^2)	5e-14	82
Vapor and air, $k_{r,w}$ (m^2)	10e-14	82
Relative permeability		
Water, $k_{r,w}$	Equation 5.34	15
Vapor and air, $k_{r,g}$	Equation 5.35	15
Capillary diffusivity (water), $D_{w,cap}$ (m^2/s)	$1\times10^{-9}exp(-2.8+2M)$	83
Binary diffusivity, $D_{eff,g},(m^2/s)$	$2.6\times10^{-6}\varepsilon_g$	48
Specific heat capacity		
Solid, c_{ps} $(cal/g\ ^0C)$	$0.406+0.00146T+$ $0.203M-0.0249M^2$	121
Water, c_{pw} $(J/kg\ K)$	4178	29
Vapor, c_{pv} $(J/kg\ K)$	2062	29
Air, c_{pa} $(J/kg\ K)$	1006	29
Thermal conductivity		
Solid, K_s, $(W/m\ K)$	$0.272+0.309\,ln(M)$	29
Water, K_w, $(W/m\ K)$	0.6542	29
Vapor, K_v, $(W/m\ K)$	0.026	29
Air, K_a, $(W/m\ K)$	0.026	29
Density		
Solid, ρ_s (kg/m^3)	1530	
Water, ρ_w (kg/m^3)	998	
Vapor, ρ_v (kg/m^3)	Ideal gas law	
Air, ρ_a (kg/m^3)	Ideal gas law	
Latent heat of vaporization, $\lambda(J/kg)$	2.26e6	
Equilibrium vapor pressure, $p_{v,eq}$ (Pa)	$p_{sat}(T)exp(-0.0267M^{-1.656}$ $+0.0107exp(-1.287M)$ $M^{1.1513}ln[p_{sat}(T)])$	
Ambient pressure, P_{amb} (Pa)	101325	
Mass transfer coefficient, h_m (m/s)	0.01	Lewis analogy
Heat transfer coefficient, h $(W/m^2\ K)$	100.78	104
Ambient temperature, $T_{amb}(K)$	300	

Evaporation rate constant, $k_e vap$ (/s)	1e-3	48
Viscoelastic parameter, F (N)	Equations 5.37 and 5.38	62
Initial Conditions		
Porosity, ϕ_0	0.02	
Moisture content on a dry basis, M_0	4.56	130
Vapor mass fraction, $\omega_{v,0}$	0.01	
Temperature, T_0 (K)	300	
Displacement, $\boldsymbol{u}_s$ (m)	0	

5.4 Remarks on Numerical Implementation of the Model in Commercial Software

Numerical implementation of similar models for transport in rigid porous materials or in swelling porous materials that are elastic has been successfully accomplished by Halder et al. (2007) [48], Rakesh (2010) [95] and Dhall (2011) [39] using a commercially available finite element software, COMSOL Multiphysics 4.1 (Comsol Inc., Burlington, MA). Thus, it is proposed that this model be implemented using this commercial software.

However, the model presented here has more complexity for numerical implementation, that is, nonlinear viscoelasticity is involved. COMSOL Multiphysics 4.1 currently does not have capabilities for direct implementation of nonlinear viscoelasticity. The built in hyperelastic material model in COMSOL Multiphysics

calculates the 2nd Piola Kirchhoff stress $\boldsymbol{S}^0$ in Equation (5.25). $\boldsymbol{Q}_i$ needs to be calculated by integrating the evolution Equation (5.28) and then the second term in the right hand side of Equation (5.28) needs to be added to the stress expression $\boldsymbol{S}^0$ in COMSOL Multiphysics. The integration of $\boldsymbol{Q}_i$ is accomplished by adding eight PDEs based on a two-term Prony series for a 2D axisymmetric body (see Equation (5.39)).

$$\begin{pmatrix} Q_{RR,1} & 0 & Q_{RZ,1} \\ & Q_{\Phi\Phi,1} & 0 \\ sym & & Q_{ZZ,1} \end{pmatrix} \text{ and } \begin{pmatrix} Q_{RR,2} & 0 & Q_{RZ,2} \\ & Q_{\Phi\Phi,2} & 0 \\ sym & & Q_{ZZ,2} \end{pmatrix} \tag{5.39}$$

where R, Z and Φ are the coordinates in the undeformed cylindrical coordinate system.

The implementation of nonlinear viscoelasticity in COMSOL Multiphysics 4.1 is accomplished using the procedure described above. Results are obtained for the uncoupled problem with solid mechanics only. These results can then be used for the fully coupled problem. In the following two sections, a test case is first considered to validate the code and then solutions for the uncoupled problem with solid mechanics only are presented.

5.4.1 Test case: solid cylinder under external pressure

As a validation of the code, a solid cylinder under external pressure is considered, since exact elastic as well as linear viscoelastic solutions are known to this problem.

Both linear and nonlinear viscoelastic numerical solutions are obtained for this case. The geometry with boundary conditions is shown in Figure 5.5. Elastic solutions to this problem are that both the radial and the hoop stresses are equal to the applied external pressure and the radial displacement is a linear function of the radial coordinate *r*. Using the correspondence principle for linear viscoelasticity, one could easily obtain that the radial and hoop stresses are also equal to the applied external pressure in this case.

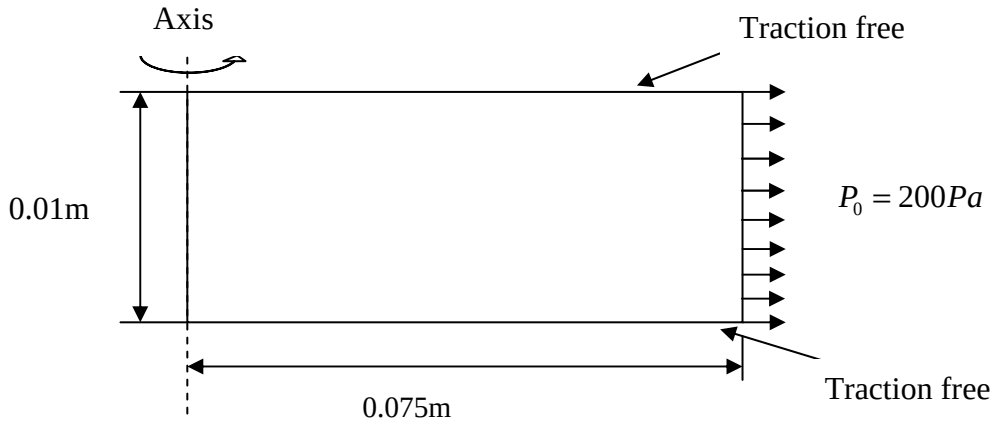

Figure 5.5: Schematic of solid cylinder under external pressure.

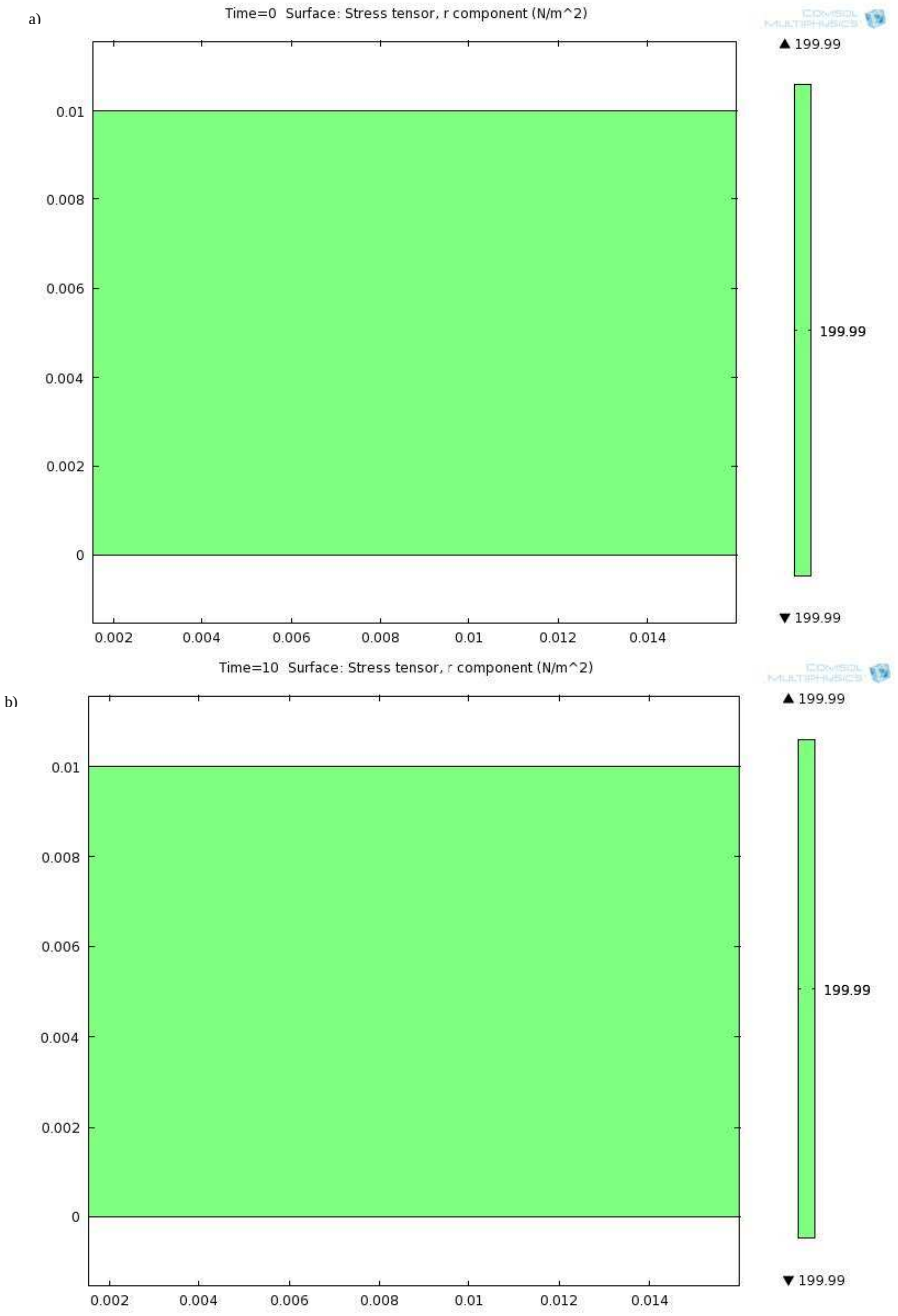

Figure 5.6: Linear viscoelastic solution: radial stress distribution at a) t=0 and b) t=10s for the test case.

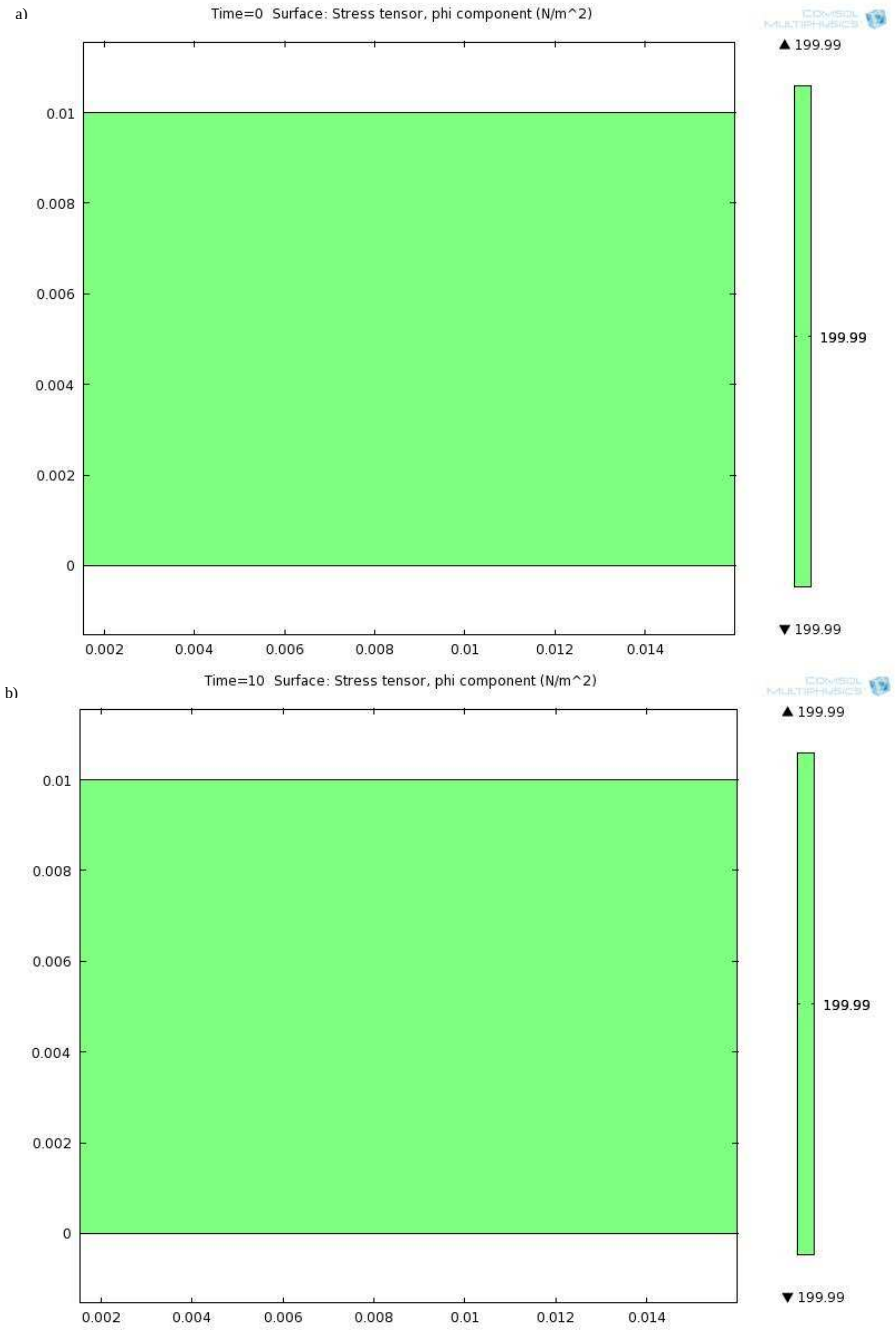

Figure 5.7: Linear viscoelastic solution: hoop stress distribution at a) t=0 and b) t=10s for the test case.

a)

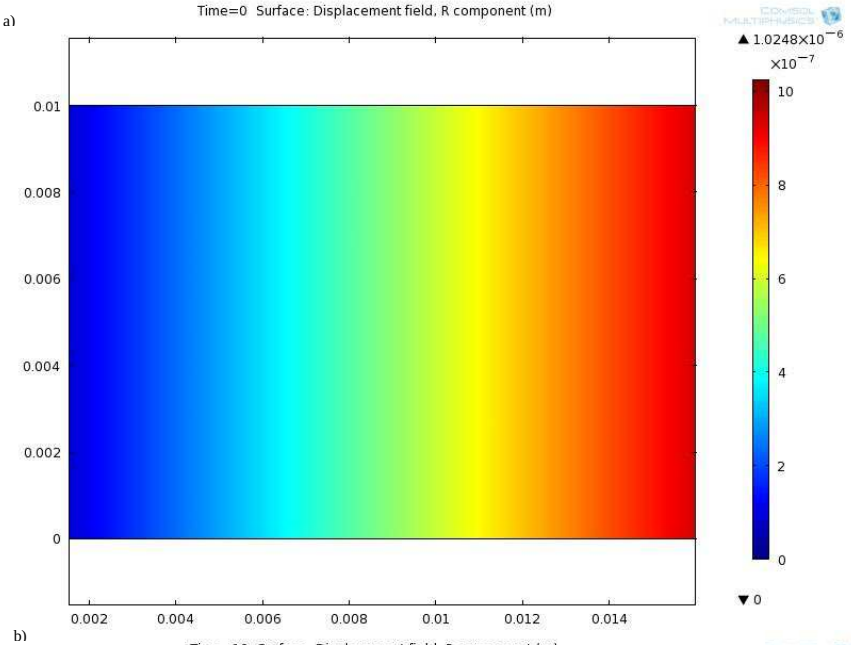
Time=0 Surface: Displacement field, R component (m)
▲ 1.0248×10⁻⁶
×10⁻⁷
10
8
6
4
2
0
▼ 0
0.01
0.008
0.006
0.004
0.002
0
0.002
0.004
0.006
0.008
0.01
0.012
0.014

b)

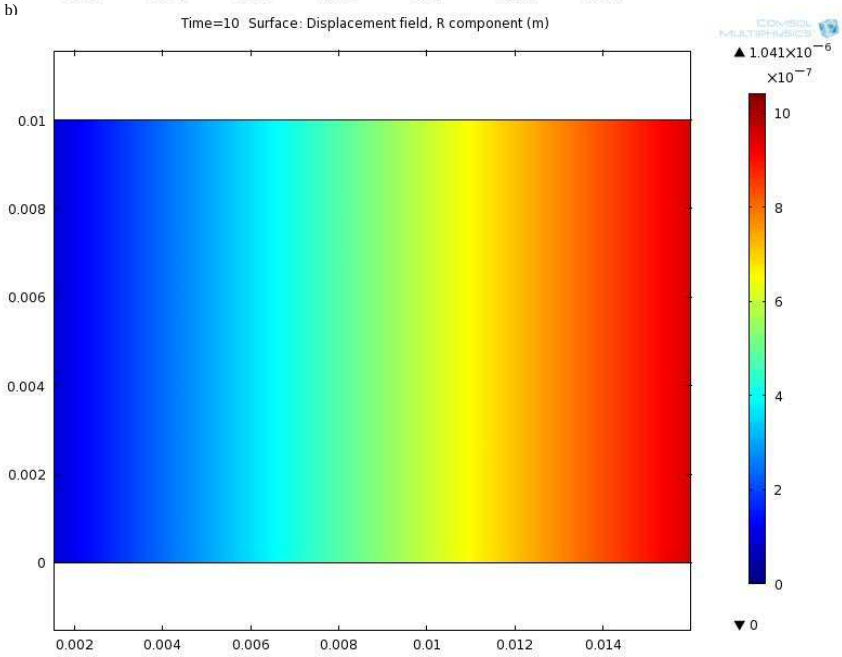
Time=10 Surface: Displacement field, R component (m)
▲ 1.041×10⁻⁶
×10⁻⁷
10
8
6
4
2
0
▼ 0
0.01
0.008
0.006
0.004
0.002
0
0.002
0.004
0.006
0.008
0.01
0.012
0.014

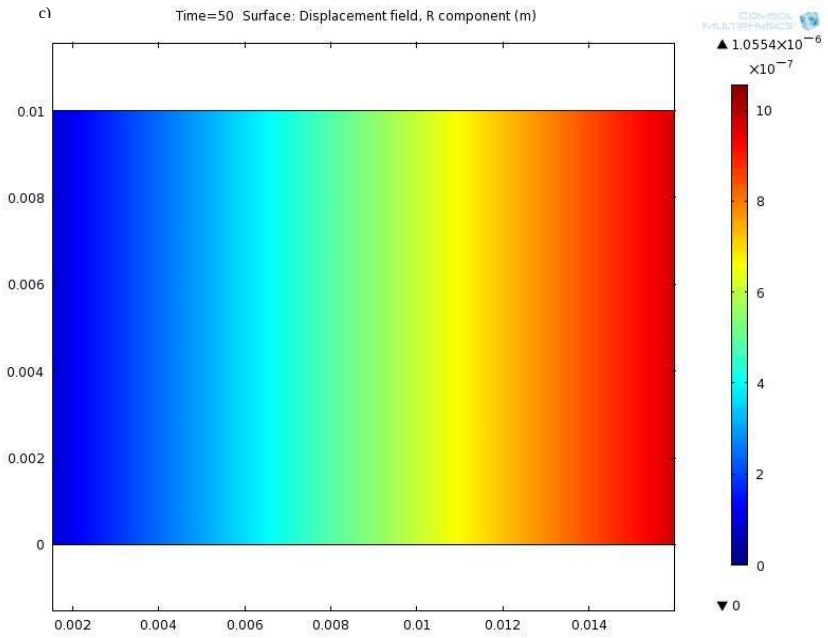

Figure 5.8: Linear viscoelastic solution: radial displacement at a) t=0, b) t=10s and c) t=50s for the test case for the test case.

From Figures 5.6 and 5.7, we could find that the numerical solutions for the radial stress and hoop stress agree with the analytical solution (t=0s gives the elastic solution of the problem). $\sigma_{r\phi}$ and $\sigma_{\phi z}$ are numerically calculated to be zero at all times, which is expected as 2D axisymmetry is considered. It is observed from the numerical solution that the radial displacement is a linear function of r at t=0s and the creep rate is observed to decrease as time t gets larger (Figure 5.8).

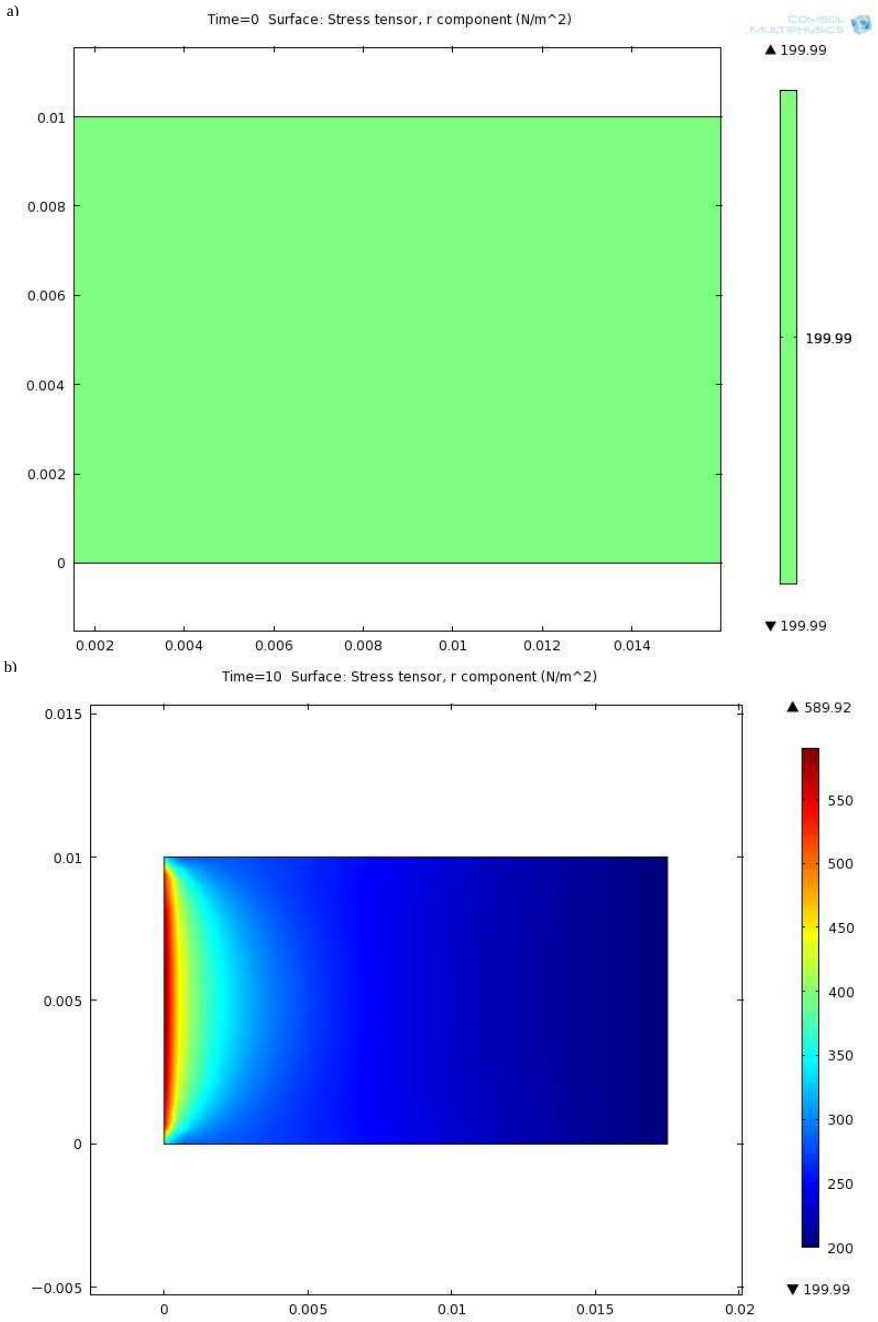

Figure 5.9: Nonliear viscoelastic solution: radial stress distribution at t=0 and t=10s for the test case.

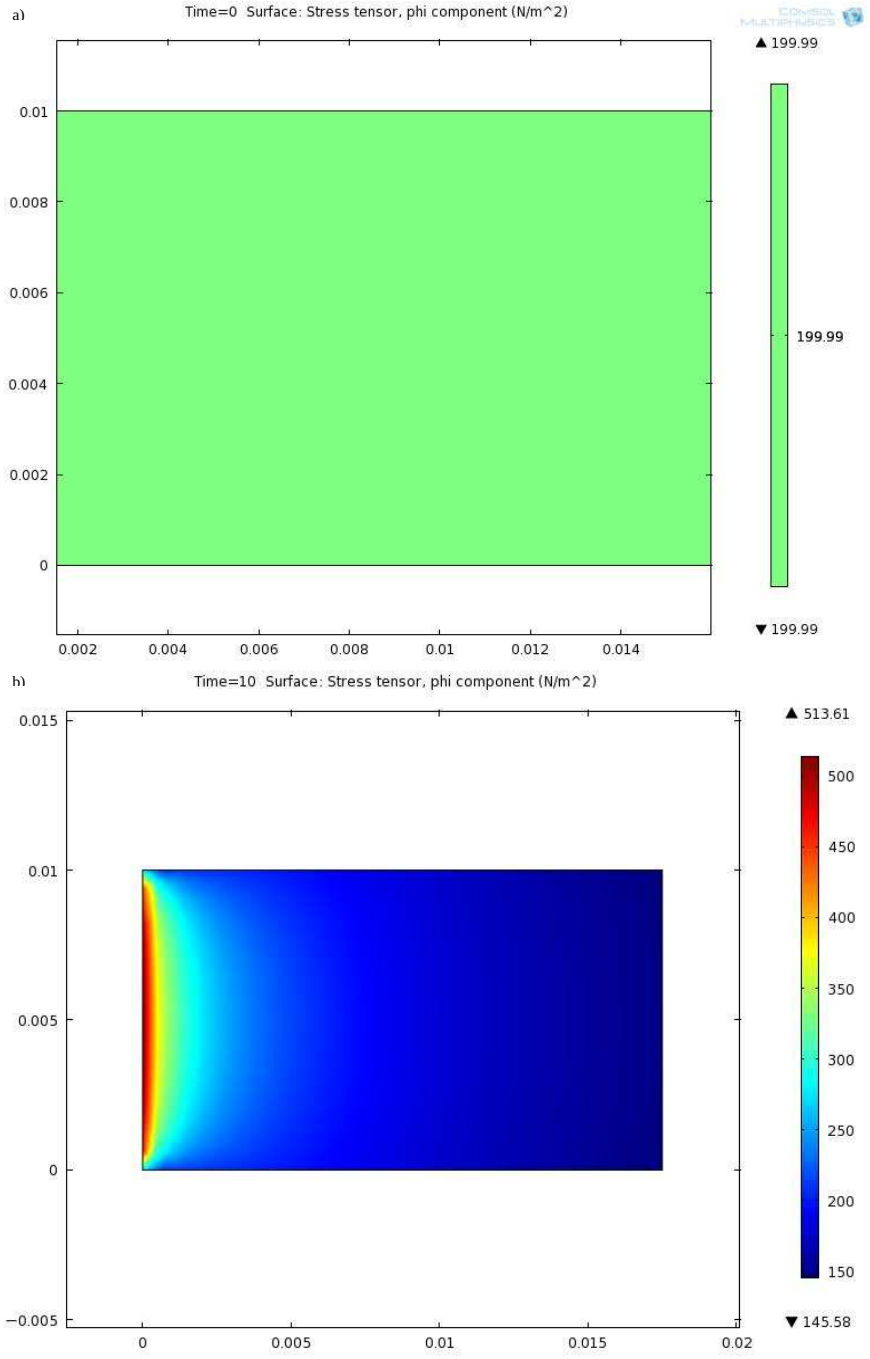

Figure 5.10: Nonliear viscoelastic solution: hoop stress distribution at *t*=0 and *t*=10s for the test case.

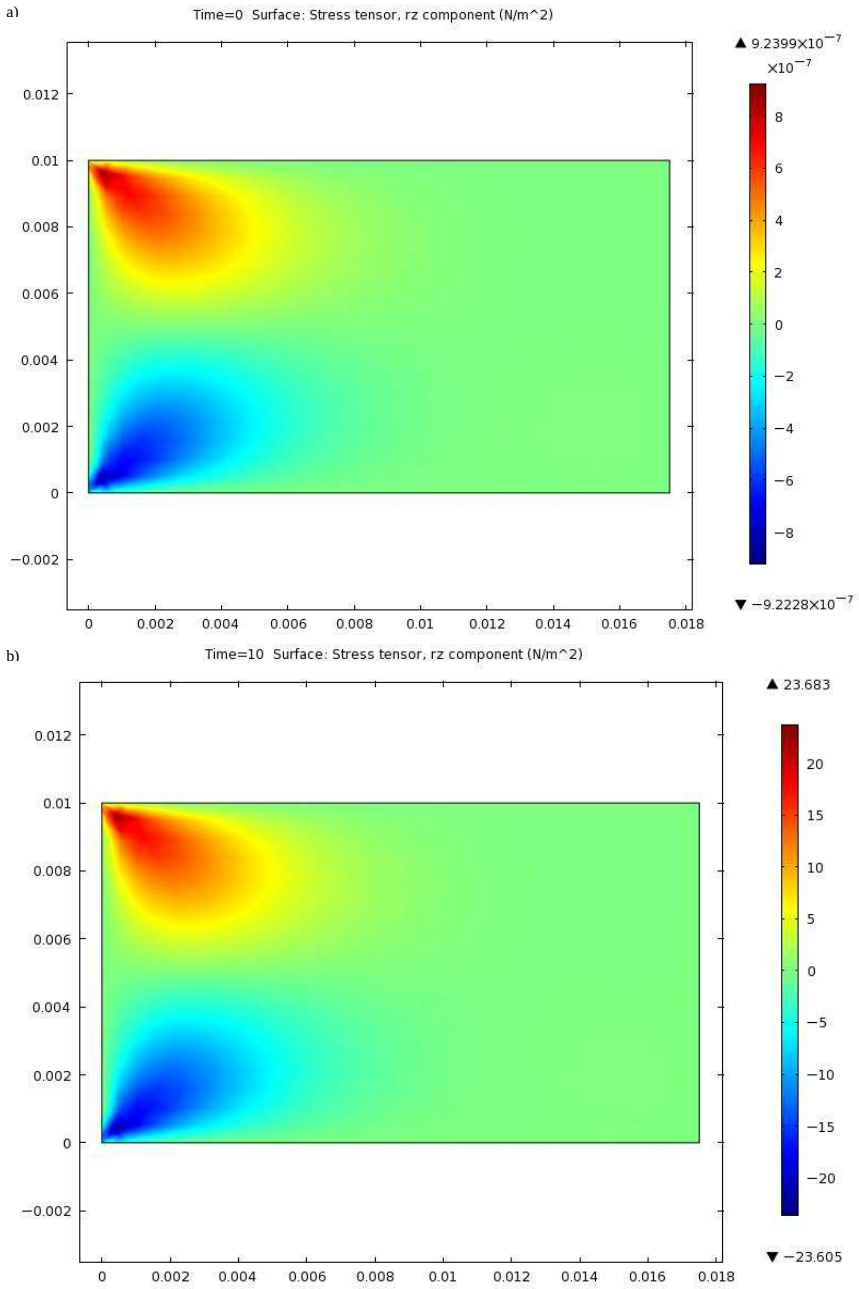

Figure 5.11: Nonliear viscoelastic solution: σ_{rz}, the Cauchy shear stress in rz direction, distribution at *t*=0s and *t*=10s for the test case.

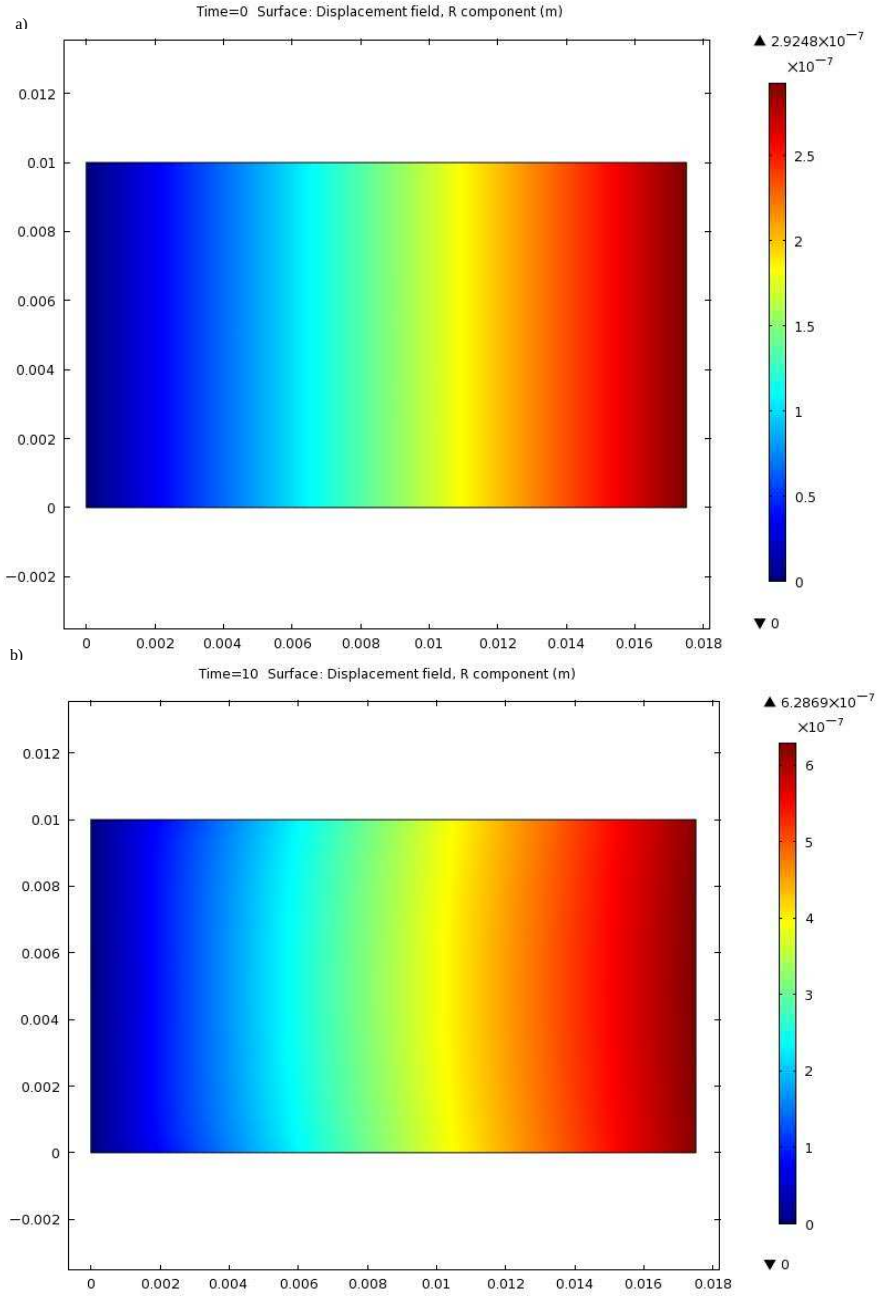

Figure 5.12: Nonliear viscoelastic solution: radial displacement at t=0 and t=10s for the test case for the test case.

Nolinear viscoelstic solutions are shown in Figures 5.9-5.12. At t=0s, numerical solutions are seen to agree with the elastic solutions. Due to geometric nonlinearity

and the fact that the stresses are functions of the material properties, at t=10s, stress redistributions are observed for both the radial and the hoop stresses. Both of the stresses increase around the center line of the solid cylinder and remain independent of z (equals the external pressure) near the outer surface. The stresses around the center line increase very slowly at smaller times and stress redistribution becomes stronger as time t increases. The shearing stress σ_{rz} is essentially zero in this problem.

5.4.2 Uncoupled problem: solid cylinder with body forces

For the uncoupled problem with solid mechanics only, body forces are prescribed in both the r and z directions (Figure 5.13); this is because, in the two-way coupled problem, body force is the driving force in the linear momentum balance equation (5.20).

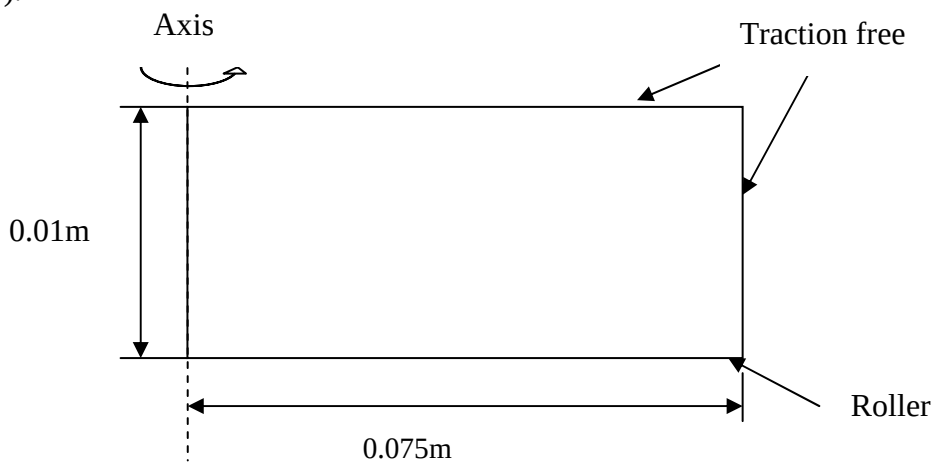

Figure 5.13: Schematic of solid cylinder with boundary conditions.

As is shown in Equations (5.37) and (5.38), relaxation parameters are functions of moisture contents. For this uncoupled problem, results are obtained for two moisture contents: M = 2.3 and M = 0.3. Stresses distributions are shown in Figures 5.14-5.17. The outer and upper surfaces are traction free and the radial stress σ_{rr} and axial stress σ_{zz} are found to be zero for these surfaces, respectively. At lower moisture contents, the material is more rigid and higher stresses are found compared to those at higher moisture contents. Fracture is more likely to occur when stresses are higher and this agrees with the fact that cracks are formed in dehydrated products, for example, dehydrated potato cubes.

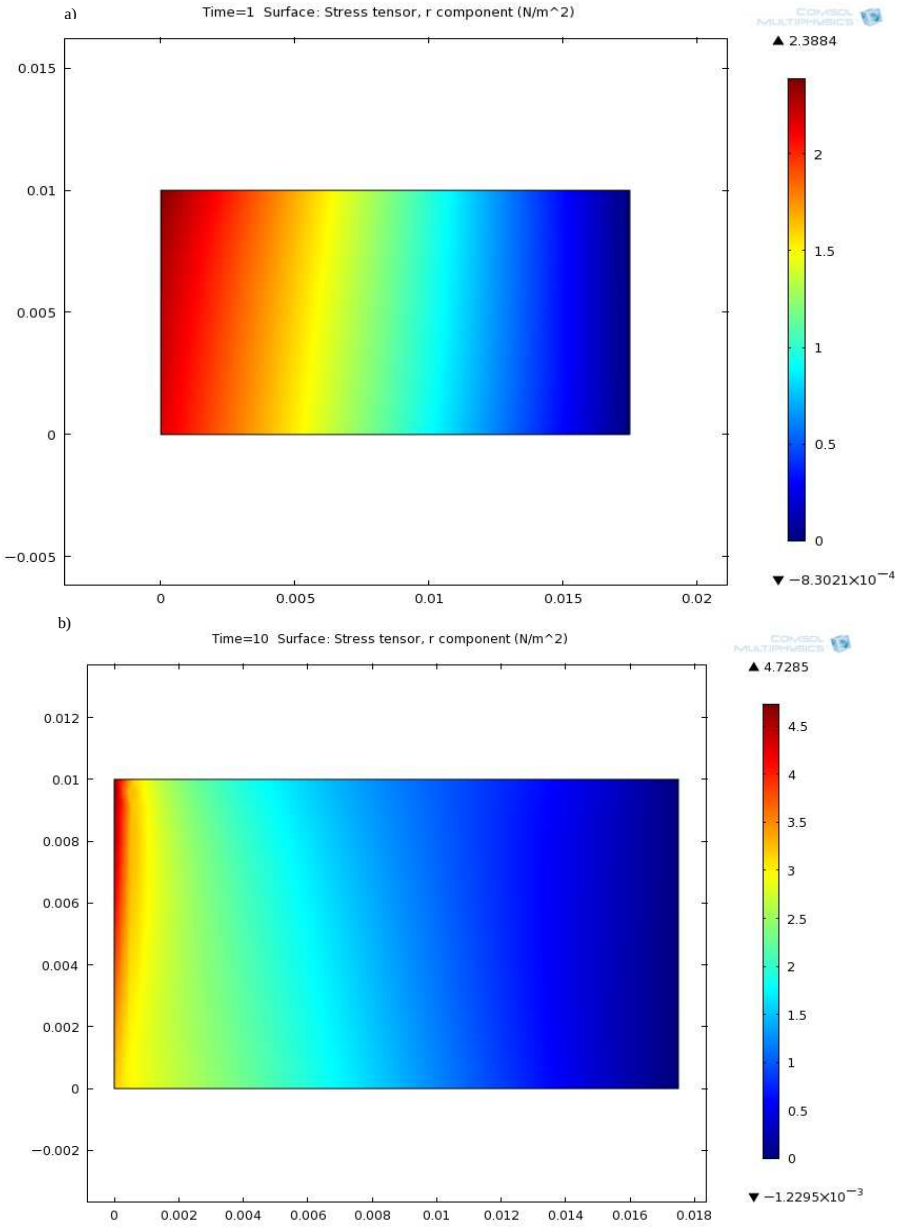
a)
Time=1 Surface: Stress tensor, r component (N/m^2)
▲ 2.3884
▼ −8.3021×10^−4
b)
Time=10 Surface: Stress tensor, r component (N/m^2)
▲ 4.7285
▼ −1.2295×10^−3

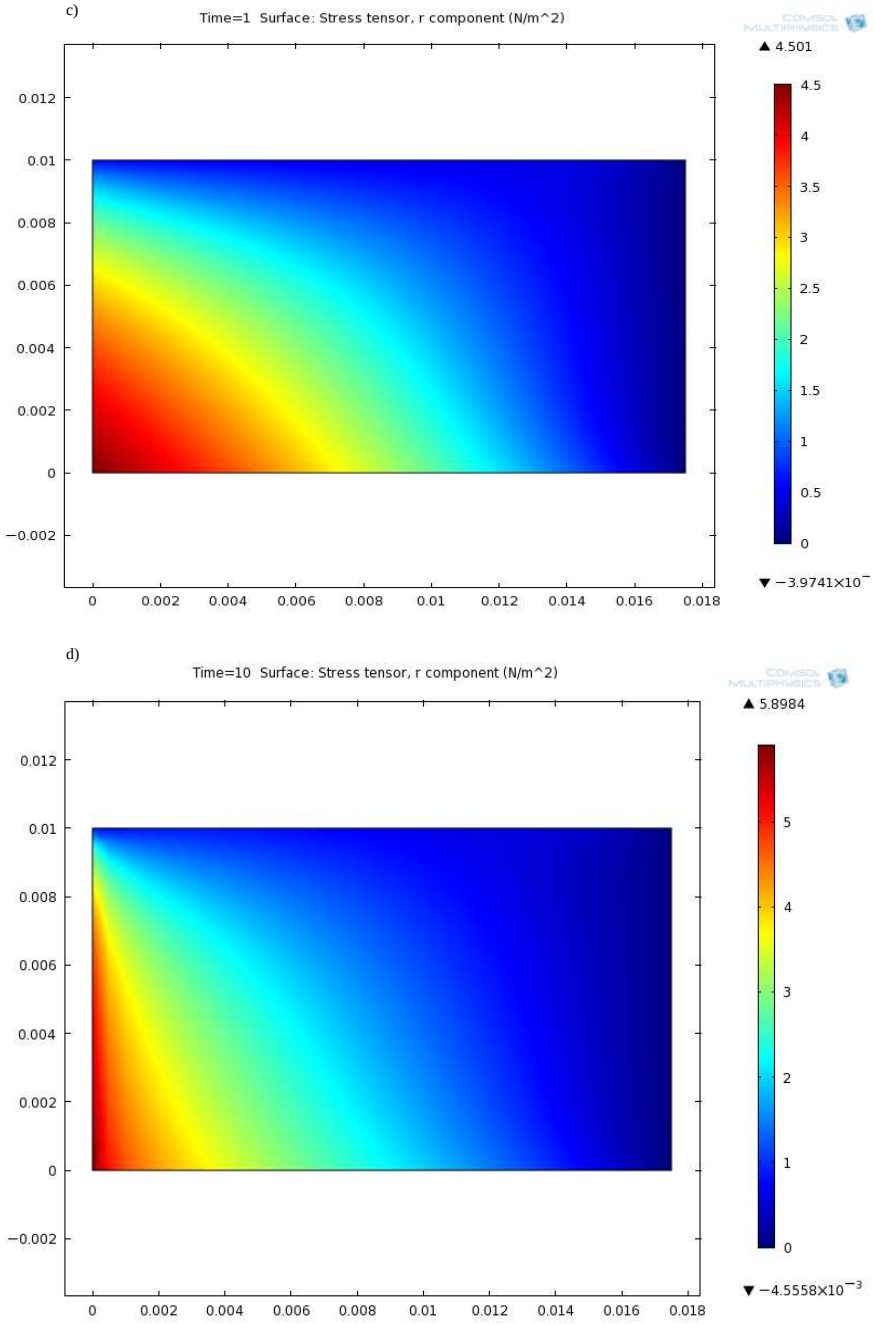

Figure 5.14: Radial stresses at different times and moisture contents: a) *t*=1s, *M*=2.3; b) *t*=10s, *M*=2.3; c) *t*=1s, *M*=0.3; d) *t*=10s, *M*=0.3.

a)

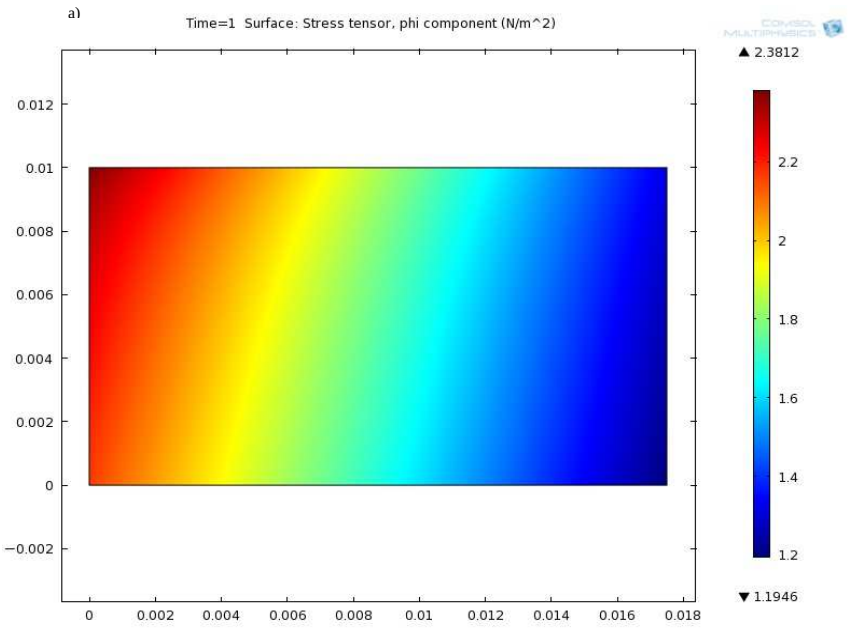
Time=1 Surface: Stress tensor, phi component (N/m^2)
▲ 2.3812
2.2
2
1.8
1.6
1.4
1.2
▼ 1.1946
0.012
0.01
0.008
0.006
0.004
0.002
0
−0.002
0
0.002
0.004
0.006
0.008
0.01
0.012
0.014
0.016
0.018

b)

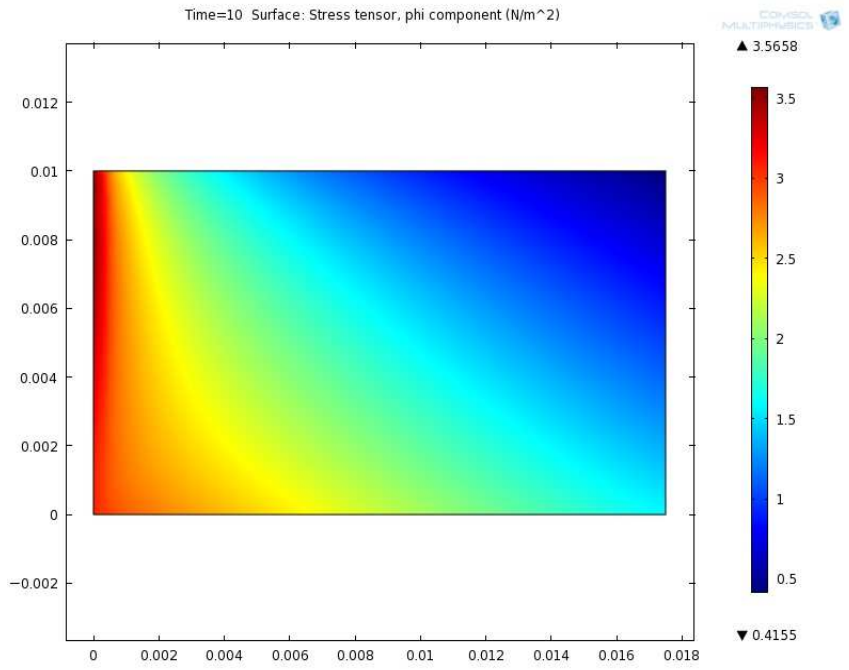
Time=10 Surface: Stress tensor, phi component (N/m^2)
▲ 3.5658
3.5
3
2.5
2
1.5
1
0.5
▼ 0.4155
0.012
0.01
0.008
0.006
0.004
0.002
0
−0.002
0
0.002
0.004
0.006
0.008
0.01
0.012
0.014
0.016
0.018

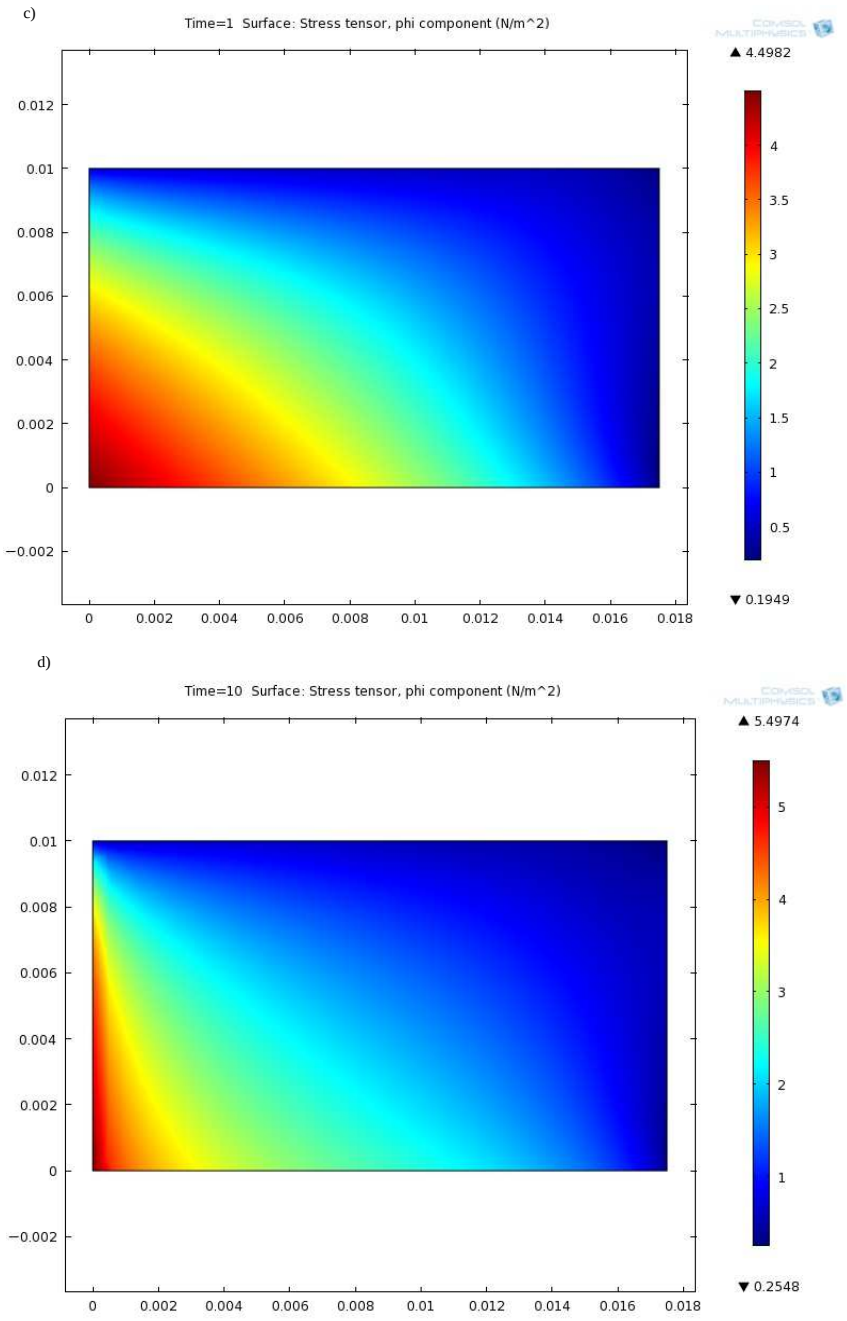

Figure 5.15: Hoop stresses at different times and moisture contents: a) t=1s, M=2.3; b) t=10s, M=2.3; c) t=1s, M=0.3; d) t=10s, M=0.3.

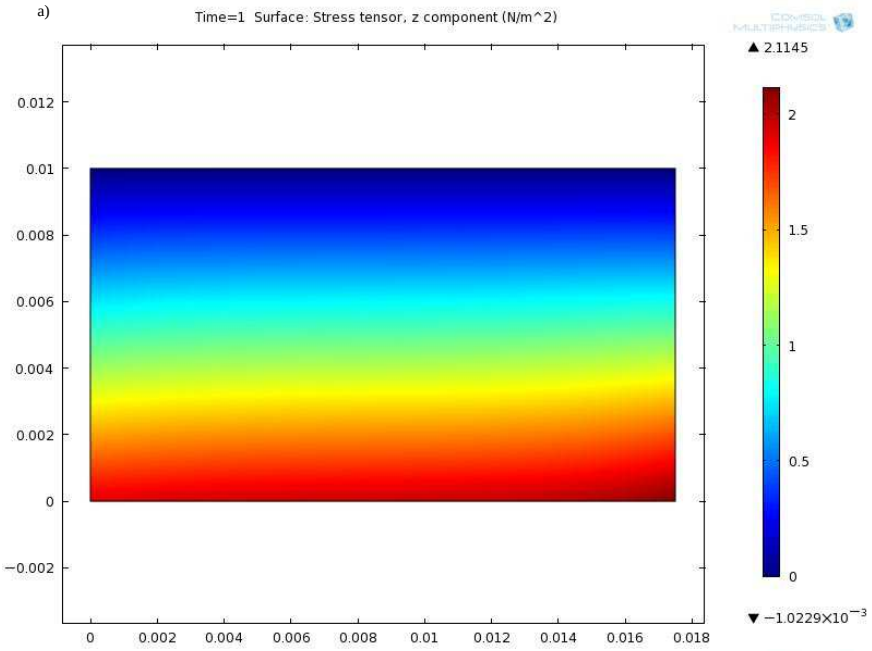
a)
Time=1 Surface: Stress tensor, z component (N/m^2)
▲ 2.1145
2
1.5
1
0.5
0
▼ −1.0229×10^−3
0.012
0.01
0.008
0.006
0.004
0.002
0
−0.002
0
0.002
0.004
0.006
0.008
0.01
0.012
0.014
0.016
0.018

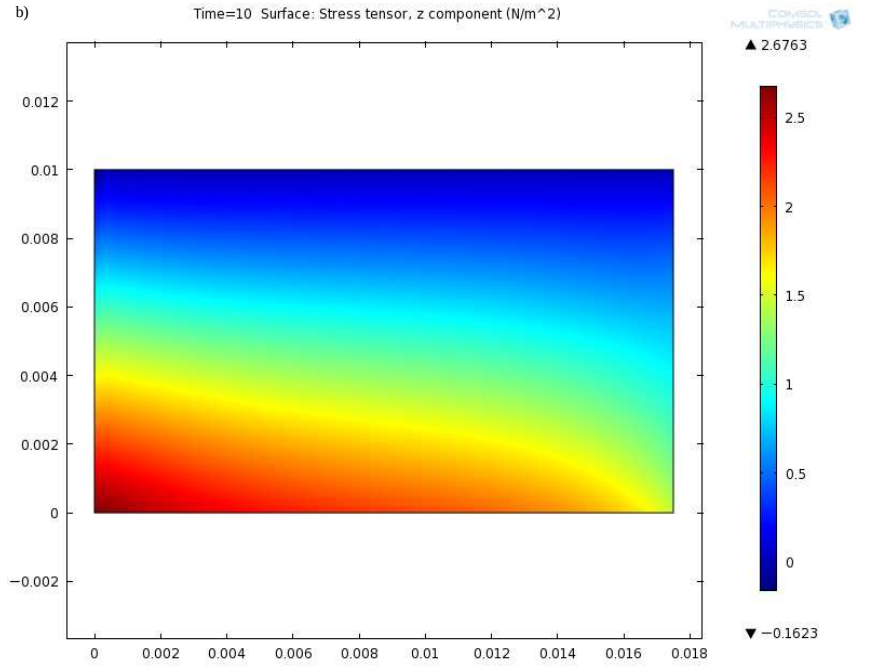
b)
Time=10 Surface: Stress tensor, z component (N/m^2)
▲ 2.6763
2.5
2
1.5
1
0.5
0
▼ −0.1623
0.012
0.01
0.008
0.006
0.004
0.002
0
−0.002
0
0.002
0.004
0.006
0.008
0.01
0.012
0.014
0.016
0.018

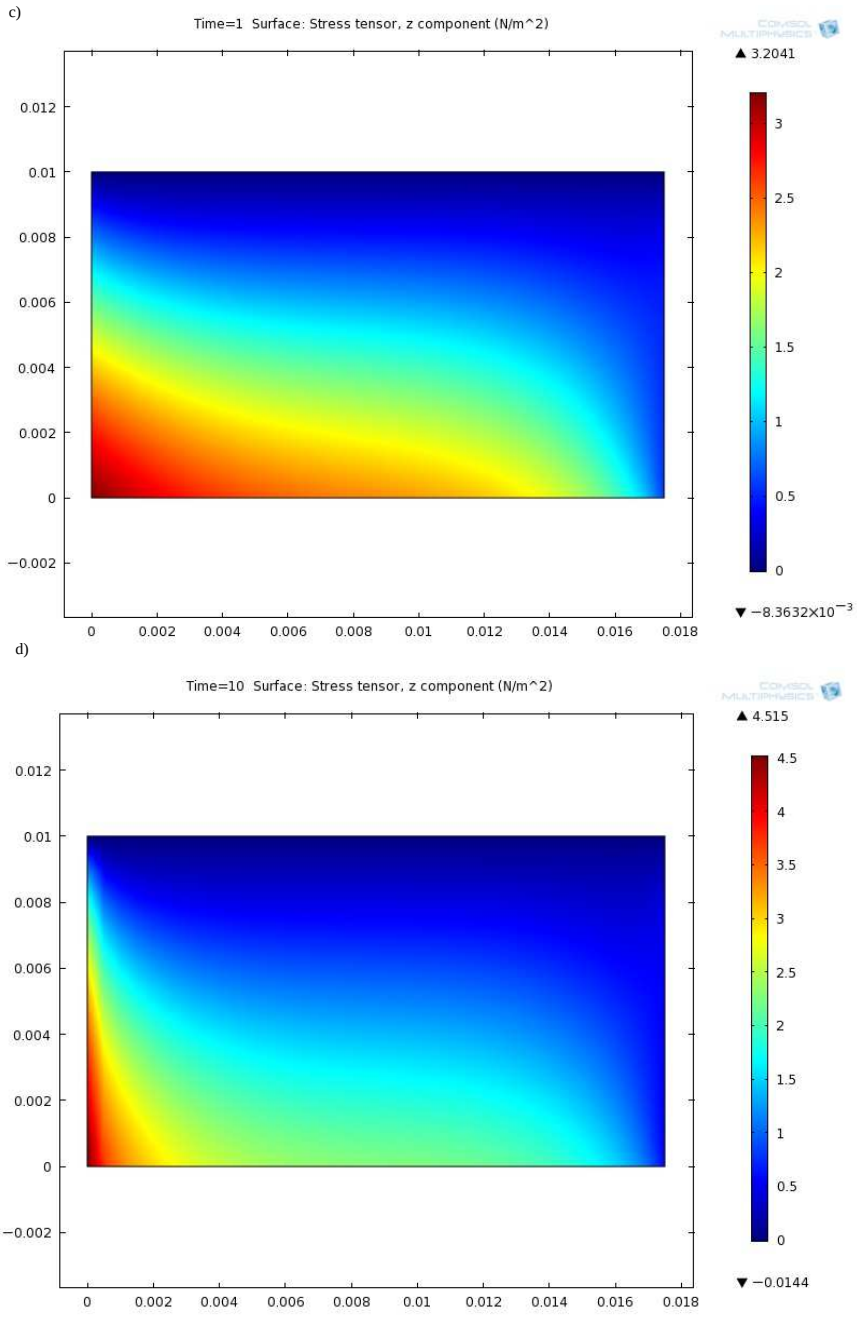

Figure 5.16: σ_{zz} at different times and moisture contents: a) t=1s, M=2.3; b) t=10s, M=2.3; c) t=1s, M=0.3; d) t=10s, M=0.3.

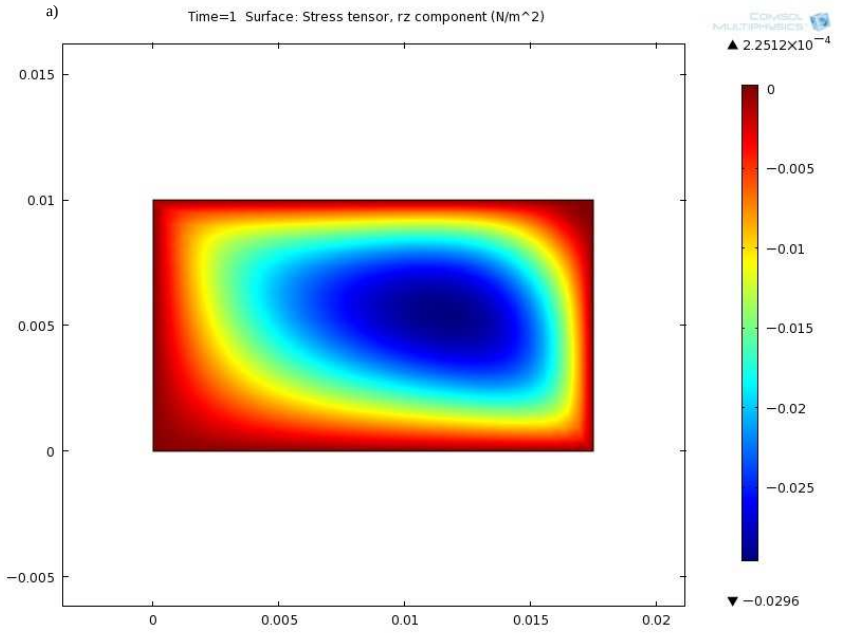
a)
Time=1 Surface: Stress tensor, rz component (N/m^2)
▲ 2.2512×10^−4
0
−0.005
−0.01
−0.015
−0.02
−0.025
▼ −0.0296
0.015
0.01
0.005
0
−0.005
0
0.005
0.01
0.015
0.02

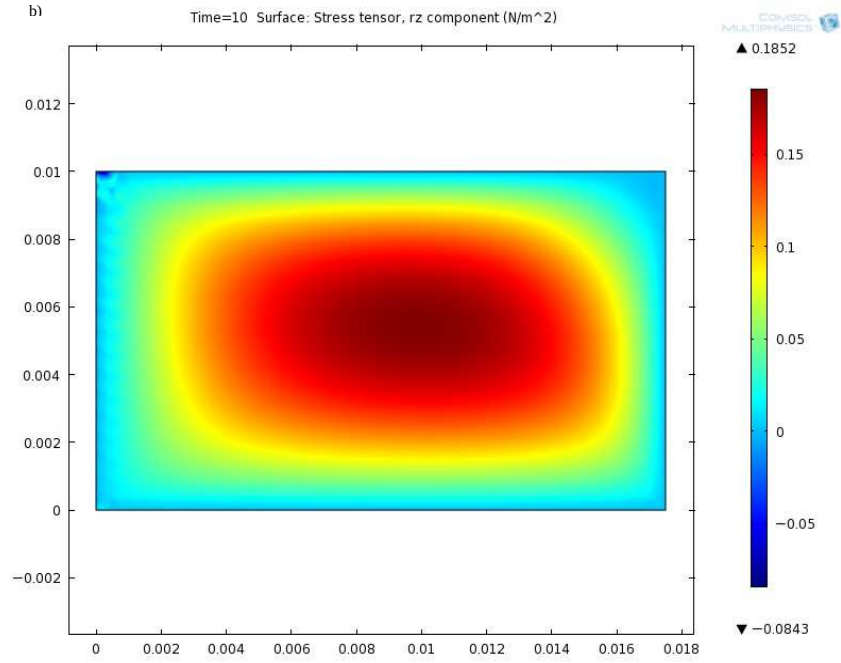
b)
Time=10 Surface: Stress tensor, rz component (N/m^2)
▲ 0.1852
0.15
0.1
0.05
0
−0.05
▼ −0.0843
0.012
0.01
0.008
0.006
0.004
0.002
0
−0.002
0
0.002
0.004
0.006
0.008
0.01
0.012
0.014
0.016
0.018

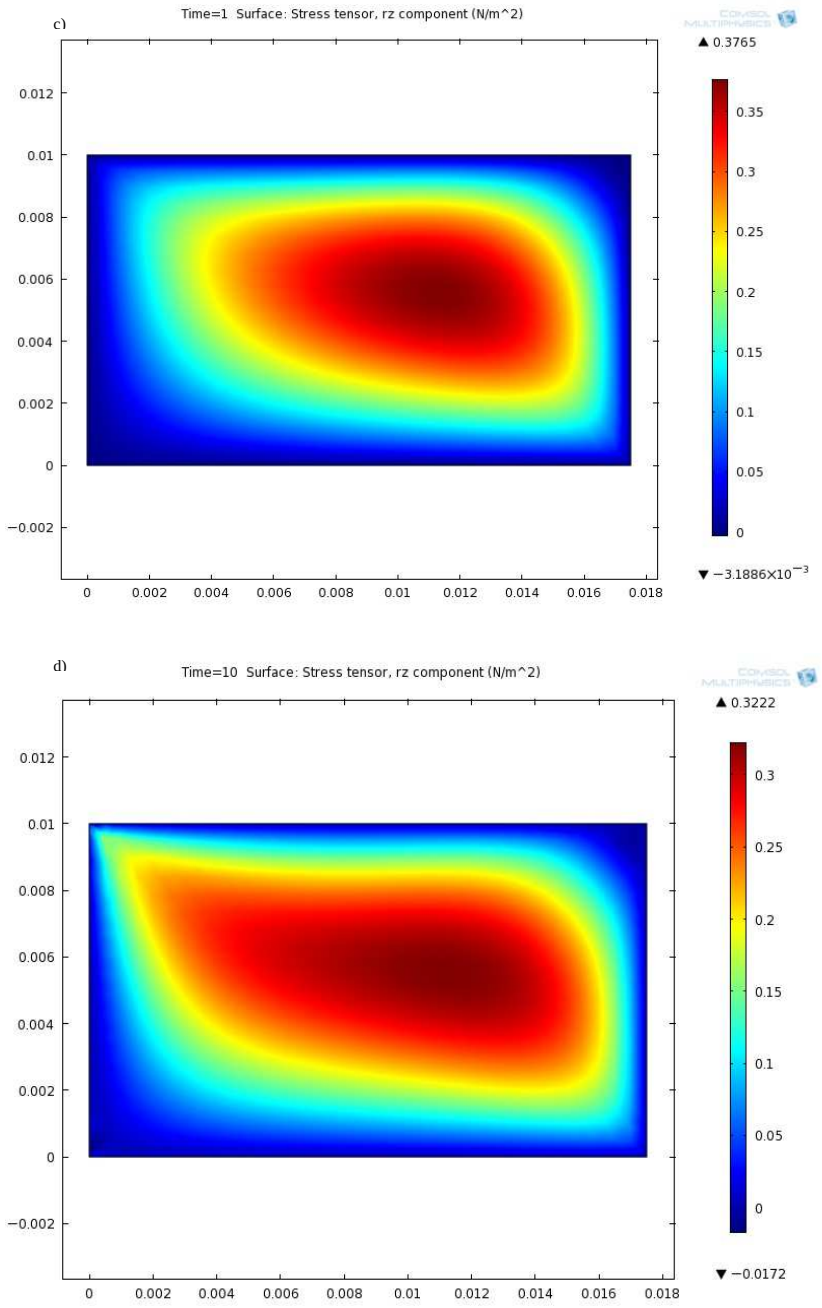

Figure 5.17: σ_{rz} at different times and moisture contents: a) t=1s, M=2.3; b) t=10s, M=2.3; c) t=1s, M=0.3; d) t=10s, M=0.3.

a)

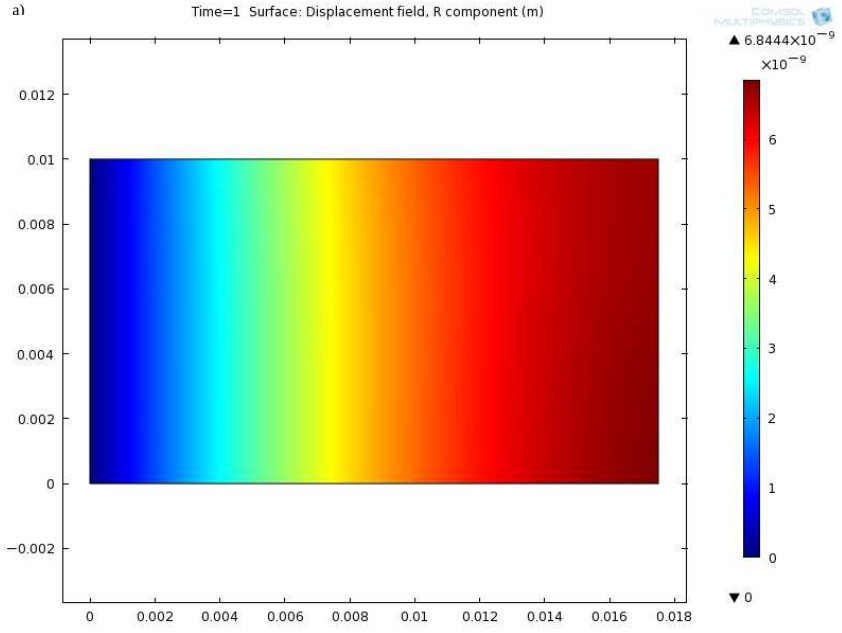
Time=1 Surface: Displacement field, R component (m)
▲ 6.8444×10⁻⁹
×10⁻⁹
6
5
4
3
2
1
0
▼ 0
0.012
0.01
0.008
0.006
0.004
0.002
0
−0.002
0
0.002
0.004
0.006
0.008
0.01
0.012
0.014
0.016
0.018

b)

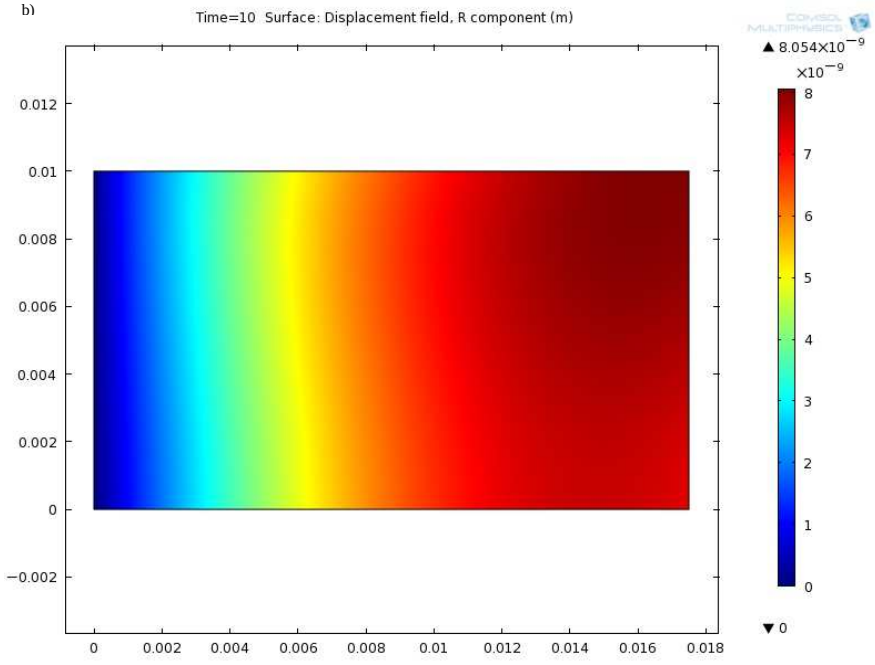
Time=10 Surface: Displacement field, R component (m)
▲ 8.054×10⁻⁹
×10⁻⁹
8
7
6
5
4
3
2
1
0
▼ 0
0.012
0.01
0.008
0.006
0.004
0.002
0
−0.002
0
0.002
0.004
0.006
0.008
0.01
0.012
0.014
0.016
0.018

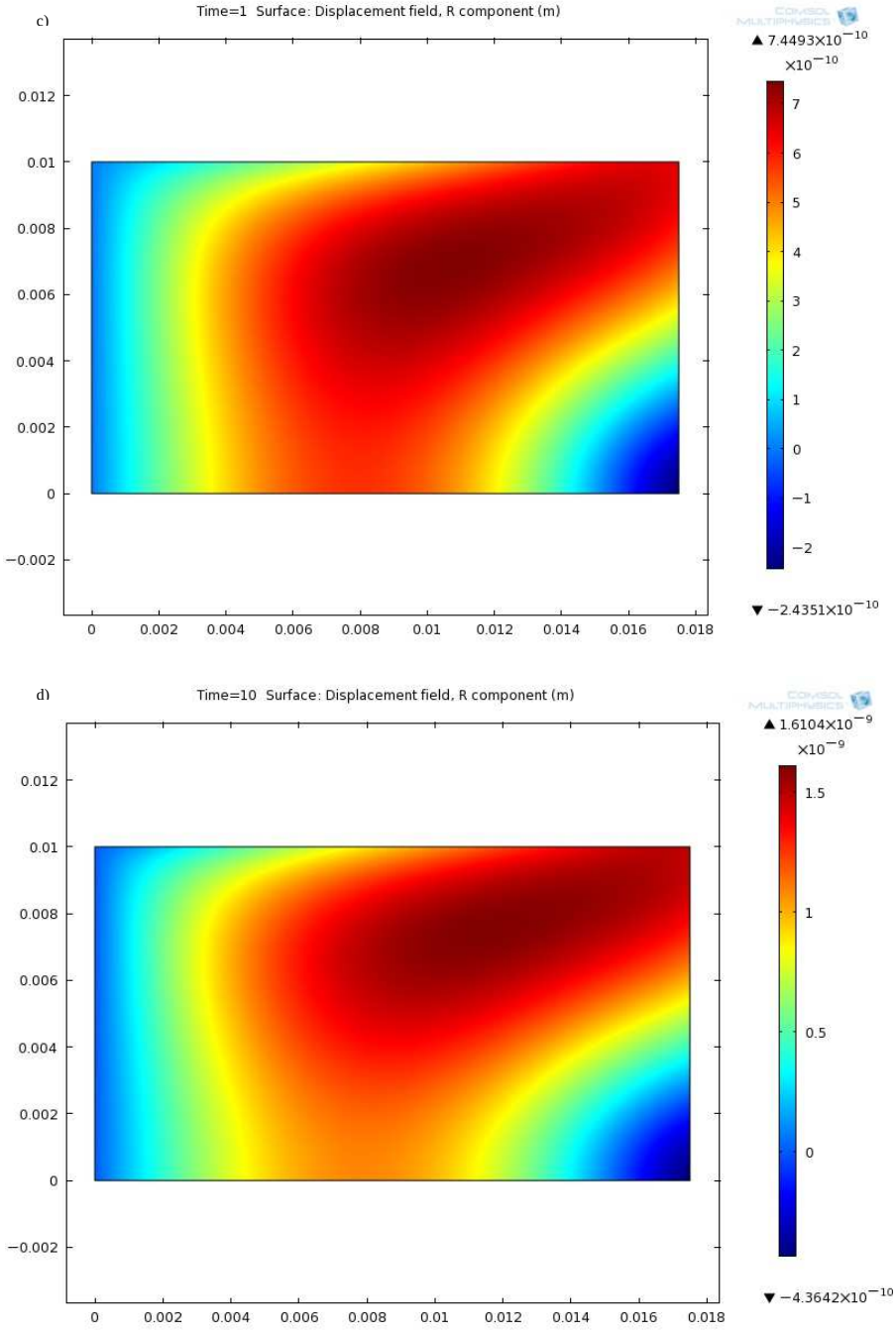

Figure 5.18: Radial displacement at different times and moisture contents: a) t=1s, M=2.3; b) t=10s, M=2.3; c) t=1s, M=0.3; d) t=10s, M=0.3.

a)

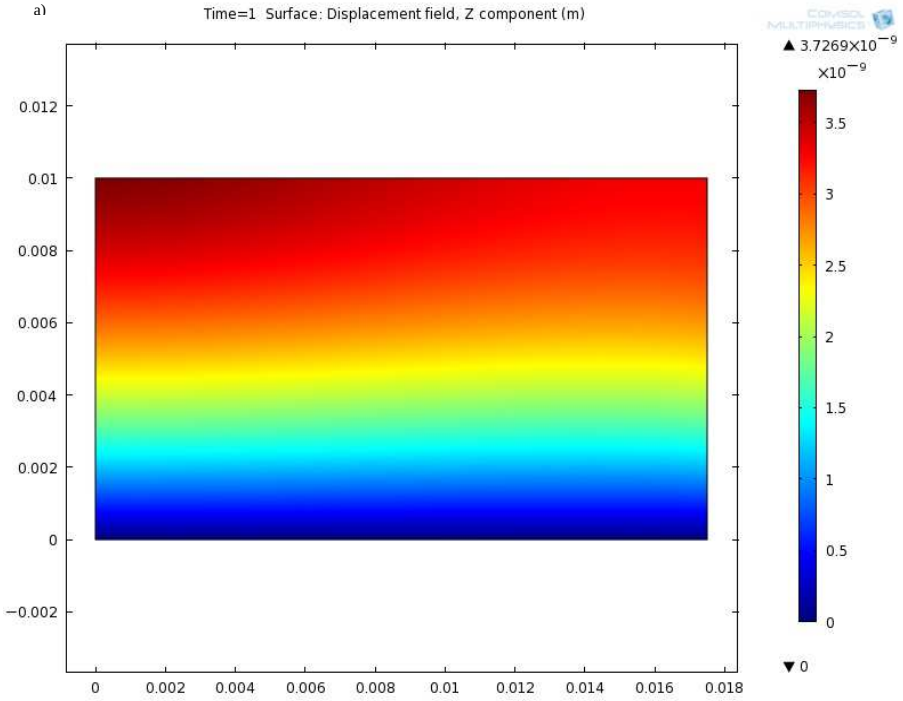
Time=1 Surface: Displacement field, Z component (m)
▲ 3.7269×10⁻⁹
×10⁻⁹
3.5
3
2.5
2
1.5
1
0.5
0
▼ 0
0.012
0.01
0.008
0.006
0.004
0.002
0
−0.002
0
0.002
0.004
0.006
0.008
0.01
0.012
0.014
0.016
0.018

b)

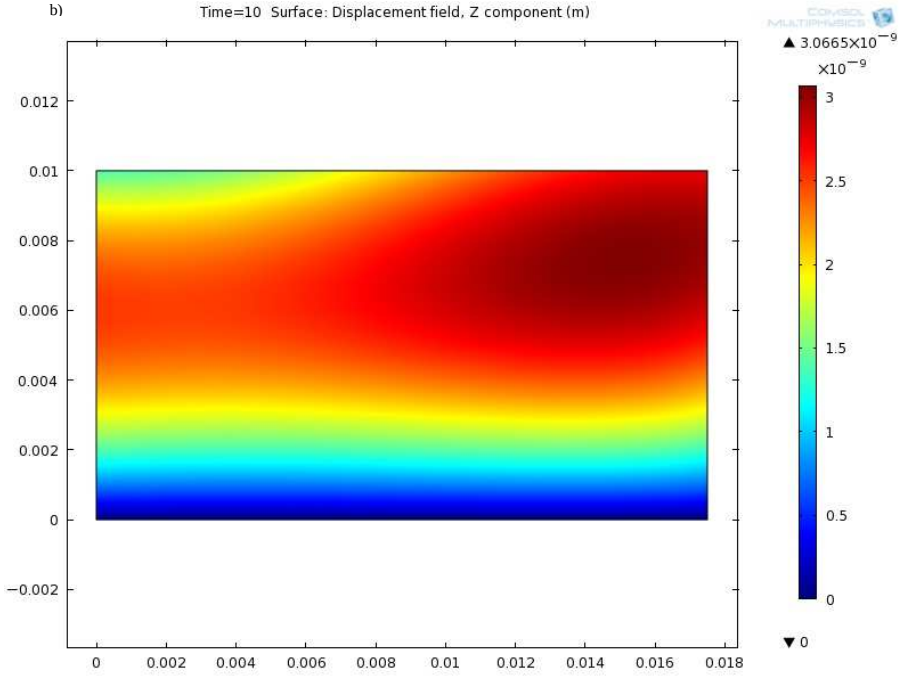
Time=10 Surface: Displacement field, Z component (m)
▲ 3.0665×10⁻⁹
×10⁻⁹
3
2.5
2
1.5
1
0.5
0
▼ 0
0.012
0.01
0.008
0.006
0.004
0.002
0
−0.002
0
0.002
0.004
0.006
0.008
0.01
0.012
0.014
0.016
0.018

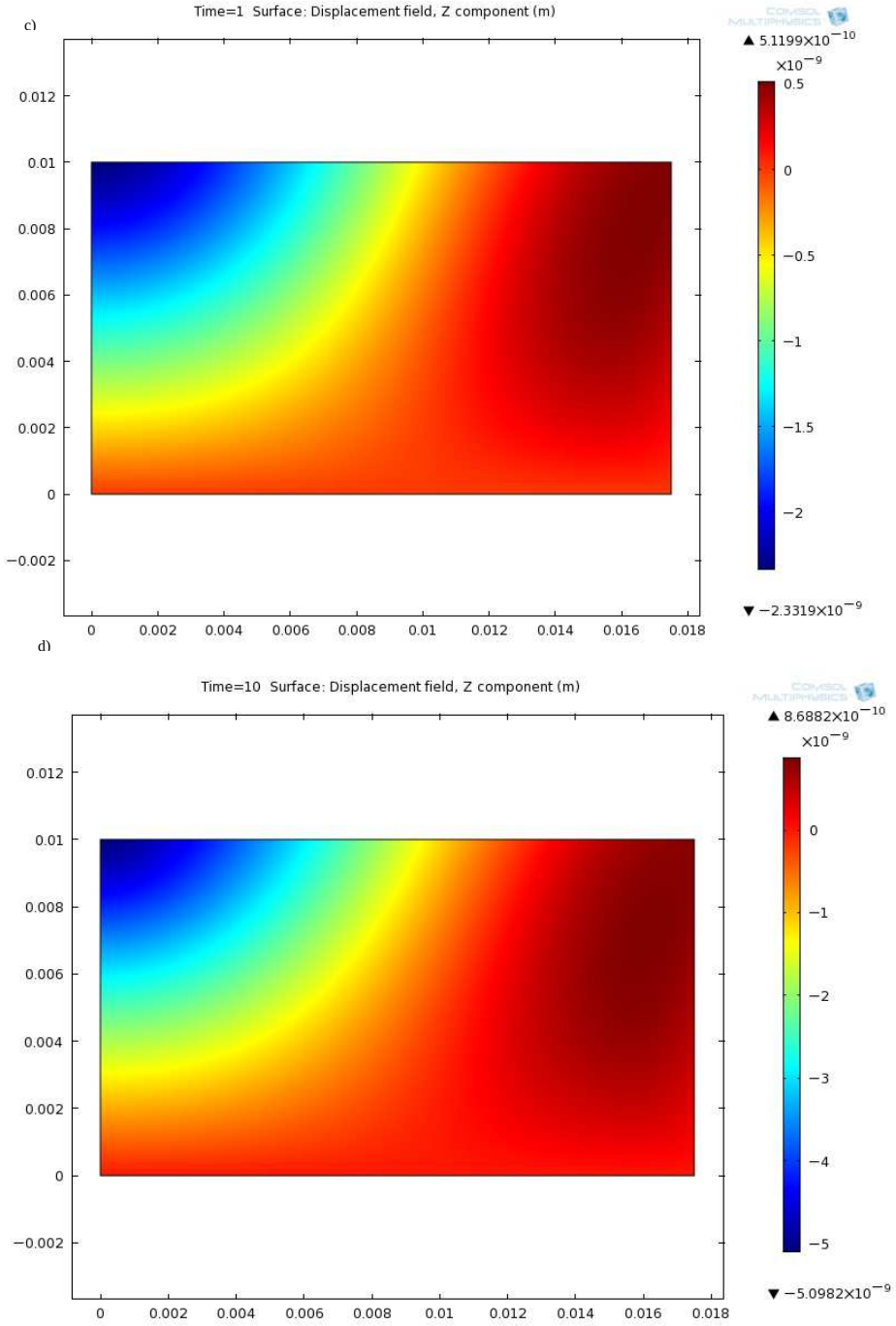

Figure 5.19: Displacement in the *z* direction at different times and moisture contents: a) *t*=1s, *M*=2.3; b) *t*=10s, *M*=2.3; c) *t*=1s, *M*=0.3; d) *t*=10s, *M*=0.3.

In Figures 5.18 and 5.19, it can be seen that when the moisture contents are lower, less deformation occurs. Shrinkage of the body decreases at lower moisture contents. These results provide useful insights for the fully two-way coupled model.

5.5 Conclusions

A physically based multiphase porous material model is developed which includes large strain viscoelasticity and is potentially capable for predicting the case hardening effect during drying of foodstuffs. The model includes mechanisms such as bulk flow, capillary flow and phase change for the water phase; bulk flow, binary diffusion and phase change for the gas phase (with vapor and air as its components) and it includes heat transfer as well as viscoelastic large deformation of the solid matrix. This fully coupled system can be implemented using the ALE algorithm and appropriate formulations are provided. Numerical implementation of this model in commercial software has been attempted with all needed input parameters listed. Numerical implementation of the uncoupled problem (solid mechanics) with large strain viscoelasticity has been accomplished in commercial software. The results provide useful insights for the fully two-way coupled problem. The model developed can be used to predict shrinkage of dehydrated food products from first principles when it deviates from water loss.

CHAPTER 6

CONCLUSIONS AND FUTURE WORK

The following remarks are in order in concluding the present dissertation.

- This dissertation is primarily motivated by the need to use fundamental physics based models to couple large strain viscoelastic deformation of the solid skeleton with mass, momentum and energy transport in unsaturated swelling porous materials (Chapter 1). The porous materials are treated as multiscale multiphase systems.
- The primary approach used in this dissertation is based on the Hybrid Mixture Theory (HMT) which involves rigorous development of a general thermomechanical theory. The key contributions of the present dissertation are in the development of a two-scale theory which, for unsaturated swelling porous systems, includes large strain viscoelasticity, and focuses on both the fluid transport and the solid deformation (Chapter 2); and in the development of a two-way coupled fluid transport model with large strain viscoelasticity in unsaturated swelling porous systems under isothermal conditions (Chapter 3).
- The model presented in this dissertation is fundamental physically based yet it can be numerically implemented without making ad-hoc assumptions. The numerical implementation of the model is accomplished using the finite element method. An example of successful model prediction is presented for water absorption in

foodstuffs (Chapter 4). It is demonstrated that including viscoelastic relaxation in such processes is necessary and important.

- Another approach which involves fundamental physics based two-way coupled modeling of large strain viscoelasticity and fluid and energy transport is also presented (Chapter 5) for an important application – drying of foodstuffs, where large strain viscoelasticity plays an important role.
- As practical impacts, the fundamental physics based model as well as the finite element model presented can be used as a generic modeling tool to predict parameters like fluid and solid contents, rehydration rate, porosity changes as well as degrees of swelling that are important indicators of food quality for rehydrated food products. Experiments may need to be carried out to obtain material properties as input parameters for the finite element model presented when applied to other rehydration processes. This is, however out of scope of this study.
- It is envisioned that as future line of studies, the theory presented in this dissertation can be used for development of models for swelling porous materials under non-isothermal conditions. Moreover, models presented in Chapter 5 and Chapter 2 can be combined as a "system approach" to study how rehydration has been affected by dehydration and thus can be used as a design tool for drying processes and to predict food quality parameters. And, the models presented in this dissertation can be extended to study other biopolymer processings where large strain viscoelasticity plays an important role.

APPENDIX A

CONSERVATION EQUATIONS

Here all the conservation equations at the macro-scale, including the conservation of mass, linear momentum, energy and entropy are listed. Details of the upscaling procedure are given in Bennethum and Cushman (1996a) [19].

A.1 Mass Balance

The macroscale mass balance for the *j*th species in phase α is given as:

$$\frac{D^{\alpha_j}(\varepsilon^\alpha \rho^{\alpha_j})}{Dt} + \varepsilon^\alpha \rho^{\alpha_j}(\nabla \bullet \boldsymbol{v}^{\alpha_j}) = \sum_{\beta \neq \alpha} \hat{e}_{\alpha_j}^{\beta} + \hat{r}^{\alpha_j} \tag{A.1}$$

Summing Equations (A.1) for *N* species gives the conservation of mass for the bulk phase:

$$\frac{D^\alpha(\varepsilon^\alpha \rho^\alpha)}{Dt} + \varepsilon^\alpha \rho^\alpha(\nabla \bullet \boldsymbol{v}^\alpha) = \sum_{\beta \neq \alpha} \hat{e}_\alpha^\beta \tag{A.2}$$

where the macroscopic species variables and their bulk counterparts are related by:

$$\rho^\alpha = \sum_{j=1}^{N} \rho^{\alpha_j} \tag{A.3}$$

$$\boldsymbol{v}^\alpha = \sum_{j=1}^{N} C^{\alpha_j} \boldsymbol{v}^{\alpha_j} \tag{A.4}$$

$$C^{\alpha_j} = \frac{\rho^{\alpha_j}}{\rho^\alpha} \tag{A.5}$$

$$\hat{e}_\alpha^\beta = \sum_{\beta \neq \alpha} \hat{e}_{\alpha_j}^{\beta} \tag{A.6}$$

They are subjected to the following restrictions:

$$\sum_{\alpha} \varepsilon^{\alpha} = 1 \tag{A.7}$$

$$\sum_{j=1}^{N} C^{\alpha_j} = 1, \alpha = s, l, a \tag{A.8}$$

$$\sum_{j=1}^{N} \hat{r}^{\alpha_j} = 1, \alpha = s, l, a \tag{A.9}$$

$$\sum_{\alpha \neq \beta} \hat{e}^{\beta}_{\alpha_j} = 0,\ j = 1, \ldots, N \tag{A.10}$$

A.2 Linear Momentum Balance

The macro-scale linear momentum balance for the the *j*th species in phase α is given as:

$$\varepsilon^{\alpha} \rho^{\alpha_j} \frac{D^{\alpha_j}(\boldsymbol{v}^{\alpha_j})}{Dt} - \nabla \bullet (\varepsilon^{\alpha} \boldsymbol{t}^{\alpha_j}) - \varepsilon^{\alpha} \rho^{\alpha_j} \boldsymbol{g}^{\alpha_j} = \sum_{\beta \neq \alpha} \hat{\mathbf{T}}^{\beta}_{\alpha_j} + \hat{i}^{\alpha_j} \tag{A.11}$$

Summing Equations (A.11) for *N* species yields the conservation of momentum for the bulk phase:

$$\varepsilon^{\alpha} \rho^{\alpha} \frac{D^{\alpha}(\boldsymbol{v}^{\alpha})}{Dt} - \nabla \bullet (\varepsilon^{\alpha} \boldsymbol{t}^{\alpha}) - \varepsilon^{\alpha} \rho^{\alpha} \boldsymbol{g}^{\alpha} = \sum_{\beta \neq \alpha} \hat{\mathbf{T}}^{\beta}_{\alpha} \tag{A.12}$$

where the macroscopic species variables and their bulk counterparts are related by:

$$\boldsymbol{t}^{\alpha} = \sum_{i=1}^{N} (\boldsymbol{t}^{\alpha_j} - \rho^{\alpha_j} (\boldsymbol{v}^{\alpha_j, \alpha})^2) \tag{A.13}$$

$$\boldsymbol{v}^{\alpha_j,\alpha} = \boldsymbol{v}^{\alpha_j} - \boldsymbol{v}^{\alpha} \tag{A.14}$$

$$\boldsymbol{g}^{\alpha} = \sum_{j=1}^{N} C^{\alpha_j} \boldsymbol{g}^{\alpha_j} \tag{A.15}$$

$$\hat{\mathbf{T}}_{\alpha}^{\beta} = \sum_{j=1}^{N} (\hat{\mathbf{T}}_{\alpha_j}^{\beta} + \mathbf{v}^{\alpha_j} \hat{e}_{\alpha_j}^{\beta}) \tag{A.16}$$

The following restrictions apply:

$$\sum_{j=1}^{N} (\hat{\mathbf{i}}^{\alpha_j} + \mathbf{v}^{\alpha_j,\alpha} \hat{r}^{\alpha_j}) = 0, \alpha = s, l, a \tag{A.17}$$

$$\sum_{\beta \neq \alpha} (\hat{\mathbf{T}}_{\alpha_j}^{\beta} + \mathbf{v}^{\alpha_j} \hat{e}_{\alpha_j}^{\beta}) = 0,\ j = 1, \ldots, N \tag{A.18}$$

A.3 Energy Balance

The macroscale conservation of energy for the *j*th species in phase α is given by:

$$\varepsilon^{\alpha} \rho^{\alpha_j} \frac{D^{\alpha_j}(e^{\alpha_j})}{Dt} - \nabla \bullet (\varepsilon^{\alpha} \boldsymbol{q}^{\alpha_j}) - \varepsilon^{\alpha} \mathbf{t}^{\alpha_j} : \nabla \boldsymbol{v}^{\alpha_j} - \varepsilon^{\alpha} \rho^{\alpha_j} h^{\alpha_j} = \sum_{\beta \neq \alpha} \hat{Q}_{\alpha_j}^{\beta} + \hat{Q}^{\alpha_j} \tag{A.19}$$

Summing Equations (A.19) for N species yields the conservation of energy for the bulk phase:

$$\varepsilon^{\alpha} \rho^{\alpha} \frac{D^{\alpha}(e^{\alpha})}{Dt} - \nabla \bullet (\varepsilon^{\alpha} \boldsymbol{q}^{\alpha}) - \varepsilon^{\alpha} \mathbf{t}^{\alpha} : \nabla \boldsymbol{v}^{\alpha} - \varepsilon^{\alpha} \rho^{\alpha} h^{\alpha} = \sum_{\beta \neq \alpha} \hat{Q}_{\alpha}^{\beta} \tag{A.20}$$

where the relationships of the macroscopic species variables and their bulk counterparts are:

$$e^{\alpha} = \sum_{j=1}^{N} C^{\alpha_j} (e^{\alpha_j} + \frac{1}{2} \boldsymbol{v}^{\alpha_j,\alpha} \bullet \boldsymbol{v}^{\alpha_j,\alpha}) \tag{A.21}$$

$$\boldsymbol{q}^{\alpha} = \sum_{j=1}^{N} [\boldsymbol{q}^{\alpha_j} + \boldsymbol{t}^{\alpha_j} \bullet \boldsymbol{v}^{\alpha_j,\alpha} - \rho^{\alpha_j} (e^{\alpha_j} + \frac{1}{2} \boldsymbol{v}^{\alpha_j,\alpha} \bullet \boldsymbol{v}^{\alpha_j,\alpha}) \boldsymbol{v}^{\alpha_j,\alpha}] \tag{A.22}$$

$$h^{\alpha} = \sum_{j=1}^{N} C^{\alpha_j} (h^{\alpha_j} + \boldsymbol{g}^{\alpha_j} \bullet \boldsymbol{v}^{\alpha_j,\alpha}) \tag{A.23}$$

$$\hat{Q}_{\alpha}^{\beta} = \sum_{j=1}^{N} [\boldsymbol{v}^{\alpha_j,\alpha} + \hat{\boldsymbol{T}}_{\alpha_j}^{\beta} \bullet \boldsymbol{v}^{\alpha_j,\alpha} + \hat{e}_{\alpha_j}^{\beta} (e^{\alpha_j,\alpha} + \frac{1}{2} \boldsymbol{v}^{\alpha_j,\alpha} \bullet \boldsymbol{v}^{\alpha_j,\alpha}) \boldsymbol{v}^{\alpha_j,\alpha}] \tag{A.24}$$

They are subjected to the following restrictions:

$$\sum_{j=1}^{N} [\hat{Q}^{\alpha_j} + \hat{\boldsymbol{i}}^{\alpha_j} \bullet \boldsymbol{v}^{\alpha_j,\alpha} + \hat{r}^{\alpha_j} (e^{\alpha_j} + \frac{1}{2} \boldsymbol{v}^{\alpha_j,\alpha} \bullet \boldsymbol{v}^{\alpha_j,\alpha}) \boldsymbol{v}^{\alpha_j,\alpha}] = 0, \alpha = s, l, a \tag{A.25}$$

$$\sum_{\beta \neq \alpha} [\hat{Q}_{\alpha_j}^{\beta} + \hat{\boldsymbol{T}}_{\alpha_j}^{\beta} \bullet \boldsymbol{v}^{\alpha_j,\alpha} + \hat{e}_{\alpha_j}^{\beta} (e^{\alpha_j} + \frac{1}{2} \boldsymbol{v}^{\alpha_j} \bullet \boldsymbol{v}^{\alpha_j}) \boldsymbol{v}^{\alpha_j,\alpha}] = 0, \; j = 1, \ldots, N \tag{A.26}$$

A.4 Entropy Balance

The macroscale conservation of energy for the *j*th species in phase α is:

$$\varepsilon^{\alpha} \rho^{\alpha_j} \frac{D^{\alpha_j} \eta^j}{Dt} - \nabla \bullet (\varepsilon^{\alpha} \boldsymbol{\phi}^{\alpha_j}) - \varepsilon^{\alpha} \rho^{\alpha_j} b^{\alpha_j} = \sum_{\alpha \neq \beta} \hat{\Phi}_{\alpha_j}^{\beta} + \hat{\eta}^{\alpha_j} + \Lambda^{\alpha_j} \tag{A.27}$$

Summing Equations (A.27) for *N* species yields the entropy balance for the bulk phase:

$$\varepsilon^{\alpha} \rho^{\alpha_j} \frac{D^{\alpha} \eta^j}{Dt} - \nabla \bullet (\varepsilon^{\alpha} \boldsymbol{\phi}^{\alpha}) - \varepsilon^{\alpha} \rho^{\alpha} b^{\alpha} = \sum_{\alpha \neq \beta} \hat{\Phi}_{\alpha}^{\beta} + \Lambda^{\alpha} \tag{A.28}$$

where the macroscopic species variables are related to their bulk counterparts by:

$$\eta^{\alpha} = \sum_{j=1}^{N} C^{\alpha_j} \eta^{\alpha_j} \tag{A.29}$$

$$\boldsymbol{\phi}^{\alpha} = \sum_{j=1}^{N} (\boldsymbol{\phi}^{\alpha_j} - \rho^{\alpha_j} \mathbf{v}^{\alpha_j,\alpha} \eta^{\alpha_j}) \tag{A.30}$$

$$b^{\alpha} = \sum_{j=1}^{N} C^{\alpha_j} b^{\alpha_j} \tag{A.31}$$

$$\hat{\Phi}^{\beta}_{\alpha} = \sum_{j=1}^{N} (\hat{\Phi}^{\beta}_{\alpha_j} + \hat{e}^{\beta}_{\alpha_j} \eta^{\alpha_j,\alpha}) \tag{A.32}$$

And the following restrictions hold:

$$\sum_{j=1}^{N} (\hat{\eta}^{\alpha_j} + \hat{r}^{\alpha_j} \eta^{\alpha_j}) = 0, \alpha = s, l, a \tag{A.33}$$

$$\sum_{\beta \neq \alpha} (\hat{\Phi}^{\beta}_{\alpha_j} + \hat{e}^{\beta}_{\alpha_j} \eta^{\alpha_j}) = 0,\ j = 1, \ldots, N \tag{A.34}$$

A.5 Total Entropy Inequality

As we mentioned before, we have assumed that the system is at local thermal equilibrium, resulting in only one temperature for all phases and their species:

$$T^{s_j} = T^{l_j} = T^{\alpha_j} = T^{s} = T^{l} = T^{\alpha} = T \tag{A.35}$$

Also, we have assumed that the system is thermodynamically simple:

$$\phi^{\alpha_j} = \frac{\alpha_j}{T} \tag{A.36}$$

and

$$b^{\alpha_j} = \frac{h^{\alpha_j}}{T} \tag{A.37}$$

We perform a Legendre transformation to convert the internal energy e^{α_j} into the Helmoltz free energy A^{α_j}:

$$A^{\alpha_j} = e^{\alpha_j} + T\eta^{\alpha_j} \tag{A.38}$$

where

$$A^{\alpha} = \sum_{j=1}^{N} C^{\alpha_j} A^{\alpha_j} \tag{A.39}$$

We obtain the total entropy inequality by eliminating h^{α_j} from the energy and entropy balance:

$$\begin{aligned}
\Lambda = \sum_{\alpha} [& -\frac{\varepsilon^{\alpha}\rho^{\alpha}}{T}\left(\frac{D^{\alpha}A^{\alpha}}{Dt} + \eta^{\alpha}\frac{D^{\alpha}T}{Dt}\right) + \frac{\varepsilon^{\alpha}}{T}\left(\sum_{j=1}^{N} \boldsymbol{t}^{\alpha_j}\right) : \boldsymbol{d}^{\alpha}] \\
& + \frac{\varepsilon^{\alpha}}{T^2}(\nabla T)\bullet[\boldsymbol{q}^{\alpha} - \sum_{j=1}^{N}(\boldsymbol{t}^{\alpha_j}\bullet\boldsymbol{v}^{\alpha_j,\alpha} - \rho^{\alpha_j}\boldsymbol{v}^{\alpha_j,\alpha}(A^{\alpha_j} + \frac{1}{2}\boldsymbol{v}^{\alpha_j}\bullet\boldsymbol{v}^{\alpha_j}))] \\
& - \frac{1}{T}\sum_{j=1}^{N}[\hat{\boldsymbol{T}}^{\beta}_{\alpha_j} + \hat{i}^{\alpha_j} + \nabla(\varepsilon^{\alpha}\rho^{\alpha}A^{\alpha_j})]\bullet\boldsymbol{v}^{\alpha_j,\alpha} \\
& + \sum_{j=1}^{N}\frac{\varepsilon^{\alpha}}{T}(\boldsymbol{t}^{\alpha_j} - \rho^{\alpha_j}A^{\alpha_j}\boldsymbol{I}) : \nabla\boldsymbol{v}^{\alpha_j,\alpha} \\
& - \frac{1}{T}\sum_{\alpha\neq\beta}\hat{\boldsymbol{T}}^{\beta}_{\alpha}\bullet\boldsymbol{v}^{\alpha,s} - \frac{1}{2T}\sum_{j=1}^{N}(\boldsymbol{v}^{\alpha_j,\alpha})^2(\hat{e}^{\beta}_{\alpha_j} + \hat{r}^{\alpha_j}) \\
& - \frac{1}{T}\sum_{\alpha\neq\beta}(A^{\alpha} + \frac{1}{2}\boldsymbol{v}^{\alpha,s}\bullet\boldsymbol{v}^{\alpha,s})] \geq 0
\end{aligned} \tag{A.40}$$

APPENDIX B

COMPLEXITIES WITH THREE-SCALE UNSATURATED SWELLING SYSTEMS

We have mentioned before that complexities arise in a three-scale theory when the system is considered as unsaturated. To see this, we need to look at the transport equation and linear momentum balance of the solid phase in a three-scale theory. In this Appendix, we present the details of the derivation of the transport equation and linear momentum balance for the solid phase for a three-scale unsaturated swelling porous system. This is based on the work by Singh et al. (2003a, 2003b) [107, 108], in which four phases, solid *sA*, vicinal fluid *wA*, bulk phase *B* and bulk phase *C*, are considered. Here we assume isothermal conditions. The solid phase is assumed to be incompressible. The vicinal fluid and the bulk fluid B are the same and assumed to be incompressible. The third phase *C* is taken as air.

B.1 Vicinal Fluid

The mass conservation of the vicinal fluid is given by (A.5) in Singh et al. (2003b) [108]:

$$\frac{D^{wA}(\varepsilon^{wA}\rho^{wA})}{Dt}+\varepsilon^{wA}\rho^{wA}(\nabla\bullet\boldsymbol{v}^{wA})=\varepsilon^{wA}\rho^{wA}\hat{e}_l^{wA} \tag{B.1}$$

where we have replaced ε^{A} by ε^{wA} as we have mentioned before that the upscaling technique is modified slightly (Cushman et al., 2004) [34]. The right hand side is nonzero as mass could be transferred between the vicinal water and the bulk phase water. We rewrite the above equation as:

$$\rho^{wA}[\dot{\varepsilon^{wA}} + (\nabla \bullet \varepsilon^{wA} \boldsymbol{v}^{wA,sA}) + \varepsilon^{wA} \nabla \bullet \boldsymbol{v}^{sA}] = \varepsilon^{wA} \rho^{wA} \hat{e}_{l}^{wA} \tag{B.2}$$

Darcy's law for the vicinal fluid is simplified as:

$$\boldsymbol{v}^{wA,sA} = (\boldsymbol{R}^{wA})^{-1}[-\varepsilon^{wA} \rho^{wA} \frac{\partial A^{wA}}{\partial \varepsilon^{wA}} \nabla \varepsilon^{wA} - \varepsilon^{wA} \rho^{wA} \sum_{m=1}^{q} \frac{\partial A^{l}}{\partial \boldsymbol{E}^{(m)sA}} : \nabla \boldsymbol{E}^{(m)sA}] \tag{B.3}$$

The third term on the right side of equation (5.30) in Singh et al. (2003b) [108] is neglected because the vicinal fluid interacts with the bulk phase water only through the boundaries and it is assumed that for such systems the bulk fluid does not affect the free energy of the vicinal fluid. Gravity and higher order effects are also ignored. The second term in the above represents the effect of vicinal water concentration on the flow and the coefficient is known as the swelling potential, while the viscoelastic effect on the flow is accounted for in the third term.

B.2 Bulk Phase Fluid B

Mass conservation of the bulk phase *B* is given by (A.7) in Singh et al. (2003b) [108] and is written as:

$$\rho^{l}[\dot{\varepsilon^{l}} + (\nabla \bullet \varepsilon^{l} \boldsymbol{v}^{l,sA}) + \varepsilon^{l} \nabla \bullet \boldsymbol{v}^{sA}] = \varepsilon^{l} \rho^{l} \hat{e}_{wA}^{l} \tag{B.4}$$

Darcy's law is given as:

$$\boldsymbol{v}^{l,sA} = \quad (\boldsymbol{R}^{l})^{-1}(-\varepsilon^{l}\rho^{l}\frac{\partial A^{l}}{\partial \varepsilon^{l}}\nabla\varepsilon^{l}) \tag{B.5}$$

The second term is related to the capillary pressure and this resembles the classical Darcy's law.

B.3 Transport Equation

As the mass transferred between the vicinal fluid and the bulk fluid add up to zero $\varepsilon^{l}\rho^{l}\hat{e}^{l}_{wA} + \varepsilon^{wA}\rho^{wA}\hat{e}^{wA}_{l} = 0$, we add Equation (B.1) and Equation (B.4) and use the notation:

$$\varepsilon^{f} = \varepsilon^{wA} + \varepsilon^{l} \tag{B.6}$$

where ε^{f} is the total volume fraction of the vicinal fluid and the volume fraction of the bulk fluid *B*; we obtain:

$$\begin{aligned}\dot{\varepsilon}^{l} - \nabla\bullet\{&\frac{k^{f}}{\mu^{f}}\boldsymbol{I}[K^{2}\varepsilon^{f}(\varepsilon^{wA}\rho^{wA}\frac{\partial A^{wA}}{\partial \varepsilon^{wA}}) + (1-K)^{2}\varepsilon^{f}(\varepsilon^{l}\rho^{l}\frac{\partial A^{l}}{\partial \varepsilon^{l}}) \\ &+\varepsilon^{f}\varepsilon^{A}\frac{\partial p^{wA}}{\partial \varepsilon^{wA}}]\nabla\varepsilon^{f} - K^{2}\varepsilon^{f}(\varepsilon^{f}\rho^{wA}\sum_{m=1}^{q}\frac{\partial A^{wA}}{\partial \overset{(m)sA}{\boldsymbol{E}}} : \nabla\overset{(m)sA}{\boldsymbol{E}})\} + \varepsilon^{f}\nabla\cdot\boldsymbol{v}^{sA}\end{aligned} \tag{B.7}$$

where

$$(\boldsymbol{R}^{l})^{-1} = (\boldsymbol{R}^{wA})^{-1} = \frac{k^{f}}{\mu^{f}}\boldsymbol{I} \tag{B.8}$$

and we follow Singh et al. (2003b) [108] to assume a linear relationship between ε^{wA} and ε^{f}:

$$\varepsilon^{wA} = K\varepsilon^{f} \tag{B.9}$$

Then,

$$\varepsilon^{l} = (1-K)\varepsilon^{f} \tag{B.10}$$

We define the Fickian diffusion coefficient as:

$$D \equiv \frac{k^{f}}{\mu^{f}}[K^{2}\varepsilon^{f}(\varepsilon^{wA}\rho^{wA}\frac{\partial A^{wA}}{\partial \varepsilon^{wA}}) + (1-K)^{2}(\varepsilon^{l}\rho^{l}\frac{\partial A^{l}}{\partial \varepsilon^{l}}) + \varepsilon^{f}\varepsilon^{A}\frac{\partial p^{wA}}{\partial \varepsilon^{wA}}K] \tag{B.11}$$

The Laplace transform technique is used to convert the fifth term in Equation (B.7) into an integral form and Equation (B.7) then becomes:

$$\dot{\varepsilon}^{f} - \nabla\cdot(D\nabla\varepsilon^{f}) - \nabla\cdot[\int_{0}^{t}\boldsymbol{B}(t-\tau):(\nabla\dot{\boldsymbol{E}}^{sA})\,d\tau] + \varepsilon^{f}\nabla\cdot\boldsymbol{v}^{sA} = 0 \tag{B.12}$$

where **B** is defined by:

$$\boldsymbol{B}(t) = \frac{k^{f}}{\mu^{f}}K^{2}\varepsilon^{f\,2}\rho^{wA}\boldsymbol{M}(t) \tag{B.13}$$

and

$$\boldsymbol{M}(t) = \sum_{m=0}^{p}\frac{\partial A^{wA}}{\partial \overset{(m)sA}{\boldsymbol{E}}}\frac{d\delta}{dt}(t) \tag{B.14}$$

Equation (B.12) is the transport equation which needs to be solved simultaneously with the solid phase equations. This is different from Equation (2.53) in Singh et al. (2003b) [108]because phase *C* is not immobile anymore and relation (2.19) in Singh et al. (2003b) [108] is no longer valid.

We have discussed before that the linearity assumption Equation (B.9) is not justified. However, without relating the volume fraction of the vicinal fluid and that of the bulk phase *B*, it is very difficult to combine the two phases.

B.4 Solid Phase

Linear momentum balance of the solid phase is given below (Here we ignore gravity and inertial effects):

$$\nabla\bullet(\varepsilon^{A}\boldsymbol{t}^{sA}) = -\sum_{\alpha\equiv wA,l,a}\rho^{sA}\varepsilon^{sA}\hat{\boldsymbol{T}}_{\alpha}^{sA} \tag{B.15}$$

The right hand side is the linear momentum transferred from other phases to the solid phase and could not be obtained directly. We use the restriction:

$$\rho^{\alpha}\varepsilon^{\alpha}(\hat{\boldsymbol{T}}_{\alpha}^{\beta}+\hat{e}_{\alpha}^{\beta}\boldsymbol{v}^{\alpha})+\rho^{\beta}\varepsilon^{\beta}(\hat{\boldsymbol{T}}_{\beta}^{\alpha}+\hat{e}_{\beta}^{\alpha}\boldsymbol{v}^{\beta})=0,\alpha,\beta=wA,sA,l,a,\alpha\neq\beta \tag{B.16}$$

and Equation (B.15) is equivalent to:

$$\nabla\bullet(\varepsilon^{A}\boldsymbol{t}^{sA}) = \rho^{wA}\varepsilon^{wA}\hat{\boldsymbol{T}}_{sA}^{wA}+\rho^{l}\varepsilon^{l}\hat{\boldsymbol{T}}_{sA}^{l}+\rho^{a}\varepsilon^{a}\hat{\boldsymbol{T}}_{sA}^{a} \tag{B.17}$$

From the linear momentum balance for phase $\alpha,\alpha=wA,l,a$, the following relationships can be obtained:

$$\rho^{wA}\varepsilon^{wA}[\hat{\boldsymbol{T}}_{wA}^{sA}+\hat{\boldsymbol{T}}_{wA}^{l}+\hat{\boldsymbol{T}}_{wA}^{a}]=\nabla(\rho^{wA}\varepsilon^{wA}) \tag{B.18}$$

$$\rho^{l}\varepsilon^{l}[\hat{\boldsymbol{T}}_{l}^{sA}+\hat{\boldsymbol{T}}_{l}^{wA}+\hat{\boldsymbol{T}}_{l}^{a}]=\nabla(\rho^{l}\varepsilon^{l}) \tag{B.19}$$

$$\rho^{a}\varepsilon^{a}[\hat{\boldsymbol{T}}_{a}^{sA}+\hat{\boldsymbol{T}}_{a}^{wA}+\hat{\boldsymbol{T}}_{a}^{l}]=\nabla(\rho^{a}\varepsilon^{a}) \tag{B.20}$$

Note that the mass transferred between the vicinal fluid and the bulk phase B is nonzero. All other mass transfers between phases vanish. Thus, if we add the above three equations up, terms cancel on the left hand side except for those that appear on the right hand side, as well as $\rho^{wA}\varepsilon^{wA}\hat{\boldsymbol{T}}^{l}_{wA}$ and $\rho^{l}\varepsilon^{l}\hat{\boldsymbol{T}}^{wA}_{l}$ on the left hand side. This is because in Equation (B.16), $\hat{e}^{l}_{wA}$ and $\hat{e}^{wA}_{l}$ are not zero. However, since no information is available for the momentum transfer between the vicinal fluid and the bulk phase l, we assume that:

$$\rho^{wA}\varepsilon^{wA}\hat{\boldsymbol{T}}^{l}_{wA}+\rho^{l}\varepsilon^{l}\hat{\boldsymbol{T}}^{wA}_{l}=0 \tag{B.21}$$

Thus, the linear momentum balance of the solid phase is given as:

$$\nabla\bullet(\varepsilon^{A}\boldsymbol{t}^{sA})=\nabla(p^{wA}\varepsilon^{wA})+\nabla(p^{l}\varepsilon^{l})+\nabla(p^{a}\varepsilon^{a}) \tag{B.22}$$

The stress-strain relationship is of the form:

$$\boldsymbol{t}^{sA}=-p^{sA}\boldsymbol{I}+\boldsymbol{t}^{seA}+\boldsymbol{t}^{shA}+\sum_{m=0}^{p}\boldsymbol{F}(G^{sA}{}^{(m)sA}_{\boldsymbol{E}})\boldsymbol{F}^{T} \tag{B.23}$$

The Terzaghi stress $\boldsymbol{t}^{seA}$ and the hydration stress $\boldsymbol{t}^{shA}$ are given respectively by:

$$\boldsymbol{t}^{seA}=\rho^{sA}\boldsymbol{F}\frac{\partial A^{sA}}{\partial \boldsymbol{E}^{sA}}\boldsymbol{F}^{T} \tag{B.24}$$

$$\boldsymbol{t}^{shA}=\rho^{wA}\boldsymbol{F}\frac{\partial A^{wA}}{\partial \boldsymbol{E}^{sA}}\boldsymbol{F}^{T} \tag{B.25}$$

In Equation (B.22), the volume fraction of the particle *A* composed of the solid phase *sA* and the vicinal fluid *wA* appears. The solid phase linear momentum balance is difficult to implement without separation of the volume fraction ε^{sA} from ε^{A}. It appears difficult to carry out this separation.

APPENDIX C

DETAILS OF SOME CALCULATIONS IN CHAPTER 4

We list the details of some calculations that arise in the residuals and their gradients that arise in Chapter 4.

C.1 $grad\,\varepsilon^s$ *and Its Gradient*

$$grad\,\varepsilon^s = \frac{\partial \varepsilon^s}{\partial X} = -\frac{\varepsilon_0^s}{J^2}\frac{\partial J}{\partial X} \tag{C.1}$$

and $\frac{\partial J}{\partial X}$ is given as:

$$\begin{aligned}
\frac{\partial J}{\partial X} &= \frac{\partial}{\partial X}(1+\frac{\partial u}{\partial X}) \\
&= \frac{\partial}{\partial \xi}(\frac{\partial u}{\partial X})\frac{\partial \xi}{\partial X} \\
&= \frac{\partial}{\partial \xi}(\frac{\partial [N]}{\partial \xi}\{u\}\frac{\partial \xi}{\partial X})\frac{\partial \xi}{\partial X} \\
&= \frac{\partial^2 [N]}{\partial \xi^2}\{u\}(\frac{\partial \xi}{\partial X})^2 + \frac{\partial [N]}{\partial \xi}\{u\}\frac{\partial \xi}{\partial X}\frac{\partial}{\partial \xi}\frac{\partial \xi}{\partial X} \\
&= \frac{\partial^2 [N]}{\partial \xi^2}\{u\}(\frac{\partial \xi}{\partial X})^2 + \frac{\partial [N]}{\partial \xi}\{u\}\frac{\partial \xi}{\partial X}\frac{\partial}{\partial \xi}\frac{1}{\frac{\partial X}{\partial \xi}} \\
&= \frac{\partial^2 [N]}{\partial \xi^2}\{u\}(\frac{\partial \xi}{\partial X})^2 + \frac{\partial [N]}{\partial \xi}\{u\}\frac{\partial \xi}{\partial X}(-\frac{1}{(\frac{\partial X}{\partial \xi})^2})\frac{\partial^2 [N]}{\partial \xi^2}\{X\} \\
&= \frac{\partial^2 [N]}{\partial \xi^2}\{u\}(\frac{\partial \xi}{\partial X})^2 - \frac{\partial [N]}{\partial \xi}\{u\}(\frac{\partial \xi}{\partial X})^3\frac{\partial^2 [N]}{\partial \xi^2}\{X\}
\end{aligned} \tag{C.2}$$

So:

$$grad\varepsilon^s = -\frac{\varepsilon_0^s}{J^2}[\frac{\partial^2[N]}{\partial\xi^2}\{u\}(\frac{\partial\xi}{\partial X})^2 - \frac{\partial[N]}{\partial\xi}\{u\}(\frac{\partial\xi}{\partial X})^3\frac{\partial^2[N]}{\partial\xi^2}\{X\}] \quad \text{(C.3)}$$

and:

$$\begin{aligned}\frac{\partial grad\varepsilon^s}{\partial\{u\}} = &-\frac{\varepsilon_0^s}{J^2}[\frac{\partial^2[N]}{\partial\xi^2}(\frac{\partial\xi}{\partial X})^2 - \frac{\partial[N]}{\partial\xi}(\frac{\partial\xi}{\partial X})^3\frac{\partial^2[N]}{\partial\xi^2}\{X\}] \\ &+\frac{2\varepsilon_0^s}{J^3}[\frac{\partial^2[N]}{\partial\xi^2}\{u\}(\frac{\partial\xi}{\partial X})^2 - \frac{\partial[N]}{\partial\xi}\{u\}(\frac{\partial\xi}{\partial X})^3\frac{\partial^2[N]}{\partial\xi^2}\{X\}]\frac{\partial J}{\partial\{u\}}\end{aligned} \quad \text{(C.4)}$$

C.2 Permeability and Its Gradients

The gradients of the permeability k^l are given by:

$$\frac{\partial k^l}{\partial\{\varepsilon^l\}} = \frac{3k^i([N]\{\varepsilon^l\})^2[N]}{(1-\varepsilon^s)^3} \quad \text{(C.5)}$$

$$\frac{\partial k^l}{\partial\{u\}} = -\frac{3k^i([N]\{\varepsilon^l\})^3\varepsilon_0^s}{J^2(1-\varepsilon^s)^4}\frac{\partial J}{\partial\{u\}} \quad \text{(C.6)}$$

C.3 the Gradients of a_w

For simplicity, first define the following from Equation (4.46):

$$a \equiv 0.138 - 10.4\times10^{-4}T \quad \text{(C.7)}$$

$$b \equiv \frac{1}{0.396 + 11.6\times10^{-4}T} \quad \text{(C.8)}$$

Then, the gradients of a_w are given as:

$$\frac{\partial a_w}{\partial\{\varepsilon^l\}} = \frac{\frac{b}{a}(M/a)^{(b-1)}}{(1+(M/a)^b)^2}\frac{\partial M}{\partial\{\varepsilon^l\}} \tag{C.9}$$

$$\frac{\partial}{\partial\{\varepsilon^l\}}\frac{a_w}{\varepsilon^l} = \frac{\frac{b}{a}(M/a)^{(b-1)}}{(1+(M/a)^b)^2}\frac{\partial}{\partial\{\varepsilon^l\}}\frac{\partial M}{\partial\varepsilon^l} + \frac{\frac{b(b-1)}{a^2}(M/a)^{(b-2)} - \frac{b(b+1)}{a^2}(M/a)^{(2b-2)}}{(1+(M/a)^b)^3}\frac{\partial M}{\partial\varepsilon^l}\frac{\partial M}{\partial\{\varepsilon^l\}} \tag{C.10}$$

C.4 the Gradients of Diffusivity D

$$\begin{aligned}\frac{\partial D}{\partial\{\varepsilon^l\}} &= \frac{[N]k^l RT}{\mu v_l}[\ln(a_w) + \frac{\varepsilon^l}{a_w}\frac{\partial a_w}{\partial\{\varepsilon^l\}}] + \frac{\varepsilon^l RT}{\mu v_l}\frac{\partial k^l}{\partial\{\varepsilon^l\}}[\ln(a_w) + \frac{\varepsilon^l}{a_w}\frac{\partial a_w}{\partial\varepsilon^l}] \\ &+ \frac{\varepsilon^l k^l RT}{\mu v_l}[\frac{1}{a_w}\frac{\partial a_w}{\partial\{\varepsilon^l\}} + \frac{[N]}{a_w}\frac{\partial a_w}{\partial\varepsilon^l} - \frac{\varepsilon^l}{a_w^2}\frac{\partial a_w}{\partial\varepsilon^l}\frac{\partial a_w}{\partial\{\varepsilon^l\}} + \frac{\varepsilon^l}{a_w}\frac{\partial}{\varepsilon^l}\frac{\partial a_w}{\partial\varepsilon^l}]\end{aligned} \tag{C.11}$$

$$\frac{\partial D}{\partial\{u\}} = \frac{[N]\{\varepsilon^l\}RT}{\mu v_l}[\ln(a_w) + \frac{[N]\{\varepsilon^l\}}{a_w}\frac{\partial a_w}{\partial\varepsilon^l}]\frac{\partial k^l}{\partial\{u\}} \tag{C.12}$$

C.5 the Gradients of A Defined by Equation (4.62)

$$\begin{aligned}\frac{\partial A}{\partial\{\varepsilon^l\}} &= \sum_{i=1}^{n_k} B_c K_i\{\exp(-\Delta t\bullet a_M/2\tau_i)\frac{1}{J}[B] - \frac{\Delta t}{\tau_i}\exp[-\Delta t\bullet a_M/\tau_i]H_n^{(i)}\frac{\partial a_M}{\partial\{\varepsilon^l\}} \\ &- \frac{\Delta t}{2\tau_i}\exp[-\Delta t\bullet a_M/2\tau_i]\frac{\partial a_M}{\partial\{\varepsilon^l\}}[(\frac{1}{J}[B]\{\varepsilon^l\}) - (\frac{1}{J}[B]\{\varepsilon_p^l\})|]\}\end{aligned} \tag{C.13}$$

$$\frac{\partial A}{\partial\{u\}} = \sum_{i=1}^{n_k} B_c K_i \{\exp(-\Delta t \bullet a_M / \tau_i)[[B]\{\varepsilon^l\} - [B]\{\varepsilon_p^l\}]$$

$$(-\frac{1}{J^2})\frac{\partial J}{\partial\{u\}} - \frac{\Delta t}{\tau_i}\exp[-\Delta t \bullet a_M / \tau_i]\frac{\partial a_M}{\partial\{u\}} H_n^{(i)} \qquad \text{(C.14)}$$

$$-\frac{\Delta t}{2\tau_i}\exp[-\Delta t \bullet a_M / 2\tau_i]\frac{\partial a_M}{\partial\{u\}}[(\frac{1}{J}[B]\{\varepsilon^l\})|_{n+1} - (\frac{1}{J}[B]\{\varepsilon^l\})|_n]\}$$

BIBLIOGRAPHY

[1] Abu-Ghannam, N., McKenna, B.: The application of Peleg's equation to model water absorption during the soaking of red kidney beans (Phaseolus vulgaris L.). J. Food Eng. 32, 391-401 (1997)

[2] Achanta, S.: Moisture transport in shrinking gels during drying. Ph.D thesis, Purdue University, West Lafayette, IN (1995)

[3] Achanta, S., Cushman, J.H.: Nonequilibrium swelling-pressure and capillary-pressure relations for colloidal systems. J. Colloid Interface Sci. 168, 266-268 (1994)

[4] Achanta, S., Cushman, J.H., Okos, M.R.: On multicomponent, multiphase thermomechanics with interfaces. Int. J. Eng. Sci. 32(11), 1717-1738 (1994)

[5] Achanta, S., Okos, M.R., Cushman, J.H., Kessler, D.P.: Moisture transport in shrinking gels during saturated drying. AIChE J. 43(8), 2112-2122 (1997)

[6] Akiyama, T., Hayakawa, K.: Heat and moisture transfer and hygrophysical changes in elastoplastic hollow cylinder-food during drying. J. Food Sci. 65(2), 315-323 (2000)

[7] Akiyama, T., Lui, H., Hayakawa, K.: Hygrostress-multicrack formation and propagation in cylindrical viscoelastic food undergoing heat and moisture transfer processes. Int. J. Heat Mass Trans. 40(7), 1601-1609 (1997)

[8] Arslan, N., Togrul, H.: Modelling of water sorption isotherms of marcaroni stored in a chamber under controled humidity and thermodynamic approach. J. Food Eng. 69, 133-145 (2005)

[9] Atkins, P., de Paula, J.: Physical Chemistry (7th ed.). W. H. Freeman, New York (2002)

[10] Aversa, M., Curcio, S., Calabro, V., Iorio, G.: An analysis of the transport phenomena occurring during food drying process. J. Food Eng. 78(3), 922-932 (2007)

[11] Bachmat, Y., Bear, J.: Macroscopic modeling of transport phenomena in porous media. 1: The continuum approach. Transp. Porous Media. 1, 213-240 (1986)

[12] Baggio, P., Bonacina, C., Schrefler, B.A.: Some considerations on modeling heat and mass transfer in porous media. Transp. Porous Media. 28, 233-251 (1997)

[13] Bai, Y., Rahman, M.S., Perera, C.O., Smith, B., Melton, L.D.: Structural changes in apple rings during convection air-drying with controlled temperature and humidity. J. Agric. Food Chem. 50(11), 3179-3185 (2002)

[14] Bakalis, S., Kyritsi, A., Karathanos, V.T., Yanniotis, S.: Modelling of rice hydration using finite elements. J. Food. Eng. 94(3-4), 321-325 (2009)

[15] Bear, J.: Dynamics of fluids in porous media. Dover, New York (1972)

[16] Bear, J., Bachmat Y.: Macroscopic modeling of transport phenomena in porous media. 2: Applications to mass, momentum and energy transport. Transp. Porous Media. 1, 241-269 (1986)

[17] Belytschko, T., Liu, W.K., Moran, B.: Nonlinear finite elements for continua and structures. John Wiley & Sons, Ltd (2000)

[18] Bennethum, L.S.: Theory of flow and deformation of swelling porous materials at the macroscale. Comput. Geotech. 34, 267-278 (2007)

[19] Bennethum, L.S., Cushman, J.H.: Multiscale, hybrid mixture theory for swelling systems. 1. Balance laws. Int. J. Eng. Sci. 34(2), 125-145 (1996a)

[20] Bennethum, L.S., Cushman, J.H.: Multiscale, hybrid mixture theory for swelling systems. 2. Constitutive theory. Int. J. Eng. Sci. 34(2), 147-169 (1996b)

[21] Bennethum, L.S., Cushman, J.H., Murad, M.A.: Clarifying mixture theory and the macroscale chemical potential for porous media. Int. J. Eng. Sci. 34(14), 1611-1621 (1996c)

[22] Bennethum, L.S., Murad, M.A., Cushman, J.H.: Modified Darcy's law, Terzaghi's effective stress principle and Fick's law for swelling clay soils. Comput. Geotech. 20(3-4), 245-266 (1997)

[23] Bennethum, L.S., Murad, M.A., Cushman, J.H.: Macroscale thermodynamics and the chemical potential for swelling porous media. Transp. Porous Media. 39(2), 187-225 (2000)

[24] Bennethum, L.S., Weinstein, T.: Three pressures in porous media. Transp. Porous Media. 54(1), 1-34 (2004)

[25]Bilbao-Sainz, C., Andres, A., Fito, P.: Hydration kinetics of dried apple as affected by drying conditions. J. Food. Eng. 68(3), 369-376 (2005)

[26]Bloksma, A.H., Bushuk, W.: Rheology and chemisty of dough. Wheat: Chemisty and Technology, 3rd Ed. Vol. 2. Y. Pomeranz, ed. Am. Assoc. Cereal Chem.: St. Paul, MN (1988)

[27] Cafieri, S., Chillo, S., Mastromatteo, M.,Suriano, N., Del Nobile, M.A.: A mathematical model to predict the effect of shape on pasta hydration kinetic during cooking and overcooking. J. Cereal Sci. 48, 857-862 (2008)

[28] Carminati, A., Kaestner, A., Lehmann, P., Flühler, H.: Unsaturated water flow across soil aggregate contacts. Adv. Water Resour. 31(9), 1221-1232 (2008)

[29] Choi, Y., Okos, M.R.: Thermal properties of liquid foods – review. In: Okos, M.R. (editor). Physical and Chemical Properties of Food Saint Joseph, Michigan: American Society of Agricultural Engineers, 35-77 (1986)

[30] Christensen, R.M.: Theory of Viscoelasticity (2nd Edition). Dover Publications (2003)

[31] Coleman, B.D., Noll, W.: The thermodynamics of elastic materials with heat conduction and viscosity. Arch. Rational Mech. Anal. 13, 167-178 (1963)

[32] Cunningham, S.E., McMinn, W.A.M., Magee, T.R.A., Richardson, P.S.: Modelling water absorption of pasta during soaking. J. Food Eng. 82(4), 600-607 (2007)

[33] Cunningham, S.E., McMinn, W.A.M., Magee, T.R.A., Richardson, P.S.: Effect of processing conditions on the water absorption and texture kinetics of potato. J. Food Eng. 84(2), 214-223 (2008)

[34] Cushman, J.H., Singh, P.P., Bennethum, L.S.: Toward rational design of drug delivery substrates: II. Mixture theory for three-scale biocompatible polymers and a computational example. Multiscale Modeling Simul. 2(2), 335-357 (2004)

[35] Datta, A.K.: Hydraulic permeability of food tissues. Int. J. Food. Prop. 9, 767-780 (2006)

[36] Datta, A.K.: Porous media approaches to studying simultaneous heat and mass transfer in food processes. I: Problem formulations. J. Food Eng. 80(1), 80-95 (2007)

[37]De Temmerman, J., Verboven, P., Delcour, J.A., Nicolai, B., Ramon, H.: Drying model for cylindrical pasta shapes using desorption isotherms. J. Food. Eng. 86, 414-421 (2008)

[38] Dejmek, P., Miyawaki, O.: Relationship between the electrical and rheological properties of potato tuber tissue after various forms of processing. Biosci. Biotechnol. Bichem., 66(6), 1218-1223 (2002)

[39] Dhall, A.: Multiphase transport in deformable phase-changing porous materials. Ph.D thesis. Cornell University, Ithaca NY (2011)

[40]Dincer, T.D., Esin, A.: Sorption isotherms for macaroni. J. Food. Eng. 27, 211-228 (1996)

[41] Erbas, M., Ertugay, M.F., Certel, M.: Moisture adsorption behaviour of semolina and farina. J. Food. Eng. 69, 191-198 (2005)

[42] Eringen, A.C.: A continuum theory of swelling porous elastic soils. Int. J. Eng. Sci. 32, 1337-1349 (1994)

[43] Fang, S., Wang, Z., Hu, X., Datta, A.K.: Hot-air drying of whole fruit Chinese jujube (Zizyphus jujube Miller): physicochemical properties of dried products. Int. J. Food Sci. Technol. 44, 1415-1421 (2009)

[44]Fardet, A., Hoebler, C., Djelveh, G., Barry, J-L.: Restricted bovine serum albumin diffusion through the protein network of pasta. J. Agric. Food. Chem. 46, 4635-4641 (1998)

[45] Flory, P.J.: Thermodynamic relations for highly elastic materials. Trans. Faraday Soc. 57, 829-838 (1961)

[46]Garcia-Pascual, P., Sanjuan, N., Bon. J., Carreres, J., Mulet, A.: Rehydration process of Boletus edulis mushrooms: characteristic and modelling. J. Sci. Food. Agric. 85, 1397-1404 (2005)

[47] Gray, W.G., Schrefler, B.A., Pesavento, F.: The solid phase stress tensor in porous media mechanics and the Hill-Mandel condition. J. Mech. Phys. Solids. 57, 539-554 (2009)

[48]Halder, A., Dhall, A., Datta, A.K.: An improved, easily implementable porous media based model for deep-fat frying - Part I: Model development and input parameters. Food and Bioproducts Processing. 85(C3), 209-219 (2007)

[49] Hassanizadeh, M., Gray, W.G.: General conservation equation for multi-phase systems: 1. Averaging procedure. Adv. Water Resour. 2, 131-144 (1979a)

[50] Hassanizadeh, M., Gray, W.G.: General conservation equation for multi-phase systems: 2. Mass, momenta, energy, and entropy equations. Adv. Water Resour. 2, 191-208 (1979b)

[51] Hassanizadeh, M., Gray W.G.: General conservation equations for multiphase systems: 3 Constitutive theory for porous media flow. Adv. Water Resour. 3, 25-40 (1980)

[52] Hassanizadeh, M., Gray, W.G.: Mechanics and thermodynamics of multiphase flow in porous media including interface boundaries. Adv. Water Resour. 13(4), 169-186 (1990)

[53] Hassini, L., Azzouz, S., Peczalski, R., Belghith, A.: Estimation of potato moisture diffusivity from convective drying kinetics with correction for shrinkage, J. Food Eng. 79, 47-56 (2007)

[54] Holzapfel, G.A.: Nonlinear Solid Mechanics: A Continuum Approach for Engineering. Wiley (2000)

[55]Iciek, J., Krysiak, W.: Effect of air parameters on the quality of dried potato cubes. Drying Technol. 27, 1316-1324 (2009)

[56] Itaya, Y., Kobayashi, T., Hayakawa, K.: Three-dimensional heat and moisture transfer with viscoelastic strain-stress formation in composite food during drying. Int. J. Heat Mass Trans. 38(7), 1173-1185 (1995)

[57] Izumi, M., Hayakawa, K.: Heat and moisture transfer and hygrostress crack formation and propagation in cylindrical, elastoplastic food. Int. J. Heat Mass Trans. 38(6), 1033-1041 (1998)

[58]Karathanos, V.T., Kanellopoulos, N.K., Belessiotis, V.G.: Development of porous structure during air drying of agricultural plant products. J. Food. Eng. 29, 167-183 (1996)

[59] Kaviany, M.: Principles of heat transfer in porous media. Springer Verlag, New York (1991)

[60]Krokida, M.K.,Maroulis, Z.B.: Effect of drying method on shrinkage and porosity. Drying Technol. 15(10), 2441-2458 (1997)

[61]Krokida, M.K., Marinos-Kouris, D.: Rehydration kinetics of dehydrated products. J. Food Eng. 57(1), 1-7 (2003)

[62]Krokida, M.K., Maroulis, Z.B., Marinos-Kouris, D.: Viscoelastic behavior of dehydrated carrot and potato, Drying Technol. 16 (3-5), 687-703 (1998)

[63]Lagoudaki, M., Demertzis, P.G., Kontominas, M.G.: Moisture adsorption behaviour of pasta products. Lebensm. Wiss. u. Technol. 26, 512-516 (1993)

[64]Lee, K.T., Farid, M., Nguang, S.K.: The mathematical modelling of the rehydration characteristics of fruits. J. Food. Eng. 72(1), 16-23 (2006)

[65]Lee, C.H., Kim, C.W.: Studies on the rheological property of Korean noodles. I. Viscoelastic behaviour of wheat flour noodle and wheat-sweet potato starch noodle.

Korean J. Food Sci. Technol. 15(2), 183-188 (1983)

[66] Liu, I.S.: Method of Lagrange multipliers for exploitation of the entropy principle. Arch. Rational Mech. Anal. 46, 131-148 (1972)

[67] Lozano, J.E., Rotstein, E., Urbicain, M.J.: Total porosity and open-pore porosity in the drying of fruits. J. Food Sci. 45, 1403-1407 (1980)

[68] Lozano, J.E., Rotstein, E., Urbicain, M.J.: Shrinkage, porosity and bulk density of foodstuffs at changing moisture contents. J. Food Sci. 48, 1497-1502, 1553 (1983)

[69]Machado, M.F., Oliveria, F.A.R., Cunha, L.M.: Effect of milk fat and total solids concentration on the kinetics of moisture uptake by ready-to-eat breakfast cereal. Int. Food Sci. Technol. 34, 47-57 (1999)

[70]Markowski, M., Bondaruk, J., Blaszczak, W.: Rehydration behavior of vacuum-microwave-dried potato cubes. Drying Technol. 27(2), 296-305 (2009)

[71] Maroulis, Z.B., Kiranoudis, C.T., Marinos-Kouris, D.: Heat and mass transfer modeling in air drying of foods. J. Food. Eng. 26, 113-130 (1995)

[72]Maskan, M.: Effect of maturation and processing on water uptake characteristics of wheat. J. Food. Eng. 47, 51-57 (2001)

[73] Marabi, A., Livings, S., Jacobson, M., Saguy, I.S.: Normalized Weibull distribution for modelling rehydration of food particulates. Eur. Food. Res. Technol. 217, 311-318 (2003)

[74] Mayor, L., Sereno, A.M.: Modelling shrinkage during convective drying of food materials: a review. J. Food Eng. 61, 373-386 (2004)

[75]Meda, L., Ratti, C.: Rehydration of freeze dried strawberries at varying temperatures. J. Food. Process. Eng. 28(3), 233-246 (2005)

[76] Misra, R.N., Young, J.H.: Numerical solution for simultaneous moisture diffusion and shrinkage during soybean drying. Trans. ASAE. 1277-1282 (1980)

[77] Moreira, R., Figueiredo, A., Sereno, A.: Shrinkage of apple disks during drying by warm air convection and freeze drying. Drying Technol. 18(1&2), 279-294 (2000)

[78] Murad, M.A., Bennethum, L.S., Cushman, J.H.: A Multiscale theory of swelling porour-media. 1. Application to one-dimensional consolidation. Transp. Porous Media. 19(2), 93-122 (1995)

[79] Murad, M.A., Cushman, J.H.: Multiscale flow and deformation in hydrophilic swelling porous media. Int. J. Eng. Sci. 34(3), 313-338 (1996)

[80] Murad, M.A., Cushman, J.H.: Multiscale theory of swelling porous media: II. Dual porosity models for consolidation of clays incorporating physicochemical effects. Transp. Porous Media. 28(1), 69-108 (1997)

[81] Murad, M.A., Cushman, J.H.: Thermomechanical theories for swelling porous media with microstructure. Int. J. Eng. Sci. 38(5), 517-564 (2000)

[82]Ni, H.: Multiphase moisture transport in porous media under intensive microwave heating, PhD thesis, Cornell University (1997)

[83] Ni, H., Datta, A.K.: Heat and moisture transfer in baking of potato slabs. Drying Technol. 17(10), 2069-2092 (1999)

[84] Ogden, R.W.: Nonlinear Elastic Deformations. John Wiley, (Dover reprint) (1984)

[85] Park, K.J.: Diffusional model with and without shrinkage during salted fish muscle drying. Drying Technol. 16 (3-5), 889-905 (1998)

[86]Peleg, M.: An empirical model for the description of moisture sorption curves. J. Food Sci. 53(4), 1216-1219 (1988)

[87] Perre, P., Moyne, C.: Processes related to drying. 2. Use of the same model to solve transfers both in saturated and unsaturated porous-media. Drying Technol. 9(5), 1153-1179 (1991)

[88] Perre, P., Turner, I.W.: A 3-D version of TransPore: a comprehensive heat and mass transfer computational model for simulating the drying of porous media. Int. J. Heat Mass Transfer. 42(24), 4501-4521 (1999)

[89]Planinic, M., Velic, D., Thomas, S., Bilic, M., Bucic, A.: Modelling of drying and rehydration of carrots using the Peleg's model. Eur. Food. Res. Technol. 221, 446-451 (2005)

[90] Ponsart, G., Vasseur, J., Frias, M., Duquenoy, A., Meot, J.M.: Modelling of stress due to shrinkage during drying of spaghetti. J. Food Eng. 57(3), 277-285 (2003)

[91] Pruess, K.: TOUGH2-A General-Purpose Numerical Simulator for Multiphase Fluid and Heat Flow. LBNL-29400, UC-251, Earth Sciences Division, Lawrence Berkeley National Laboratory, Berkeley, CA (1991)

[92] Purandara, B.K., Varadarajan, N., Venkatesh, B.: Simultaneous transport of water and solutes under transient unsaturated flow conditions - A case study. J. Earth Syst. Sci. 117(4), 477-487 (2008)

[93] Rahman, M.S., Perera, C.O., Chen, X.D., Driscoll, R.H., Potluri, P.L.: Density, shrinkage and prosity of Calamari Mantle Meat during air drying in a cabinet dryer as a function of water content. J. Food Eng. 30, 135-145 (1996)

[94] Rahman, M.S., Potluri, P.L.: Shrinkage and density of squid flesh during air drying. J. Food Eng. 12, 133-143 (1990)

[95] Rakesh, V.: Transport in rigid and deformable hygroscopic porous media during electromagnetic and combination heating. Ph.D thesis. Cornell University, Ithaca NY (2010)

[96] Ramana, S.V., Taylor, A.J.: Dynamic measurement of tissue rigidity during freezing and cooking of vegetables. J. Sci. Food Agric. 58, 261-266 (1992)

[97] Ratti, C.: Shrinkage during drying of foodstuffs. J. Food Eng. 23(1), 91-105 (1994)

[98] Ratti, C., Crapiste, G.H., Rotstein, E.: A new water sorption equilibrium expression for solid foods based on thermodynamic considerations. J. Food Sci. 54(3), 738-747 (1989)

[99]Ruiz Diaz, G., Martinez-Monzo, P., Chiralt, A.: Modelling of dehydration-rehydration of orange slices in combined microwave/air drying. Innovat. Food. Sci. Emerg. Technol. 4, 203-209 (2003)

[100]Saguy, I.S., Marabi, A., Wallach, R.: New approach to model rehydration of dry food particulates utilizing principles of liquid transport in porous media. Trends. Food. Sci. Technol. 16(11), 495-506 (2005)

[101]Sanjuan, N., Simal, S., Bon, J., Mulet, A.: Modelling of broccoli stems rehydration process. J. Food. Eng. 41(1), 27-31 (1999)

[102]Sasaki, T., Kohyama, K., Yasui, T., Satake, T.: Rheological properties of white salted noodles with different amylose content at small and large deformation. Cereal Chem. 81(2), 226-231 (2004)

[103] Schrefler, B.A.: Mechanics and thermodynamics of saturated/unsaturated porous materials and quantitative solutions. Appl. Mech. Rev. 55(4), 351-388 (2002)

[104]Simal, S., Berna, A., Mulet, A., Rossello, C.: A method for the calculation of the heat transfer coefficient in potato drying, J. Sci. Food Agric. 63, 365-367 (1993)

[105] Simo, J.C., Hughes, T.J.R.: Computational Inelasticity. Springer-Verlag (1997)

[106] Singh, P.P.: Effect of viscoelastic relaxation on fluid and species transport in biopolymeric materials. Ph.D thesis, Purdue University, West Lafayette, IN (2002)

[107] Singh, P.P., Cushman, J.H., Maier, D.E.: Three scale thermomechanical theory for swelling biopolymeric systems. Chem. Eng. Sci. 58, 4017-4035 (2003a)

[108] Singh, P.P., Cushman, J.H., Maier, D.E.: Multiscale fluid transport theory for swelling biopolymers. Chem. Eng. Sci. 58, 2409-2419 (2003b)

[109] Singh, B., Gupta, A.K.: Mass transfer kinetics and determination of effective diffusivity during convective dehydration of pre-osmosed carrot cubes. J. Food. Eng. 79(2), 459-470 (2007)

[110] Singh P.P., Maier D.E., Cushman J.H., Campanella O.H.: Effect of viscoelastic relaxation on moisture transport in foods. Part II: sorption and drying of soybeans. J. Math. Biol. 49, 20–34 (2004)

[111]Sopade, P.A., Ajisegiri, E.S., Badau, M.H.: The use of Peleg's equation to model water absorption in some cereal grains during soaking. J. Food. Eng. 15, 269-283 (1992)

[112]Sozer, N., Dalgic, A.C.: Modeling of rheological characteristics of various spaghetti types. European Food Research and Technol. 225(2), 183-190 (2007)

[113] Srikiatden, J., Roberts, J.S.: Predicting moisture profiles in potato and carrot during convective hot air drying using isothermally measured effective diffusivity. J. Food. Eng. 84(4), 516-525 (2008)

[114]Stamatopoulos, A.: Contribution à l'étude théorique et expérimentale du séchage des pâtes alimentaires, PhD Thesis, University of Montpellier, Montpellier, France (1986)

[115]Sung, W.C., Stone, M.: Microstructural studies of pasta and starch pasta. J. Mar. Sci. Tech. 13(2), 83-88 (2005)

[116]Takhar S.P., Kulkkarni, M.V., Huber, K.: Dynamic viscoelastic properties of pasta as a function of temperature and water content. J. Texture Studies. 37, 696-710 (2006)

[117] Treloar, L.R.G.: The elasticity of a network of long-chain molecules-I. Trans. Faraday Soc. 39, 36-41 (1943a)

[118] Treloar, L.R.G.: The elasticity of a network of long-chain molecules-II. Trans. Faraday Soc. 39, 241-246 (1943b)

[119] Tsukada, T., Sakai, N., Hayakawa, K.: Computerized model for strain-stress analysis of food undergoing simultaneous heat and mass transfer. J. Food Sci. 56(5), 1438-1445 (1991)

[120] Vazquez, G., Chenlo, F., Morera, R., Costoyas, A.: The dehydration of garlic. 1. Desorption isotherms and modeling of drying kinetics. Drying Technol. 17(6), 1095-1108 (1999)

[121]Wang, N., Brennan, J.G.: Thermal conductivity of potato as a function of moisture content. J. Food Eng. 17, 153-160 (1992)

[122] Wang, N., Brennan, J.G.: The influence of moisture content and temperature on the specific heat of potato measured by differential scanning calorimetry. J. Food Eng. 19, 303-310 (1993)

[123] Wang, N., Brennan, J.G.: Changes in structure, density and porosity of potato during dehydration. J. Food Eng. 24(1), 61-76 (1995)

[124]Weerts, A.H., Martin, D.R., Lian, G., Melrose, J.R.: Modelling the hyration of foodstuffs. Simulat. Model. Pract. Theor. 13(2), 119-128 (2005)

[125]Weibull, W.: A statistical distribution function of wide applicability. J. Appl. Mech.-Trans. ASME. 18(3), 193-197 (1951)

[126] Weinstein, T.F., Bennethum, L.S.: On the derivation of the transport equation for swelling porous materials with finite deformation. Int. J. Eng. Sci. 44, 1408-1422 (2006)

[127] Weinstein, T.F., Bennethum, L.S., Cushman, J.H.: Two-Scale, Three-Phase Theory for swelling Drug Delivery Systems. Part I: Constitutive Theory. J. Pharm. Sci. 97(5), 1878-1903 (2008a)

[128]Weinstein, T.F., Bennethum, L.S., Cushman, J.H.: Two-Scale, Three-Phase Theory for swelling Drug Delivery Systems. Part II: Flow and transport models. J. Pharm. Sci. 97(5), 1904-1915 (2008b)

[129] Willis, B., Okos, M., Campanella, O.: Effects of glass transition on stress development during drying of a shrinking food system. Proceedings of the sixth conference of food engineering (CoFE'99). 451-496 (1999)

[130]Yadollahinia, A., Latifi, A., Mahdavi, R.: New method for determination of potato slice shrinkage during drying. Comput. Electron. Agric. 65, 268-274 (2009)

[131] Yang, H., Sakai, N., Watanabe, M.: Drying model with non-isotropic shrinkage deformation undergoing simultaneous heat and mass transfer. Drying Technol. 19(7), 1441-1460 (2001)

[132] Zhang, J., Datta, A.K., Mukherjee, S.: Transport processes and large deformation during baking of a bread. AICHE J. 51(9), 2569-2580 (2005)

[133]Zhu, H., Dhall, A., Mukherjee, S., Datta, A.K.: A model for flow and deformation in unsaturated swelling porous media. Transp. Porous Media. 84, 335-369 (2010)

[134] Zhu, H., Mukherjee, S., Dhall, A.: A finite element analysis and coupling between water absorption and swelling of foodstuffs during soaking. Transp. Porous Media. 88 (3), 399-419 (2011)